PNNL-22631, Rev. 1
ORP-58289

Pacific Northwest
NATIONAL LABORATORY
Proudly Operated by Battelle Since 1965

Glass Property Models and Constraints for Estimating the Glass to be Produced at Hanford by Implementing Current Advanced Glass Formulation Efforts

JD Vienna DC Skorski
DS Kim J Matyas

July 2013

U.S. DEPARTMENT OF ENERGY
Prepared for the U.S. Department of Energy under Contract DE-AC05-76RL01830

DISCLAIMER

This report was prepared as an account of work sponsored by an agency of the United States Government. Neither the United States Government nor any agency thereof, nor Battelle Memorial Institute, nor any of their employees, makes **any warranty, express or implied, or assumes any legal liability or responsibility for the accuracy, completeness, or usefulness of any information, apparatus, product, or process disclosed, or represents that its use would not infringe privately owned rights**. Reference herein to any specific commercial product, process, or service by trade name, trademark, manufacturer, or otherwise does not necessarily constitute or imply its endorsement, recommendation, or favoring by the United States Government or any agency thereof, or Battelle Memorial Institute. The views and opinions of authors expressed herein do not necessarily state or reflect those of the United States Government or any agency thereof.

PACIFIC NORTHWEST NATIONAL LABORATORY
operated by
BATTELLE
for the
UNITED STATES DEPARTMENT OF ENERGY
under Contract DE-AC05-76RL01830

Printed in the United States of America

Available to DOE and DOE contractors from the
Office of Scientific and Technical Information,
P.O. Box 62, Oak Ridge, TN 37831-0062;
ph: (865) 576-8401
fax: (865) 576-5728
email: reports@adonis.osti.gov

Available to the public from the National Technical Information Service
5301 Shawnee Rd., Alexandria, VA 22312
ph: (800) 553-NTIS (6847)
email: orders@ntis.gov <http://www.ntis.gov/about/form.aspx>
Online ordering: http://www.ntis.gov

This document was printed on recycled paper.
(8/2010)

PNNL-22631, Rev. 1
ORP-58289

Glass Property Models and Constraints for Estimating the Glass to be Produced at Hanford by Implementing Current Advanced Glass Formulation Efforts

JD Vienna
DS Kim
DC Skorski
J Matyas

July 2013

Prepared for
the U.S. Department of Energy
under Contract DE-AC05-76RL01830

Pacific Northwest National Laboratory
Richland, Washington 99352

Abstract

Recent glass formulation and melter testing data have suggested that significant increases in waste loading in high-level waste (HLW) and low-activity waste (LAW) glasses are possible over current system planning estimates. The data (although limited in some cases) were evaluated to determine a set of constraints and models that could be used to estimate the maximum loading of specific waste compositions in glass. It is recommended that these models and constraints be used to estimate the likely HLW and LAW glass volumes that would result if the current glass formulation studies are successfully completed. It is recognized that some of the models are preliminary in nature and will change in the coming years. In addition, the models do not currently address the prediction uncertainties that would be required before they could be used in plant operations. The models and constraints are only meant to give an indication of rough glass volumes and are not intended to be used in plant operation or waste form qualification activities. A current research program is in place to develop the data, models, and uncertainty descriptions for that purpose.

A fundamental tenet underlying the research reported in this document is the attempt to be less conservative than previous studies when developing constraints for the estimation of glass to be produced by implementing current advanced glass formulation efforts. The less conservative approach documented herein should allow for the estimate of glass masses that may be realized if the current efforts in advanced glass formulations are completed over the coming years, and are as successful as early indications suggest they may be. Because of this approach, there is an unquantifiable uncertainty in the ultimate glass volume projections due to model prediction uncertainties that must be considered, along with other system uncertainties, such as waste compositions and amounts to be immobilized, split factors between LAW and HLW, etc.

Summary

Efforts are being made to increase the loading of Hanford tank wastes in glass while maintaining adequate processability, regulatory compliance, and product quality. These efforts have significantly expanded the composition regions and waste loadings of glasses beyond the point used in current project planning models. The effort documented in this report is aimed at evaluating the current glass formulation, property, and processing data, and to use the data to develop a non-conservative set of constraints and property models that can be used to estimate the amount of glass that would be produced at Hanford if the current advanced waste glass formulation efforts were to be successfully completed according to current plans.

An accurate method of estimating glass volume to be produced from Hanford tank waste is important for making informed decisions regarding the appropriate process options to pursue, as well as estimating the likely cost and schedule for tank waste cleanup mission completion. To help gain an accurate estimate of glass volume, glass property, processing, and composition, data have been gathered from literature including the results of the ongoing advanced glass formulation program being led by the U.S. Department of Energy Office of River Protection with support from the Vitreous State Laboratory at The Catholic University of America and the Pacific Northwest National Laboratory. These data have been evaluated and used in the development of preliminary glass composition-property models as well as property and composition constraints. By combining these models and constraint sets, the reader can estimate the minimum amount of glass to be generated from Hanford tank waste with a given composition. Example calculations are supplied to ensure that the calculations are performed as intended. The models and constraints are only meant to give an indication of rough glass volumes and are not intended to be used in plant operation or waste form qualification activities. A current research program is in place to develop the data, models, and uncertainty descriptions for that purpose.

Throughout this document, a number of model coefficients and other values are reported with a higher number of figures than are significant. Ideally, the appropriate number of figures to report should be evaluated in detail. However, no such evaluation was performed. We therefore suggest using all reported figures in the model coefficients for consistency with example calculations supplied in this report.

High-Level Waste Glass Property Models

Models to constrain the composition and loading of high-level waste (HLW) glasses include models to control the amount of spinel in the melter (c_{Sp}), the sulfur tolerance of the melter feed, nepheline formation in canister-cooled glass, viscosity of the melt, product consistency test (PCT) response, and liquidus temperature (T_L) of zirconia-containing phases. Also reported are component concentration limits for model validity, chromium tolerance, and phosphate tolerance. The recommended models are given below, along with property and component concentration constraints.

The c_{sp} model is given by:

$$c_{Sp} \cong \sum_{i=1}^{p} \left(a_i + b_i T \right) g_i \qquad \text{(S.1)}$$

where a_i and b_i are the temperature-independent and temperature-dependent component coefficients listed in Table S.1, and g_i is the i^{th} component mass fraction in glass.

Table S.1. Coefficients for the Recommended c_{Sp} Model, in vol%

Component, *i*	*T*-Independent Coefficient, a_i	*T*-Dependent Coefficient, b_i, °C^{-1}
Al_2O_3	21.24545	-0.00785
B_2O_3	-14.55838	0.0078747
CaO	-76.00601	0.0646231
CdO	-50.6897	0.0621757
Cr_2O_3	-52.92551	0.1156024
F	117.44887	-0.094526
Fe_2O_3	30.882125	-0.013788
K_2O	-17.83219	0.0106531
Li_2O	91.117773	-0.098169
MgO	420.6061	-0.305744
MnO	62.003538	-0.038308
Na_2O	-4.485897	-0.007289
NiO	311.47667	-0.220915
SiO_2	-13.18649	0.009237
ZrO_2	-0.753569	0.0066262
Others	38.536088	-0.036449

The allowable weight percent SO_3 concentration in the melter feed ($w_{SO_3}^{Limit}$) is given by:

$$w_{SO_3}^{Limit} = \sum_{i=1}^{p} s_i n_i + s_{Li_2O \times Li_2O} n_{Li_2O}^2 \qquad \text{(S.2)}$$

where s_i is the i^{th} component coefficient given in Table S.2, $s_{Li_2O \times Li_2O}$ is the coefficient for normalized lithium oxide concentration squared, and n_i is the i^{th} component concentration in glass normalized to 1 after removing SO_3: $n_i = g_i / 1 - g_{SO_3}$, where g_i is the i^{th} component mass fraction in glass.

Table S.2. Coefficients for the Recommended w_{SO_3} Model, in wt%

Components, i	Coefficients, s_i
Al_2O_3	-0.803866
B_2O_3	3.0983142
CaO	5.6570336
Cl	-29.77093
Cr_2O_3	-7.5784
Li_2O	3.2746409
Na_2O	2.7845163
P_2O_5	4.4652267
SiO_2	-0.542488
SrO	2.6347706
TiO_2	6.3907736
V_2O_5	6.2747968
ZnO	4.2286005
ZrO_2	-1.291709
Other	0.1221757
$Li_2O \times Li_2O$	179.71011

The composition effects on nepheline are significantly more non-linear than those for c_{Sp} or w_{SO_3}, therefore a neural network (NN) model is used to predict its precipitation. Accordingly, the probability of nepheline formation during slow cooling (P) for a given glass is given by:

$$P = \left[1 + Exp\left(a_0 + a_1 N_1 + a_2 N_2 + a_3 N_3\right)\right]^{-1} \tag{S.3}$$

where N_1, N_2, and N_3 are three nodes of the form

$$N_\alpha = TanH\left[\frac{1}{2}\left(w_{\alpha,0} + \sum_{i=1}^{p} w_{\alpha,i} g_i\right)\right] \tag{S.4}$$

where $w_{\alpha,i}$ is the i^{th} component coefficient for the α^{th} node and g_i is the i^{th} component mass fraction in glass. The model coefficients are listed in Table S.3.

Table S.3. Coefficients for the Recommended Nepheline Probability Model

Variable	*Prenodal*, a_0	Node 1 Coefficients, $w_{1,i}$	Node 2 Coefficients, $w_{2,i}$	Node 3 Coefficients, $w_{3,i}$
a_α	13.2882662868656	16.1270533249324	-4.26025610502183	-4.97044005504938
$w_{\alpha,0}$	-	-0.368504314788528	2.59230438483144	-17.6191838468361
w_{α,Al_2O_3}	-	-16.3361586053405	32.506920415784	-71.1921457263483
w_{α,B_2O_3}	-	7.92706218213264	-145.236120123692	-46.6794443749077
$w_{\alpha,CaO}$	-	1.96944639904736	141.41874985731	81.2090543151236
w_{α,Li_2O}	-	-6.37113637206031	96.2610336261315	421.585615170079
w_{α,Na_2O}	-	-10.1383393382153	-71.9972897111855	349.303887885242
w_{α,SiO_2}	-	7.98567618444061	49.559194772126	-48.7817648739116

The viscosity at 1150°C (η_{1150}) was modeled previously and used again in this study. The form of the equation is:

$$Ln[\eta_{1150}] = \sum_{i=1}^{p} h_i g_i + selected \left\{ \sum_{i=1}^{p-1} \sum_{j=i}^{p} h_{ij} g_i g_j \right\} \quad \text{(S.5)}$$

where h_i and g_i are the i^{th} component coefficient and mass fraction in glass, respectively. Table S.4 lists the model coefficients.

Table S.4. Coefficients for the Recommended η_{1150} Model, in Ln[Pa·s]

Model Term, i	Coefficient, h_i
Al_2O_3	10.6085
B_2O_3	-9.37529
BaO	-3.41816
CaO	-6.9328
F	-12.3445
K_2O	-3.82491
La_2O_3	-4.96954
Li_2O	-39.0249
MgO	-3.23141
MnO	-6.88677
Na_2O	-9.63275
P_2O_5	5.305007
PbO	-23.1436
SiO_2	9.368089
SrO	-4.35052
UO_3	2.151455
ZnO	-2.69626
ZrO_2	7.14044
Others	-0.09027
$B_2O_3 \times B_2O_3$	24.59262
$Na_2O \times B_2O_3$	-26.9571
$Li_2O \times Li_2O$	47.35918
$Na_2O \times Al_2O_3$	17.51718
$CaO \times Al_2O_3$	-8.13474

A model for the average natural logarithm of normalized PCT boron, lithium, and sodium response was developed with the form:

$$\mathrm{Ln}\left[PCT\right] = \sum_{i=1}^{p} b_i g_i + b2_{Al_2O_3} g_{Al_2O_3}^2 + b3_{Al_2O_3} g_{Al_2O_3}^3 + b4_{Al_2O_3} g_{Al_2O_3}^4 \qquad \text{(S.6)}$$

where b_i and g_i are the i^{th} component coefficient and mass fraction in glass. The coefficients are listed in Table S.5.

Table S.5. Coefficients for the Recommended Ln[PCT] Model, in Ln[g/m^2]

Model Term, i	Coefficient, b_i
Al_2O_3	-103.76
B_2O_3	10.75627
CdO	15.74204
F	26.97387
Fe_2O_3	-2.574697
K_2O	11.64107
Li_2O	23.52778
MgO	10.4331
MnO	4.028527
Na_2O	15.27193
SiO_2	-2.827361
SO_3	20.6466
TiO_2	-11.8236
ZrO_2	-6.265786
Others	-0.595703
$(Al_2O_3)^2$	1166.629
$(Al_2O_3)^3$	-5871.868
$(Al_2O_3)^4$	10289.47

A model for the T_L of zirconium-containing phases was developed and published previously and recommended for use here. This model has the form:

$$T_L = \sum_{i=1}^{p} t_i g_i \tag{S.7}$$

where t_i and g_i are the i^{th} component coefficient and mass fraction in glass, respectively. The coefficients are listed in Table S.6.

Table S.6. Coefficients for the Recommended T_L-Zs Model, in °C

Model Term, i	Coefficient, t_i
Al_2O_3	3193.3628
B_2O_3	651.39721
LN_2O_3[(a)]	2156.4074
Li_2O	-1904.417
Na_2O	-1947.711
SrO	13011.909
ZrO_2	3747.4241
Others	1259.2233

(a) LN_2O_3 is the combined mass fractions of Y_2O_3 and all the rare-earth oxides (which are all assumed to be in the trivalent state).

The recommended property constraints are listed in Table S.7 and the recommended component concentration constraints are listed in Table S.8.

Table S.7. HLW Glass Property Constraints

Constraint	Limit
PCT Response	Ln[PCT] < 1.39
Nepheline	P < 27%
Spinel	c_{Sp} < 2 vol% at 950°C
Zirconium-containing phases	T_L-Zs < 1050°C if ZrO_2>4%
Viscosity at 1150°C	$4 < \eta_{1150} < 6$ Pa·s
P_2O_5 and CaO concentrations	$w_{P_2O_5} \times w_{CaO}$ <6.5 wt%[2]
Salt, SO_3 concentration	$w_{SO_3} < w_{SO_3}^{Limit}$
Eskolaite formation	$g_{Cr_2O_3} < 0.03$

Table S.8. HLW Glass Component Concentration Constraints, in wt%

Comp, *i*	Min	Max
Al_2O_3	1.9	29
B_2O_3	4	20
BaO	0	4.7
Bi_2O_3	0	7
CaO	0	7
CdO	0	1.5
Cr_2O_3	0	4
F	0	2.5
Fe_2O_3	0	20
K_2O	0	6
Li_2O	0	6
MgO	0	6
MnO	0	7
Na_2O	4.1	23
Nd_2O_3	0	5.9
NiO	0	3
P_2O_5	0	4.5
SiO_2	30.3	53
SrO	0	10.1
ThO_2	0	6
TiO_2	0	3.1
UO_3	0	6.3
ZnO	0	4
ZrO_2	0	13.5

Low-Activity Waste Glass Property Models

Models to constrain the composition and loading of low-activity waste (LAW) glasses include models to control the sulfur tolerance of the melter feed PCT response, Vapor Hydration Test (VHT) response, and viscosity. Also reported are component concentration limits for model validity, as well as the chromium, halide, phosphate, and alkali tolerance. The recommended models are given below along with property and component concentration constraints.

The allowable weight percent SO_3 concentration in the melter feed (w_{SO_3}) is given by:

$$w_{SO_3}^{Limit} = \sum_{i=1}^{p} s_i n_i + s_{Li_2O \times Li_2O} n_{Li_2O} n_{Li_2O} \quad \text{(S.8)}$$

where s_i is the component coefficient given in Table S.9 and n_i is the i^{th} component concentration in glass normalized to 1 after removing SO_3: $n_i = g_i / (1 - g_{SO_3})$, where g_i is the i^{th} component mass fraction in glass.

Table S.9. Coefficients for the Recommended w_{SO_3} Model, in wt%

Components, $_i$	Coefficients, s_i
Al_2O_3	-0.803866
B_2O_3	3.0983142
CaO	5.6570336
Cl	-29.77093
Cr_2O_3	-7.5784
Li_2O	3.2746409
Na_2O	2.7845163
P_2O_5	4.4652267
SiO_2	-0.542488
SrO	2.6347706
TiO_2	6.3907736
V_2O_5	6.2747968
ZnO	4.2286005
ZrO_2	-1.291709
Other	0.1221757
$Li_2O \times Li_2O$	179.71011

A model for the average natural logarithm of normalized PCT boron and sodium response was developed with the form:

$$\mathrm{Ln}\left[\mathrm{NL},\ \mathrm{g/L}\right] = \sum_{i=1}^{p} b_i g_i + selected\left\{\sum_{i=1}^{p-1}\sum_{j=i+1}^{p} b_{ij} g_i g_j\right\} \qquad \text{(S.9)}$$

where b_i and g_i are the i^{th} component coefficient and mass fraction in glass. The coefficients are listed in Table S.10.

Table S.10. Coefficients for the Recommended Ln[PCT] Model, in Ln[g/L]

Model Term, i	Coefficient, b_i
Al_2O_3	-69.07589
B_2O_3	13.020929
CaO	-7.234449
Fe_2O_3	-6.318672
K_2O	10.099748
Li_2O	27.748976
MgO	7.1092189
Na_2O	16.667725
P_2O_5	-9.063384
SiO_2	-3.07673
V_2O_5	9.3277525
ZrO_2	-8.556034
Others	-1.157161
$Al_2O_3 \times Al_2O_3$	361.93083
$CaO \times Fe_2O_3$	163.17256
$MgO \times ZrO_2$	592.93753

The composition effects on VHT are significantly more non-linear that those for w_{SO_3} and Ln[PCT], therefore an NN model is used to predict glass response to VHT. Accordingly, the VHT response (r24) for a given glass is given by the following:

r24=22.2368486728788+162.297620340354*TanH(0.5*Fn1)+146.571639705835*TanH(0.5*Fn2) (S.10)

where Fn1 and Fn2 are given by:

Fn1= -2.0234500345046 +

3.42064364061235 * TanH (0.5 * (19.6032022867479
+ -41.763025292002 * Al2O3
+ -7.2247531165788 * B2O3
+ -71.440190399197 * CaO
+ 21.4866660009179 * Fe2O3
+ -5.8285856407714 * K2O
+ 14.1674908254771 * Li2O
+ -17.712793652953 * MgO
+ 4.90653877435819 * Na2O
+ -23.999070392784 * SiO2
+ -89.261809766372 * ZrO2))
+ -1.5945608677549 * TanH (0.5 * (9.71096479446714
+ -1.7854759769145 * Al2O3
+ 35.9943209948772 * B2O3
+ -49.874405307677 * CaO
+ 23.2401360961441 * Fe2O3
+ -86.620913893724 * K2O
+ 9.56939724758103 * Li2O
+ -238.90360119104 * MgO
+ -3.2019704029069 * Na2O
+ -25.2772019420 1 * SiO2
+ 140.437932824307 * ZrO2))
+

2.31555079823014 * TanH (0.5 * (3.26429869709493
+ 104.477522837661 * Al2O3
+ 4.58157835900144 * B2O3
+ 0.85255450354859 * CaO
+ 1.1244826601591 * Fe2O3
+ 60.7067527477005 * K2O
+ 62.0556736612157 * Li2O
+ -62.402468467866 * MgO
+ 11.4599614081572 * Na2O
+ -27.425799171143 * SiO2
+ -49.853555611999 * ZrO2))
+ -4.0985855697882 * TanH (0.5 * (54.4850934035448
+ 14.0759354190093 * Al2O3
+ -77.812329749985 * B2O3
+ -24.479879404922 * CaO
+ -15.422081646139 * Fe2O3
+ -64.301191862086 * K2O
+ -106.16853767331 * Li2O
+ -75.957683994829 * MgO
+ -103.98990411707 * Na2O
+ -50.469486676587 * SiO2
+ -29.590974146236 * ZrO2))
+

2.42774575785518 * TanH (0.5 * (10.7282870519699
+ 135.592922593436 * Al2O3
+ -43.364161952728 * B2O3
+ 94.4108021418093 * CaO
+ 106.198181220628 * Fe2O3
+ -95.8928850646 * K2O
+ -62.087358826133 * Li2O
+ 8.17353548499568 * MgO
+ -36.294958232164 * Na2O
+ -44.774632983115 * SiO2
+ 52.2713874914766 * ZrO2))
+ -3.002427812819 * TanH (0.5 * (1.36554171806406
+ 8.39190437614229 * Al2O3
+ 85.1968179640575 * B2O3
+ -54.481478008755 * CaO
+ 87.6692685766409 * Fe2O3
+ -21.332583067516 * K2O
+ -0.0388979586356 * Li2O
+ 155.446663232058 * MgO
+ -25.780955827028 * Na2O
+ -2.3634111816427 * SiO2
+ -165.81210510989 * ZrO2))

Fn2= 2.60707890790828 +

-2.0838579173615 * TanH [0.5 * [19.6032022867479
+ -41.763025292002 * Al2O3
+ -7.2247531165788 * B2O3
+ -71.440190399197 * CaO
+ 21.4866660009179 * Fe2O3
+ -5.8285856407714 * K2O
+ 14.1674908254771 * Li2O
+ -17.712793652953 * MgO
+ 4.90653877435819 * Na2O
+ -23.999070392784 * SiO2
+ -89.261809766372 * ZrO2]] +

0.99511640966129 * TanH [0.5 * [9.71096479446714
+ -1.7854759769145 * Al2O3
+ 35.9943209948772 * B2O3
+ -49.874405307677 * CaO
+ 23.2401360961441 * Fe2O3
+ -86.620913893724 * K2O
+ 9.56939724758103 * Li2O
+ -238.90360119104 * MgO
+ -3.2019704029069 * Na2O
+ -25.27720194201 * SiO2
+ 140.437932824307 * ZrO2]] +

-1.8175914652203 * TanH [0.5 * [3.26429869709493
+ 104.477522837661 * Al2O3
+ 4.58157835900144 * B2O3
+ 0.85255450354859 * CaO
+ 1.1244826601591 * Fe2O3
+ 60.7067527477005 * K2O
+ 62.0556736612157 * Li2O
+ -62.402468467866 * MgO
+ 11.4599614081572 * Na2O
+ -27.425799171143 * SiO2
+ -49.853555611999 * ZrO2]] +

2.69183546569062 * TanH [0.5 * [54.4850934035448
+ 14.0759354190093 * Al2O3
+ -77.812329749985 * B2O3
+ -24.479879404922 * CaO
+ -15.422081646139 * Fe2O3
+ -64.301191862086 * K2O
+ -106.16853767331 * Li2O
+ -75.957683994829 * MgO
+ -103.98990411707 * Na2O
+ -50.469486676587 * SiO2
+ -29.590974146236 * ZrO2]] +

-1.3391192503165 * TanH [0.5 * [10.7282870519699
+ 135.592922593436 * Al2O3
+ -43.364161952728 * B2O3
+ 94.4108021418093 * CaO
+ 106.198181220628 * Fe2O3
+ -95.8928850646 * K2O
+ -62.087358826133 * Li2O
+ 8.17353548499568 * MgO
+ -36.294958232164 * Na2O
+ -44.774632983115 * SiO2
+ 52.2713874914766 * ZrO2]] +

1.9238318134371 * TanH [0.5 * [1.36554171806406
+ 8.39190437614229 * Al2O3
+ 85.1968179640575 * B2O3
+ -54.481478008755 * CaO
+ 87.6692685766409 * Fe2O3
+ -21.332583067516 * K2O
+ -0.0388979586356 * Li2O
+ 155.446663232058 * MgO
+ -25.780955827028 * Na2O
+ -2.3634111816427 * SiO2
+ -165.81210510989 * ZrO2]]

The viscosity at 1150°C (η_{1150}) was modeled previously and used again in this study. The form of the equation is:

$$Ln[\eta_T, P] = \sum_{i=1}^{p}\left(v_i + y_i/\left[T\cdot 1000\right]^2\right)g_i + selected\left\{\sum_{i=1}^{p-1}\sum_{j=i}^{p} v_{ij}g_i g_j\right\} \qquad \text{(S.11)}$$

where v_i , y_i, and g_i, are the i^{th} component temperature-independent coefficient, temperature-dependent coefficient, and mass fraction in glass, respectively; T is the absolute temperature (in K). Table S.11 lists the model coefficients.

Table S.11. Coefficients for the Recommended Ln[η] Model, in Ln[P]

Model Term, *i*	Temperature-Independent Coefficient, v_i	Temperature-Dependent Coefficient, y_i
Al_2O_3	5.5124	24.6423
B_2O_3	−42.3772	-
CaO	−10.6445	13.7793
Fe_2O_3	−4.6220	15.2036
K_2O	−0.8689	-
Li_2O	10.9390	−82.4815
MgO	−5.6188	22.7608
Na_2O	0.9073	−14.5621
P_2O_5	−0.8081	24.0339
SiO_2	1.5575	24.4077
ZrO_2	−12.0741	48.2286
Others	−9.3903	17.3800
$(B_2O_3)^2$	198.7360	-
$(Li_2O)^2$	133.6906	-
$Al_2O_3 \times Li_2O$	−136.5095	-
$(MgO)^2$	-179.8249	-

The recommended property constraints are listed in Table S.12. The waste loading rules give an estimate of the loading of waste in glass, while the property limits, combined with property models described above, allow for optimization of the glass composition along with the recommended component concentration constraints that are listed in Table S.13.

Table S.12. LAW Glass Property Constraints

Waste Loading Rules	Limit
Alkali content	$w_{Na_2O} + 0.66 w_{K_2O} < 24\,\text{wt\%}$
Alkali and sulfur content	$w_{Na_2O} + 0.66 w_{K_2O} \le 33.94 - 11.69 w_{SO_3}, \text{wt\%}$
Sulfur content	$w_{SO_3} < 1.5\,\text{wt\%}$
Halide content	$w_{SO_3} \le 1.65 - 0.725\left(w_{Cl} + 0.3 w_F + 0.4 w_{Cr_2O_3}\right), \text{wt\%}$
Property	**Limit**
Salt, SO_3 concentration	$w_{SO_3} < w_{SO_3}^{Limit}$
PCT response	Ln[PCT] < 1.386
VHT response	r24 < 50 g/m^2/d
Viscosity at 1150°C	$40 < \eta_{1150} < 60$ P

Table S.13. LAW Glass Component Concentration Constraints, in wt%

Component	Lower Limit	Upper Limit
Al_2O_3	5.0	9.0
B_2O_3	5.0	16.0
CaO	0	13.0
Fe_2O_3	0	13.0
K_2O	0	8.0
Li_2O	0	6.0
MgO	0	10.0
Na_2O	5.0	26.0
P_2O_5	0	4.5
SiO_2	30.0	51.0
SO_3	0	1.6
SnO_2	0	5.0
TiO_2	0	4.0
V_2O_5	0	4.5
ZnO	0	6.0
ZrO_2	2.6	7.0

Quality Assurance

This work was performed under the U.S. Department of Energy (DOE) Office of River Protection (ORP) Inter-Entity Work Order # M0ORV00020. The details of the work and associated requirements are documented in the test plan TP-EWG-00001 (Vienna et al. 2013). Per ORP as stated in the test plan, project work was conducted under a quality assurance program compliant with Title 10 of the Code of Federal Regulations Part 830 (10 CFR 830), "Nuclear Safety Management," Subpart A, "Quality Assurance Requirements" and DOE Order 414.1D, "Quality Assurance" and NQA-1 (ASME 2000); and it was graded in accordance with NQA-1-2000, Subpart 4.2, "Guidance on Graded Application of Quality Assurance (QA) for Nuclear-Related Research and Development." Pacific Northwest National Laboratory's (PNNL's) program is compliant with these requirements.

The PNNL QA program description implements both DOE Order 414.1D and 10 CFR 830, Subpart A. PNNL has also adopted the NQA-1-2000, Quality Assurance Program for Nuclear Facilities, as its single consensus standard for implementation of quality assurance requirements, and graded in accordance with NQA-1-2000, Subpart 4.2, "Guidance on Graded Application of Quality Assurance (QA) for Nuclear-Related Research and Development." PNNL's standards-based management system—How Do I? (HDI)—is a web-based system for communicating the QA program requirements through Laboratory-wide procedures or subject areas. All work at PNNL is subject to the applicable HDI requirements. In the facilities where work in support of this project is conducted, PNNL's "Integrated Operations Systems" is used to implement HDI and safety procedures at the benchtop. As part of the graded approach to quality assurance, this project has a formal Quality Assurance Plan (QAP) that specifies project-specific quality procedures covering technical work.

In accordance with ORP, all analytical project work was performed following the latest "Hanford Analytical Services Quality Requirements Document" (HASQARD). PNNL subcontracted to Southwest Research Institute (SwRI) for analytical services, which required HASQARD compliance. PNNL has audited and accepted SwRI services as being compliant with the HASQARD requirements, and has placed SwRI on the PNNL Evaluated Suppliers List as an acceptable supplier for analytical services in accordance with HASQARD.

No experimentation was conducted as part of the study reported here. The work reported includes the gathering of data from literature, the screening and evaluation of the data, the fitting of glass property models, and the recommendation of constraints for glass formulation based on the literature data and glass formulation experiences. These activities were performed under the QA program described above. However, the data used in the evaluations and models were taken from literature and do not always comply with the above-stated QA requirements or any defined quality assurance program. Therefore, the models reported in this document cannot be considered to comply with NQA-1 (ASME 2000) or RW-0333P (DOE 2008).

Acknowledgments

We gratefully acknowledge the financial support of the U.S. Department of Energy's Waste Treatment and Immobilization Plant Federal Project Office under the direction of Dr. Albert A. Kruger.

The authors also thank the following people for their technical review and consultations on the work leading to this report:

- Albert Kruger – ORP
- Rod Gimpel – Hanford Tank Waste Treatment and Immobilization Plant (WTP)
- Jeremy Belsher – Washington River Protection Solutions (WRPS)
- David Peeler – Savannah River National Laboratory (SRNL)
- Pavel Hrma – Consultant
- Brian Riley – PNNL
- Mary Bliss – PNNL
- Ernie Lee – WTP
- Paul Certa – WRPS
- Peter Empey – WRPS
- Kevin Fox – SRNL
- Jake Amoroso – SRNL
- Connie Herman – SRNL

This manuscript was masterfully edited by Susan Ennor. We thank Mike Schweiger, Mary Bliss, Kirsten Meier, and Mona Champion (all of PNNL) for programmatic support during the conduct of this work.

A large fraction of the data described in this report was generated by the Vitreous State Laboratory at The Catholic University of America (VSL). We are thankful to VSL for sharing their data and assistance in data evaluation and interpretation, in particular Professor Ian Pegg.

Abbreviations/Acronyms

ASTM	American Society for Testing and Materials
CCC	canister centerline cooled
CFR	Code of Federal Regulations
c_{Sp}	equilibrium concentration of spinel in the melt
CVS	composition variation study
DOE	U.S. Department of Energy
DWPF	Defense Waste Processing Facility
EA	environmental assessment
g_i	mass fraction of i^{th} component in glass
G2	WTP dynamic flowsheet model
HASQARD	Hanford Analytical Services Quality Requirements Document
HDI	how do I?
HLP	Hanford LAW product acceptance
HLW	high-level waste
HTM	high temperature melter
HTWOS	Hanford Tank Waste Operations Simulator
HWVP	Hanford Waste Vitrification Plant
ILAW	immobilized low-activity waste
INEEL	Idaho National Engineering and Environmental Laboratory
LAW	low-activity waste
MT	metric ton
ND	nepheline discriminator
n_i	normalized mass fraction of i^{th} component in glass
NAlk	normalized alkali oxide concentration
NH	normalized halogen concentration
NN	neural network
NQA	nuclear quality assurance
NSi	normalized SiO_2 concentration
OB	optical basicity
ORP	Office of River Protection
PCT	Product Consistency Test
PNNL	Pacific Northwest National Laboratory
QA	quality assurance
QAP	Quality Assurance Plan
r24	Vapor Hydration Test response rate normalized to 24 day test
RPP	River Protection Project

R^2	coefficient of determination
RMSE	root mean squared error
RSD	relative standard deviation
SRNL	Savannah River National Laboratory
SwRI	Southwest Research Institute
TanH	hyperbolic tangent
TCLP	Toxicity Characteristic Leaching Procedure
$T_{1\%}$	temperature at one volume percent crystal in equilibrium with the melt
T_L	liquidus temperature
TWRS	Tank Waste Remediation System
VHT	Vapor Hydration Test
VSL	Vitreous State Laboratory at the Catholic University of America
w_i	weight percent of the i^{th} component in glass or melter feed
WTP	Hanford Tank Waste Treatment and Immobilization Plant
WVDP	West Valley Demonstration Project

Contents

Figures

Tables

1.0 Introduction

The Hanford Tank Waste Operations Simulator (HTWOS) and the Hanford Tank Waste Treatment and Immobilization Plant (WTP) dynamic flowsheet model (G2) are software tools used to evaluate the impacts of process assumptions on the Hanford tank waste cleanup mission (Bergmann 2010; Deng 2011). Both contain modules that calculate the high-level waste (HLW) and low-activity waste (LAW) glass mass to be produced from each batch of tank waste transferred to the WTP. The sum of the glass masses over the life of the Hanford tank waste cleanup mission is a key output of the models that may significantly influence cleanup costs and schedules, which forms part of the basis for the cost and schedule baseline (e.g., the River Protection Project (RPP) system plan) (Certa et al. 2011). It is important, therefore, to incorporate the most up-to-date information on waste loading in glasses into these models.

The purpose of this report is to summarize the advancements in glass formulation and to recommend a set of glass property-composition models and constraints that can be used in HTWOS and G2 to estimate the range of likely HLW and LAW glass volumes that would result if the current glass formulation studies are continued and the models ultimately implemented. It is recognized that some of the models are preliminary in nature and will change in the coming years. In addition, the models do not currently address the prediction uncertainties that would be needed before they could be used in plant operations. The models and constraints are only meant to give an indication of rough glass volumes and are not intended to be used in plant operation or waste form qualification activities. A current research program is in place to develop the data, models, and uncertainty descriptions for that purpose.

A fundamental tenet underlying the research reported in this document is the attempt to be less conservative than previous studies when developing constraints for estimating glass to be produced by implementing current advanced glass formulation efforts. The less conservative approach documented herein should allow for the estimate of glass masses that may be realized if the current efforts in advanced glass formulations are completed over the coming years and are as successful as early indications suggest they may be. Because of this approach, there is an unquantifiable uncertainty in the ultimate glass volume projections due to model prediction uncertainties that must be considered, along with other system uncertainties, such as waste compositions and amounts to be immobilized, split factors between LAW and HLW, etc.

The advanced glass formulation efforts have largely been performed by the Vitreous State Laboratory at The Catholic University of America (VSL) under the guidance and support of the U.S. Department of Energy (DOE) Office of River Protection (ORP). Some of the research was performed by the Pacific Northwest National Laboratory (PNNL) and by the Savannah River National Laboratory (SRNL).

1.1 High-Level Waste Loading Limitations

The HLW glass volume estimates are based on optimizing the loading of the waste batch in a borosilicate glass, while simultaneously meeting a full range of predicted property and composition limits (Bergmann 2010; Gimpel 2009). The property predictions are currently based on the glass property models of (Vienna et al. 2009). The use of these models is constrained by maintaining the calculated glass composition within the range of compositions covered by glasses used to fit the models. In

addition, a normalized silica concentration ($NSi = g_{SiO_2} \Big/ \left(g_{Al_2O_3} + g_{Na_2O} + g_{SiO_2} \right)$) constraint is used to avoid the deleterious effects of nepheline formation in the product glass (Li et al. 1997).

An evaluation of the impacts of the property and component concentration constraints showed that five constraints are most influential on the estimated Hanford HLW glass volumes (Belsher and Meinert 2009):

- the temperature at one volume percent spinel crystal in the melt ($T_{1\%}$) being limited to 950°C,
- the concentration limit of SO_3 of 0.5 wt% (on a melter feed basis) to avoid the accumulation of salt in the melter,
- the concentration limits of 3.2 wt% Bi_2O_3 and 2.5 wt% P_2O_5 in glass as constrained by model-validity regions,
- the *NSi* limit of 0.62 to help avoid nepheline formation in the product, and
- the model-validity constraints for Al_2O_3 of 20 wt%.

Kim likewise found the following limiting factors, based on HTWOS 2009 model predictions, with the fraction of glass limited by each factor given parenthetically (Kim et al. 2011):

- high Al_2O_3 wastes that are limited by nepheline formation and spinel (46%),
- high Fe_2O_3 wastes (with and without significant Cr_2O_3, MnO, and NiO) forming spinel and other crystals (24%),
- high Cr_2O_3 and SO_3 wastes that are subject to data range constraints but prone to salt formation and potential eskolaite formation (20%),
- high P_2O_5 and P_2O_5+CaO wastes that are limited by phase separation and potential process upsets (9%), and
- high Na_2O wastes limited by data range constraints but prone to poor durability (1%).

These are shown graphically in Figure 1.1.

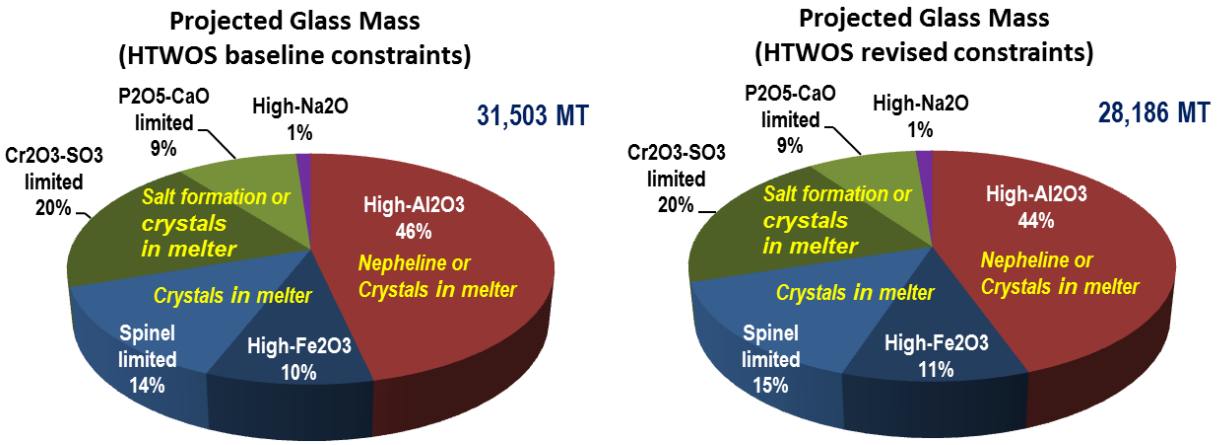

Figure 1.1. Pie Charts Showing the Distribution of HLW Glass by Limiting Factors (Kim et al. 2011)

These constraints are the subject of ongoing research to improve waste loading without significant risk and without requiring changes to planned plant equipment. Some of the improvements were documented in a revised set of constraints for use in HTWOS in 2010 (McCloy and Vienna 2010). A comparison of the glass volume results from the two constraint sets is shown in Figure 1.1.

1.2 Low-Activity Waste Loading Limitations

As with HLW, the loading of LAW in glass has been found to be limited by two factors (Kim et al. 2011; Kim and Vienna 2012; Matlack et al. 2007b; Muller et al. 2010):

- alkali content of the glass (primarily Na_2O, but also K_2O in some wastes), which causes poor chemical durability in general and more specifically fails the current WTP contract constraints for Product Consistency Test (PCT) and Vapor Hydration Test (VHT) responses (DOE 2000), and
- salt formation in the melter that is promoted by SO_3 concentration and to lesser extents Cr_2O_3, Cl, F, and P_2O_5.

The ratio of waste limited by each of those two factors depends on the constraint sets and waste composition estimates used. Two methods of estimating the loading of LAW glass are currently used in HTWOS and G2. The first method, used in the WTP G2 model (Gimpel 2010) and also programed as an option in the HTWOS model (Bergmann 2010), is based on the preliminary immobilized LAW (ILAW) glass formulation algorithm approach (Kim and Vienna 2012). A set of waste loading constraints is used to determine the target waste loading as shown graphically in Figure 1.2 through Figure 1.4.

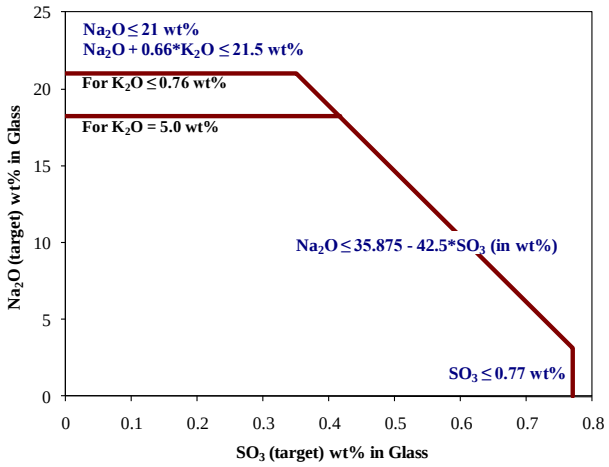

Figure 1.2. Schematic of Current WTP Glass Formulation Rules for Na_2O-SO_3 with Bounding K_2O Concentrations. Two horizontal lines represent Na_2O values for expected K_2O concentration extremes.

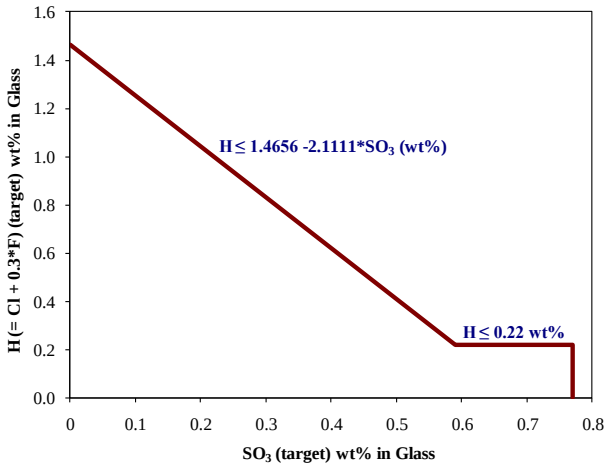

Figure 1.3. Schematic of Current WTP Halide Constraints for Cl-F-SO_3

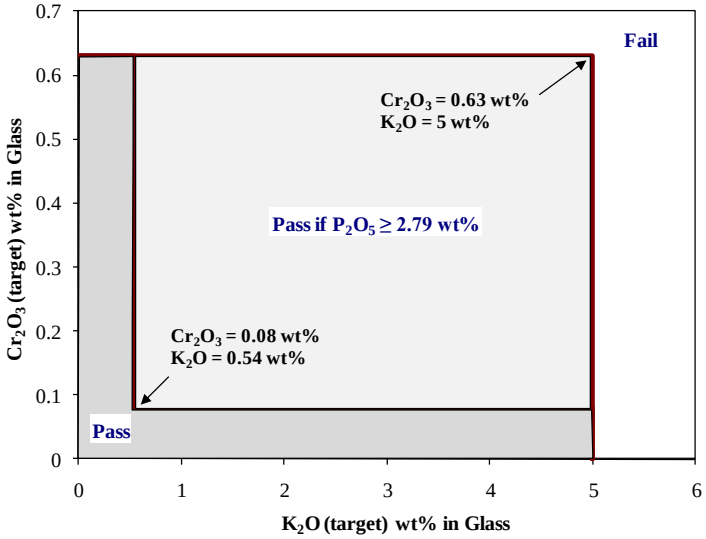

Figure 1.4. Schematic of Current WTP Halide Constraints for Cr_2O_3-K_2O-P_2O_5

Recent and ongoing glass formulation advancements have shown significant gains in LAW loadings in glass. These advancements are compared to the maximum alkali vs. sulfur loading rules of Figure 1.2 in Figure 1.5. The results of this work are summarized by Muller (2010). There is a clear increase in loading for the advanced formulations. Section 3.0 attempts to quantify the differences in glass compositions that led to this dramatic increase in projected waste loadings.

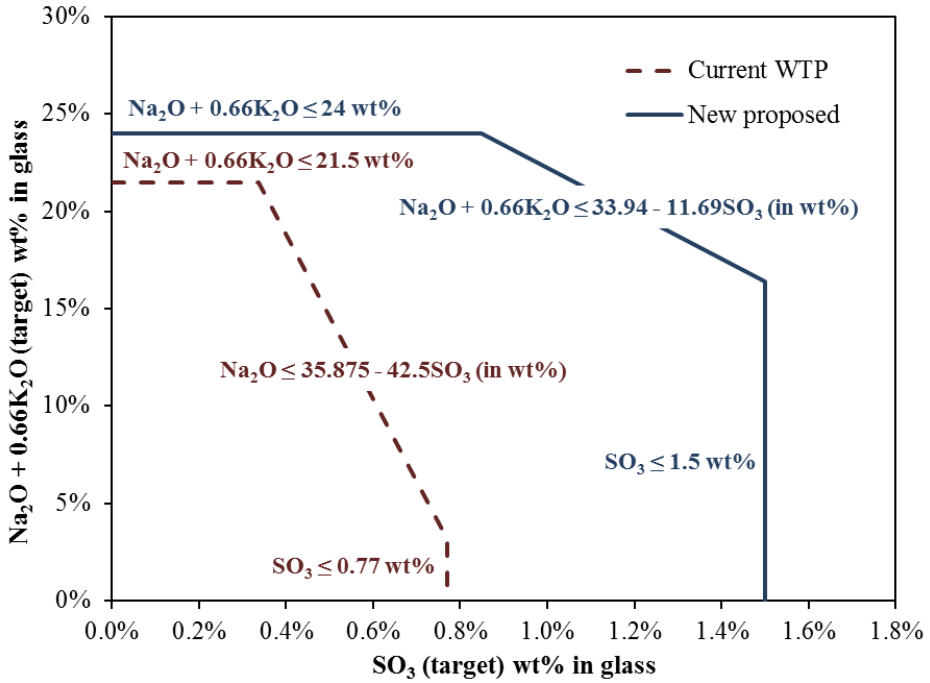

Figure 1.5. Comparison of LAW Loadings of Advanced Formulations with Those of the WTP Baseline Glass Formulation Rules (Kim 2013)

Figure 1.6 compares glass volume estimates using the two sets of waste loading estimates. This study assumed a total of 95,140 metric tons (MT) of Na_2O (70,580 MT of Na) would be vitrified (including recycles). Roughly 63% of the LAW would be vitrified in the supplemental LAW vitrification facility. The conservative and optimistic halide limits, shown in the plot, are discussed in Section 3.1.2.

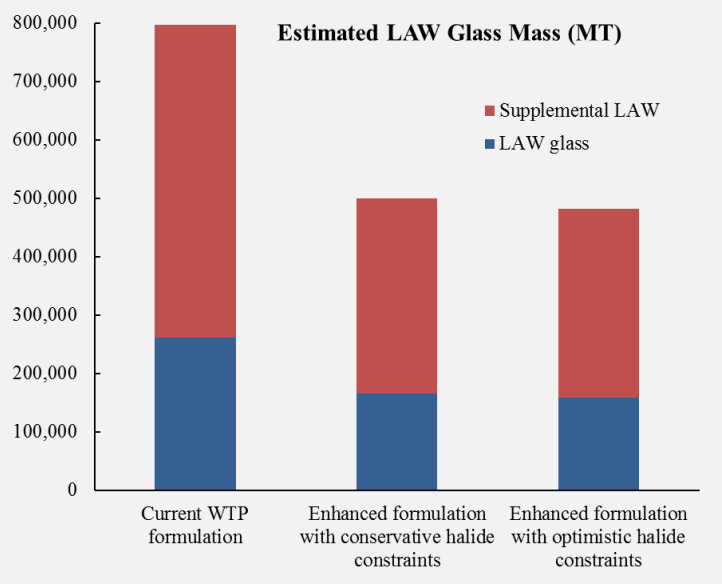

Figure 1.6. Comparison of Predicted LAW Glass Volumes Using Current WTP Formulation Rules and Advanced Glass Formulation Rules (Kim 2013)

1.3 A Note on Significant Figures

Throughout this document, a number of model coefficients and other values are reported with a higher number of figures than are significant. Ideally, the appropriate number of figures to report should be evaluated in detail. However, no such evaluation was performed. We therefore suggest using all reported figures in the model coefficients for consistency with example calculations supplied in Sections 2.10 and 3.7.

2.0 High-Level Waste Glass Constraints Set

This section summarizes the recent advances in HLW glass formulation, and recommends constraints that can be applied to estimate the amount of HLW glass that may be produced at Hanford. Spinel accumulation, sulfur tolerance, nepheline formation, chromium tolerance, viscosity, PCT response, T_L of zirconia-containing phases, and phosphate tolerance are discussed in the following subsections. The recommended constraints are then summarized and example waste loading estimates are shown.

2.1 Spinel Model

Spinel limits in the form of a liquidus temperature (T_L) constraint have been used to control glass composition at the Defense Waste Processing Facility (DWPF) and the West Valley Demonstration Project (WVDP) (Jain et al. 1992; Jantzen 1991a; Jantzen and Brown 2007a,b). VSL proposed that the T_L constraints may be too conservative and inconsistent with the presence of undissolved noble metals (Annamalai et al. 2004). This led to WTP adopting a model to predict the relatively arbitrary 1 vol% spinel temperature limit ($T_{1\%}$) of 950°C for constraining glass composition (Vienna and Kim 2008). This constraint was used as a conservative placeholder until a more technically defensible constraint is developed; it is the basis for both G2 and HTWOS glass HLW estimates. Meanwhile, it was clearly shown by a combination of laboratory testing and melter modeling that crystal fraction and crystal size are far better predictors of potential melter failure caused by spinel buildup than T_L or $T_{1\%}$ (Hrma 2002; Hrma et al. 2003; Hrma and Vienna 2003; Hrma 2010).

A study of the design and operation of the WTP HLW melter suggests that the process most likely to cause failure due to spinel accumulation is the plugging of the pour-spout riser (Matyas et al. 2010a,b). This assessment matched previous experiences with pour-spout plugging in test melters (Jantzen 1986; Rankin et al. 1982) and the DWPF melter (Jantzen et al. 2004). It is recognized, however, that crystal accumulation in the melter body must also be considered when setting an ultimate crystal content limit. To implement a more appropriate control strategy, a model is being developed and will be validated to predict the accumulation of spinel in the WTP pour-spout riser and melter body as a function of melt composition, time, and temperature (Matyas et al. 2013, 2011, 2010a). Although this model shows great promise for setting a technically defensible limit for crystallinity in the WTP HLW melter, it is not yet ready to predict glass volumes over a range of waste compositions.

One approach is to predict the equilibrium fraction of spinel (c_{Sp}) as a function of composition and temperature in the pour-spout riser. Two equations for predicting c_{Sp} as functions of composition and temperature were developed (Hrma and Vienna 2003). The first such equation is based on the freezing point depression equation for an ideal mixture:

$$c_{Sp} = c_{sp,0}\left\{1-\exp\left[-B_L\left(\frac{1}{T}-\frac{1}{T_L}\right)\right]\right\} \tag{2.1}$$

where $c_{Sp,0}$ is the equilibrium fraction of spinel as T approaches 0 K, B_L is a fit parameter related to the enthalpy of crystallization over the universal gas constant, and T is the absolute temperature in K. The parameters $c_{Sp,0}$, T_L, and B_L are then fit to melt composition (typically as first-order glass

property-composition models). Over a relatively narrow range of low c_{Sp} values, this function can be best approximated by the following:

$$c_{Sp} \cong a + bT \tag{2.2}$$

where a and b are linear fit coefficients that can likewise be fit to melt composition to yield the second equation:

$$c_{Sp} \cong \sum_{i=1}^{p} \left(a_i + b_i T\right) g_i \tag{2.3}$$

where a_i = the i^{th} component temperature-independent coefficient,
b_i = the i^{th} component temperature-dependent coefficient,
g_i = the i^{th} component mass fraction in the melt,
p = the number of components modeled, and
T = temperature (not necessarily absolute temperature) (Hrma and Vienna 2003).

A database of c_{Sp}, T, and composition was compiled and fitted to the simplified model. The database is given in Appendix B, and the resulting model is summarized in Table 2.1 and Figure 2.1. The fit is not precise (with a root mean squared error of 0.47 vol% spinel), but it should be sufficient for estimating the amount of glass to be produced from Hanford HLW. As additional data are collected, the model will be improved to better formulate successful glasses.

Table 2.1 also lists the component mass fraction ranges over which the model was fitted. Figure 2.2 shows that the data coverage across the composition region is generally quite good. Also shown in the scatterplot matrix as red circles are the ten data points removed from the fit as outliers with studentized residuals of greater than four. Only two potential reasons for outliers become obvious in the scatterplot matrix: 1) a glass with both high g_{K2O} and g_{CdO} and 2) a glass with both high g_F and g_{MnO}. However, each of those are only single data points and not a trend.

Table 2.1. Coefficients, Validity Constraints, and Summary Statistics for c_{Sp} Model

Component, i	Temperature-Independent Coefficient, a_i	Temperature-Dependent Coefficient, b_i, °C^{-1}	Min Mass Fraction, g_i	Max Mass Fraction, g_i	Statistic	Value
Al_2O_3	21.24545	-0.00785	0.02	0.29	R^2	0.7326
B_2O_3	-14.55838	0.0078747	0.03	0.203	R^2_{Adj}	0.7245
CaO	-76.00601	0.0646231	0	0.08	R^2_{Press}	0.7121
CdO	-50.6897	0.0621757	0	0.02	RMSE, vol%	0.4735
Cr_2O_3	-52.92551	0.1156024	0	0.02	#	1053
F	117.44887	-0.094526	0	0.02	Mean c_{sp}, vol%	1.152
Fe_2O_3	30.882125	-0.013788	0.026	0.20	-	-
K_2O	-17.83219	0.0106531	0	0.06	-	-
Li_2O	91.117773	-0.098169	0	0.06	-	-

Component, i	Temperature-Independent Coefficient, a_i	Temperature-Dependent Coefficient, b_i, °C^{-1}	Min Mass Fraction, g_i	Max Mass Fraction, g_i	Statistic	Value
MgO	420.6061	-0.305744	0	0.01	-	-
MnO	62.003538	-0.038308	0	0.06	-	-
Na_2O	-4.485897	-0.007289	0.04	0.25	-	-
NiO	311.47667	-0.220915	0	0.03	-	-
SiO_2	-13.18649	0.009237	0.215	0.53	-	-
ZrO_2	-0.753569	0.0066262	0	0.062	-	-
Others	38.536088	-0.036449	0	0.16	-	-
T, °C	-	-	654	1328	-	-
c_{Sp}, vol%	-	-	0	5.3	-	-

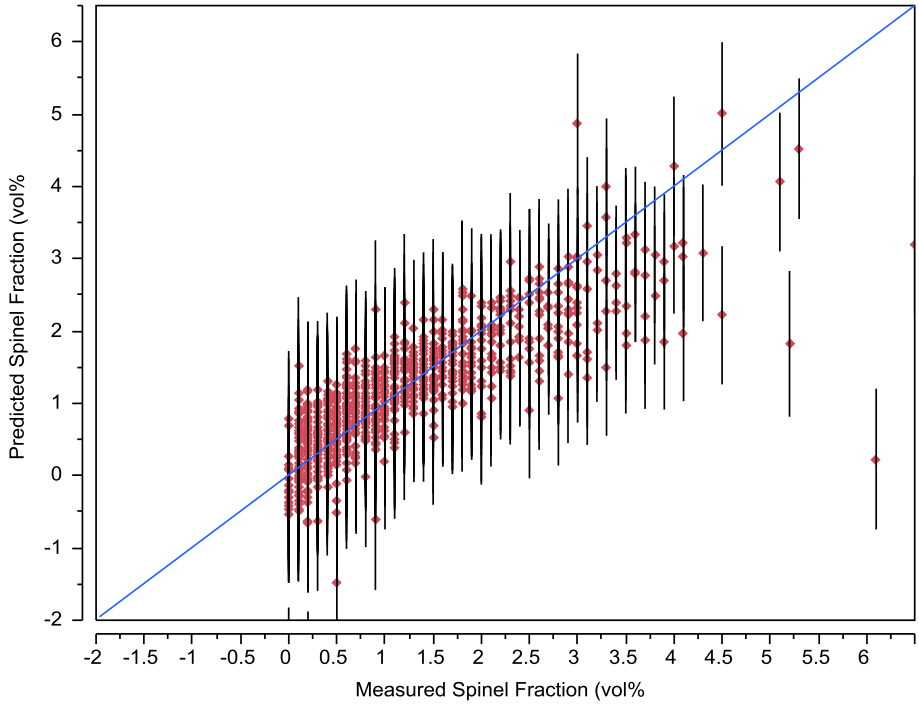

Figure 2.1. Plot of Predicted vs. Measured c_{sp} with 95% Confidence Interval for Individual Prediction, vol%

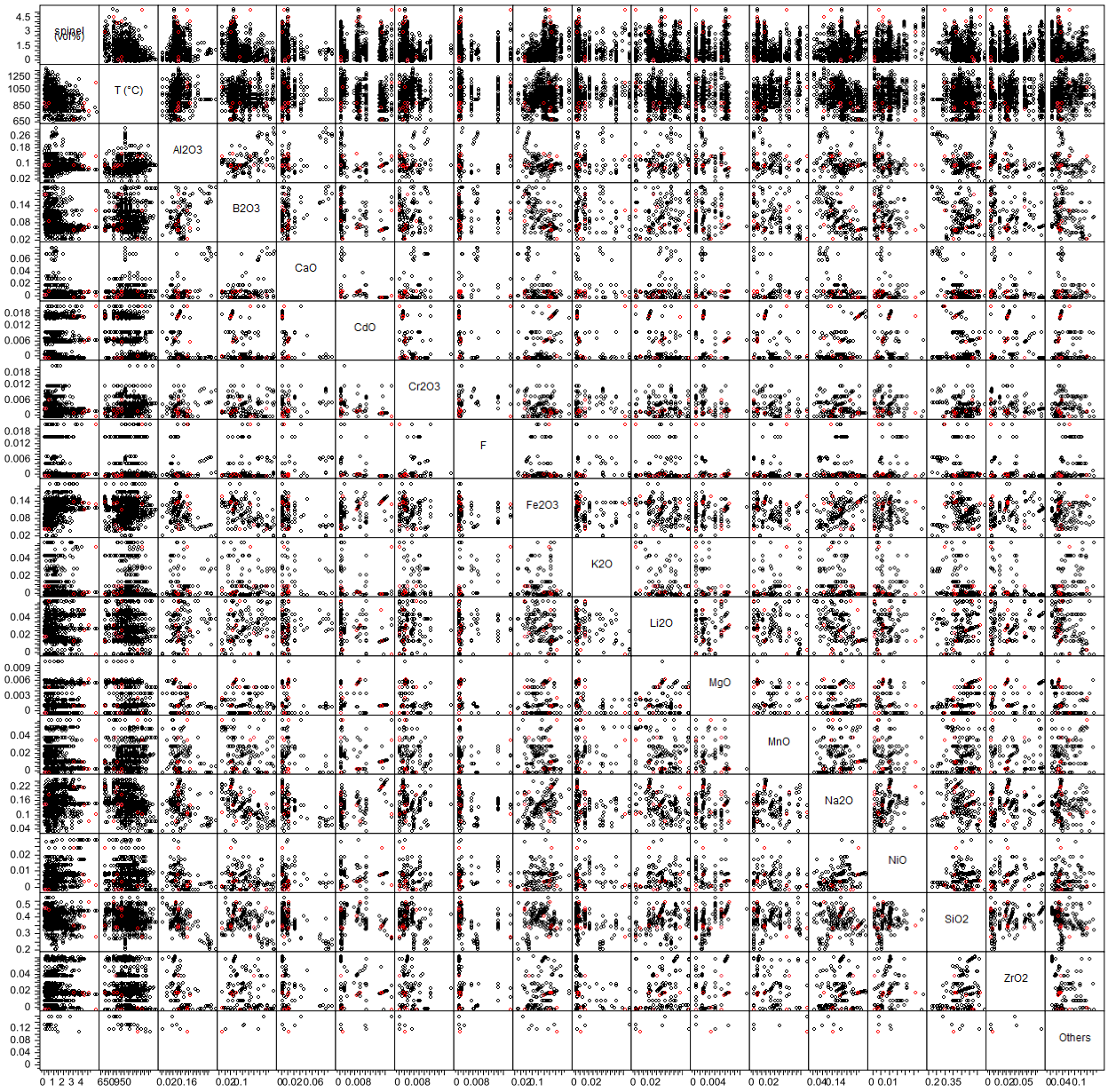

Figure 2.2. Scatterplot Matrix of Glasses Used to Fit the c_{sp} Model

The model-fit can be summarized by the coefficient of determination (R^2), which describes the fraction of the variation in data that is accounted for by the model. Three variations of the R^2 are also considered: 1) the R^2 adjusted for the number of coefficients used to fit the model (R^2_{Adj}), 2) the R^2 calculated from data used to validate the model that was not used in model fitting (R^2_{Val}), and 3) a special case of the R^2_{Val} in which each data point is "left out of the fit" in evaluating how well the model predicts the property for each data point to yield R^2_{Press}. The R^2_{Press} estimates the fraction of variability that would be explained in predicting new observations drawn from the same composition space. Another commonly reported statistic for model fitting is the root mean square error (RMSE), which is the square root of the mean squared difference between predicted and measured response values, and is an estimate

of the experimental plus measurement standard deviation if the model does not have a statistically significant lack of fit.

To calculate the R^2_{Val}, data not used in model fitting must be obtained. Because all appropriate data within the desired composition region were used in model fitting, subsets of the model data were used to validate the model. The data were sorted by c_{Sp} value. The data were then numbered 1, 2, 3, 4, 5, 1, 2, … to split them into five representative groups of roughly 20% of the data. The same model form (including the same set of terms) was then refit to subsets 2 to 5 and used to predict data in subset 1. Then the model was fit to each group of four subsets and used to predict the remaining subset in sequence. Table 2.2 summarizes the results of the model validation.

The R^2 values are all close to each other at approximately 0.74. The R^2_{Val} are all in the range of 0.72, with the exception of group 1 with an R^2_{Val} of 0.66. The average R^2_{Val} is almost identical to the R^2_{Press}value of 0.71. This model is well validated and should give predictions of unknown data within the model-validity region nearly as well as for the model-fit data.

Table 2.2. Summary of c_{sp} Model Validation

Fit Statistics	Full Model	Grp 1	Grp 2	Grp 3	Grp 4	Grp 5	Average
R^2	0.7313	0.7468	0.7314	0.7296	0.7299	0.7293	0.7334
R^2_{Adj}	0.7231	0.7372	0.7211	0.7193	0.7196	0.7189	0.7232
R^2_{Press}	0.7101	0.7213	0.7034	0.7022	0.7039	0.7018	0.7065
RMSE	0.475	0.464	0.477	0.477	0.475	0.481	0.475
$\mathrm{RMSE}_{\mathrm{Press}}$	0.486	0.477	0.492	0.491	0.488	0.495	0.489
Validation							
R^2_{Val}	-	0.6604	0.7215	0.7221	0.7249	0.7276	0.7113

To apply this model, one must select a temperature and a c_{Sp} limit at that temperature. A number of melter test campaigns have been performed with finite c_{Sp} in the melt (Barnes and Larson 1981; Baron and Smith 1988; Bjorklund 1980; Cooper et al. 1994; Dierks 1980; Goles et al. 2002; Hutson 1993; Jain and Barnes 1991; Jantzen 1986; Jantzen and Lambert 1999; Matlack et al. 2009b; McElroy 1976; McElroy et al. 1979a,b; Mendel et al. 1977; Rankin et al. 1982; Ross and Mendel 1979). The two reports of most direct interest have quantified the crystal fraction at 950°C as well as compared the crystals discharged and remaining in the melter (Goles et al. 2002; Matlack et al. 2009b). Goles et al. (2002) successfully processed a glass melt with 3.2 vol% spinel (at 950°C) in a short (120 h) test using the research scaled melter with an overflow pour-spout. They concluded that the $T_{1\%}$ < 950°C limit was too conservative, but they did not perform sufficient testing to determine an appropriate limit. Matlack et al. (2009b) performed five short tests (50 h each) with between 1.6 to 4.2 vol% spinel and eskolaite (at 950°C) using the DM-100 melter with a scaled airlift pour-spout. All the melts processed fine, with no suggestion that the concentrations may yield a problem. However, they concluded that the testing was not yet sufficient to redefine a "crystal limit" since the tests were relatively short and did not include multiple idlings.

A study was performed to determine what the relative impact would be if the crystal fraction limit was set to a value between 1% (current arbitrary limit) and 5% (extent of data used to fit the current model). The results are shown in Figure 2.3. Although the details of these calculations are beyond the scope of this report, three conclusions can be drawn: 1) the new crystal fraction model (shown as C950 in Figure 2.3) results closely match those from the previous $T_{1\%}$ at 950°C model, adding validity to this new model, 2) a significant reduction of glass volumes can be achieved by increasing the crystal limit, and 3) the additional benefits are insignificant after roughly 4 vol% spinel at 950°C, because other properties limit the loadings of waste in glass.

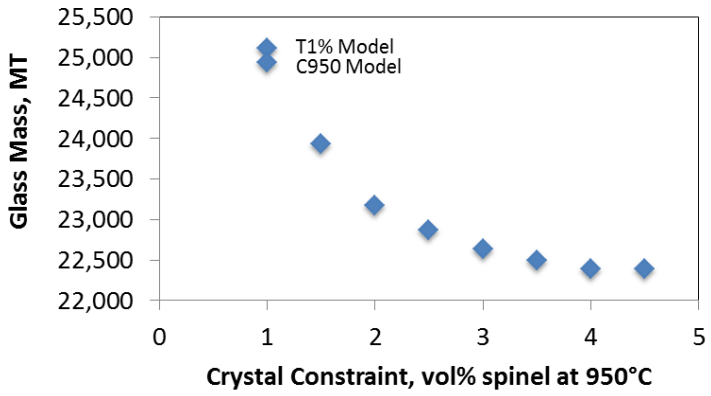

Figure 2.3. Estimated Hanford HLW Glass Volume as a Function of Crystal Concentration Constraint

Figure 2.4 shows the dimensions of the glass discharge riser for the WTP HLW melter. The pattern-filled part represents a volume of glass (~ 3.3 L) available for precipitation, growth, and accumulation of crystals during melter idling. Figure 2.5 shows the accumulated crystal layer heights that were calculated for various volume fractions of crystals in the glass and 35% packing density of crystals in the layer (a typical compaction value seen in the laboratory tests [Matyas et al. 2010b]) based on an assumption that there was enough time during idling for all of the crystals to precipitate, settle, and accumulate in the bottom of the pour-spout riser.

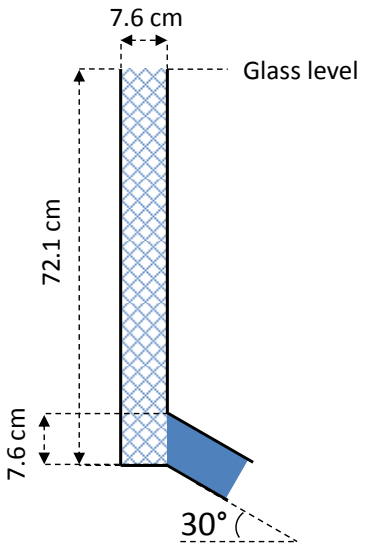

Figure 2.4. Dimensions of the Glass Discharge Riser for WTP HLW Melter

In the lab, the presence of the latency period has been demonstrated during which crystals grow but do not accumulate (Matyas et al. 2013). The length of this period varied with the glass composition, but was always longer than a day. Therefore, for a large number of short idling periods of less than a day or two, the accumulated layer in the riser, if any, should be small. However, idling periods longer than a few days can lead to thick layers that can eventually plug the riser and prevent pouring of the glass (Figure 2.5).

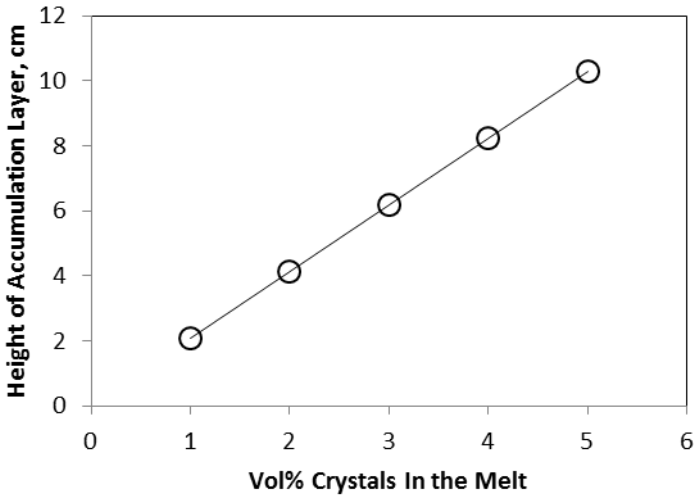

Figure 2.5. Crystal Accumulation Layer Height as a Function of Crystal vol% in the Melt

With a roughly 8-cm-high orifice in the bottom of the pour-spout riser, a reasonable accumulation height that could be envisioned is half of the height, or 4 cm, which translates to a 2 vol% crystal constraint in

the melt. Until sufficient data on spinel accumulation in the melter is obtained, a limit will be used of 2 vol% at 950°C using the model with coefficients in Table 2.1.

2.2 Sulfur Tolerance

The *Preliminary IHLW* [Immobilized High-Level Waste] *Formulation Algorithm Description* limits SO_3 mass fraction in glass (g_{SO_3}) to 0.0044 ($w_{SO_3} \leq 0.44$ wt%) based on only three melter test results available at the time of the report (Vienna and Kim 2008). The 2010 constraint report recommends a constant g_{SO_3} limit of 0.006 ($w_{SO_3} \leq 0.60$ wt%), which was the average concentration of melter tests that did not accumulate a salt from the limited tests available at the time (McCloy and Vienna 2010).

Due to the impact of g_{SO_3} limits on projected HLW glass volumes, additional testing was performed to better estimate the effect of composition on SO_3 tolerance and to refine the concentration limit. Three methods were used to evaluate g_{SO_3} in simulated HLW glasses: 1) melter tests with progressively higher concentrations of SO_3 in the melter feed, 2) SO_3 solubility measurements made by bubbling crucible melts with mixtures of SO_2 and O_2 gases, and 3) Na_2SO_4 saturation in crucible melts. The data available for these three measurement methods are summarized in Table 2.3. These data and the data discussed in this section are based on the amount of SO_3 in the melter feed rather than the fraction retained in glass. The use of wt% is on a calcined melter feed basis (e.g., after removal of volatiles such as H_2O, NO_2^-, NO_3^-, CO_3^{2-}, etc., but no removal of semivolatiles such as Cs^+ or SO_4^{2-}).

Table 2.3. HLW SO_3 Solubility, Saturation, and Melter Test Data, wt%

Glass ID	w_{SO_3}, Saturation	w_{SO_3}, Bubbling	w_{SO_3}, Melter, Max w/o Salt	w_{SO_3}, Melter, Min w/ Salt
HLW98-77	0.38	0.58	NM	NM
HLW98-86	NM[(a)]	0.73	0.44	0.5
HLW98-96	NM	0.54	NM	NM
HLW02-15	NM	0.83	NM	NM
HLW02-22	0.63	0.6	NM	NM
HLW02-24	NM	0.58	NM	NM
HLW02-26	NM	0.61	NM	NM
HLW02-43	NM	0.82	NM	NM
HLW02-46	NM	0.53	0.7	0.9
HLW02-50	NM	0.59	NM	NM
HLW03-01	NM	1.12	NM	NM
HLW03-03	0.62	0.63	NM	NM
HLW04-07	NM	0.62	0.19	0.19
HLW06-16	0.52	0.84	NM	NM
HLW06-22	1.34	1.6	NM	NM
HLW06-24	NM	0.65	NM	NM
HLW06-27	NM	0.64	NM	NM
HLW06-29	NM	0.72	NM	NM
HLW06-32	NM	0.85	NM	NM
HLW-ALG-03	NM	0.87	NM	NM
HLWS-01	0.80	1.05	NM	NM
HLWS-02	0.70	0.86	NM	NM
HLWS-03	0.78	NM	NM	NM

Glass ID	w_{SO_3}, Saturation	w_{SO_3}, Bubbling	w_{SO_3}, Melter, Max w/o Salt	w_{SO_3}, Melter, Min w/ Salt
HLWS-04	1.29	1.31	NM	NM
HLWS-05	1.38	1.30	NM	NM
HLWS-06	1.19	NM	NM	NM
HLWS-07	1.10	NM	NM	NM
HLWS-08	1.29	1.29	NM	NM
HLWS-09	1.63	1.78	1.91	NM
HLWS-10	1.55	1.74	NM	NM
HLWS-11	1.09	1.58	NM	NM
HLWS-12	1.33	1.78	NM	NM
HLWS-13	0.85	1.25	NM	NM
HLWS-14	1.18	1.25	NM	NM
HLWS-15	1.14	NM	NM	NM
HLWS-16	1.33	NM	NM	NM
HLWS-17	0.79	NM	NM	NM
HLWS-18	0.74	NM	NM	NM
HLWS-19	0.64	NM	NM	NM
HLWS-20	1.26	NM	NM	NM
HLW-NGFe2	NM	0.83	0.50	0.60
HLW04-09	NM	0.65	NM	NM
HLW-E-Bi-6	NM	0.74	NM	NM
HLW-E-Al-27	NM	1.09	NM	NM
HLW-EANa-22	NM	0.87	NM	NM
HWI-Al-19	NM	1.25	1.30	1.40
HLW98-80	NM	0.66	NM	NM
HLW98-95	NM	0.66	NM	NM

(a) NM-not measured

With so little melter test data, the correlation between melter salt separation response and crucible-scale test data is used. There is significantly more crucible-scale testing. The six glasses with both melter test and bubbling solubility data show a distinct correlation as shown in Figure 2.6. For all but the highest sulfur glass, there are two data points that represent a single measured solubility by bubbling in the crucible and two concentrations used in melter tests, the circles being salt free in the melter test and the triangles for SO_3 concentrations that accumulated salt in the melter tests. It is the circular points that are later used as the "maximum SO_3 concentration in melter tests without salt accumulation."

Figure 2.7 compares the SO_3 concentrations measured using the bubbling solubility and Na_2SO_4 saturation methods. The different symbols represent data from different reports. The strong correlation between all three methods suggests either that the more abundant crucible-scale data can be used to model sulfur tolerance or that the data can reasonably be combined into a single data set for modeling. However, the Na_2SO_4 saturation data is consistently below the bubbling solubility data (by roughly 0.2 wt% SO_3); this data must be offset by that amount before combining with the other two data sets. The validity of this approach will be revisited as we model the data as a function of target glass composition in the coming subsections.

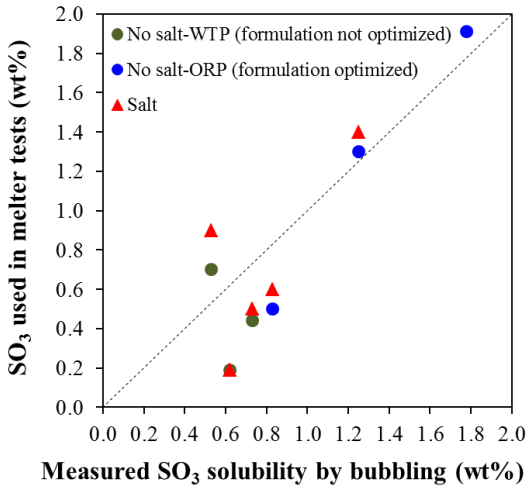

Figure 2.6. Comparison of Melter Test and Crucible-Scale Bubbling Solubility SO_3 Concentrations

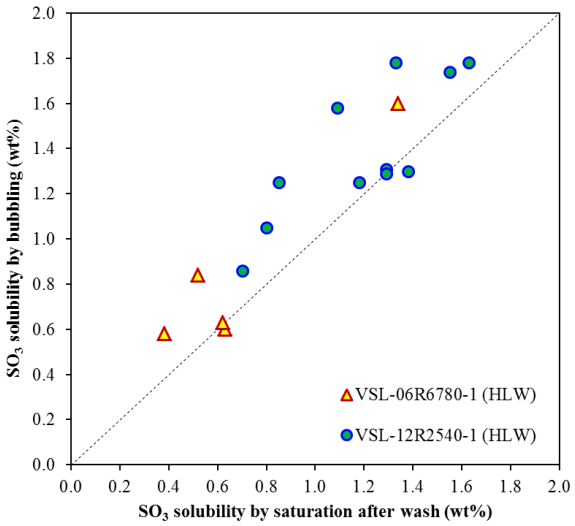

Figure 2.7. Comparison of SO_3 Concentrations by Bubbling Solubility and Na_2SO_4 Saturation Tests

The composition basis was adjusted to enable modeling. Because g_{SO_3} is both the dependent variable and part of the independent variables (mass fractions of oxides in glass), the composition was normalized after removing the concentration of SO_3:

$$n_i = \frac{g_i}{1 - g_{SO_3}} \tag{2.4}$$

where g_i is the i^{th} component mass fraction in glass and n_i is the i^{th} components normalized concentration, so that the concentrations of all components except SO_3 sum to 1.

Four approaches to modeling $w_{SO_3}^{Limit}$ were ultimately attempted using different model data sets:

1. In the first approach, the 48 crucible-scale bubbling solubility and Na_2SO_4 saturation data were combined using the following rules: if bubbling solubility data were available for a given glass, they were used (because these data most closely matched melter data) and if bubbling solubility data were not available, then the saturation data with the appropriate offset were used. The combined crucible-scale data were then fitted to composition, and are summarized in Section 2.2.1.

2. In the second approach, the maximum melter wt% SO_3 without salt accumulation ($w_{SO_3}^{Melt}$) was combined with the crucible-scale data using the rule that data were taken in order of priority for each glass: melter, bubbling solubility, then saturation plus offset. Because the melter data are the highest priority and only exist for 6 of the 48 compositions, the data were weighted to give melter data equal weight as crucible data. The combined melter and crucible-scale data were then fitted to composition, and are summarized in Section 2.2.2.

Although the HLW-only w_{SO_3} models fit the data used to fit them very well (with R^2 values of roughly 0.9), they did not validate well with R^2_{Press} and R^2_{Val} values in the 0.6 to 0.7 range. It was therefore concluded that with insufficient HLW w_{SO_3} data, an attempt would be made to fit the combined LAW and HLW w_{SO_3} data set.

3. In the third approach, the combined LAW and HLW crucible-scale (bubbling solubility and Na_2SO_4 saturation) data were combined using the following rules: if bubbling solubility data were available for a given glass, they were used (because these data most closely matched melter data) and if bubbling solubility data were not available, then the saturation data with the appropriate offset were used. The combined LAW and HLW crucible-scale data were then fitted to composition, and are summarized in Section 2.2.3.
4. In the fourth approach, the combined LAW and HLW melter- and crucible-scale data were modeled as a function of composition. Here, as in the second approach, the melter data were weighted equally with the crucible data. Likewise, the saturation data were offset by the average difference between melter and saturation wt% SO_3 (w_{SO_3}). The combined LAW and HLW melter- and crucible-scale data were then fitted to composition, and are summarized in Section 2.2.4.

The four modeling approaches are contrasted in Section 2.2.5. The results lead to a recommended final g_{SO_3} to be used in glass formulation and waste loading estimation.

2.2.1 Crucible-Scale HLW w_{SO_3} Model

There are 48 glass compositions in the HLW w_{SO_3} database. The composition region covered by these glasses is summarized in Table 2.4 and shown in a scatterplot matrix in Figure 2.8.

Table 2.4. Component Concentration Ranges for HLW w_{SO_3} Database, n_i, in Mass Fraction

Comp, *i*	Min	Max
Al_2O_3	0.019	0.239
B_2O_3	0.043	0.203
CaO	0.000	0.086
Cl	0.000	0.002
Cr_2O_3	0.000	0.008
F	0.000	0.008
Fe_2O_3	0.014	0.171
K_2O	0.000	0.016
Li_2O	0.000	0.061
MgO	0.000	0.012
MnO	0.000	0.080
Na_2O	0.037	0.200
P_2O_5	0.000	0.051
SiO_2	0.270	0.531
SrO	0.000	0.103
TiO_2	0.000	0.010
V_2O_5	0.000	0.041
ZnO	0.000	0.040
ZrO_2	0.000	0.115
Bi_2O_3	0.000	0.067
CdO	0.000	0.017
La_2O_3	0.000	0.012
NiO	0.000	0.017
ThO_2	0.000	0.060
UO_3	0.000	0.065

Figure 2.8. Scatterplot Matrix of Component Concentrations in the HLW w_{SO_3} Database (n_i in mass fraction)

The 48-glass data set is made up of 38 $w_{SO_3}^{Bubb}$ and 9 $w_{SO_3}^{Sat}$. Because there is only one data point with both $w_{SO_3}^{Melt}$ (1.91 wt%) and $w_{SO_3}^{Sat}$ (1.63 wt%), the $w_{SO_3}^{Sat}$ offset was estimated by the difference between both $w_{SO_3}^{Melt} - w_{SO_3}^{Sat}$ and $w_{SO_3}^{Bubb} - w_{SO_3}^{Sat}$, as shown graphically in Figure 2.9. The average offset is 0.185 (wt% SO_3).

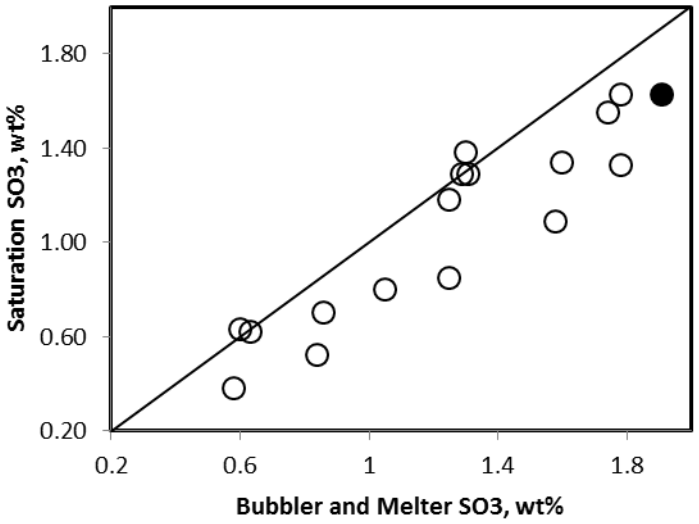

Figure 2.9. Comparison of $w_{SO_3}^{Sat}$ with $w_{SO_3}^{Bubb}$ (open points) and $w_{SO_3}^{Melt}$ (solid point)

Once properly adjusted, the 48 data were fitted to the composition according to:

$$w_{SO_3}^{Limit} = \sum_{i=1}^{p} s_i n_i \tag{2.5}$$

where $w_{SO_3}^{Limit}$ is the sulfur tolerance limit (in wt%), s_i is the i^{th} component coefficient, and n_i is the i^{th} component normalized (after removing SO_3) mass fraction. The results are shown in Figure 2.10 and summarized in Table 2.5.

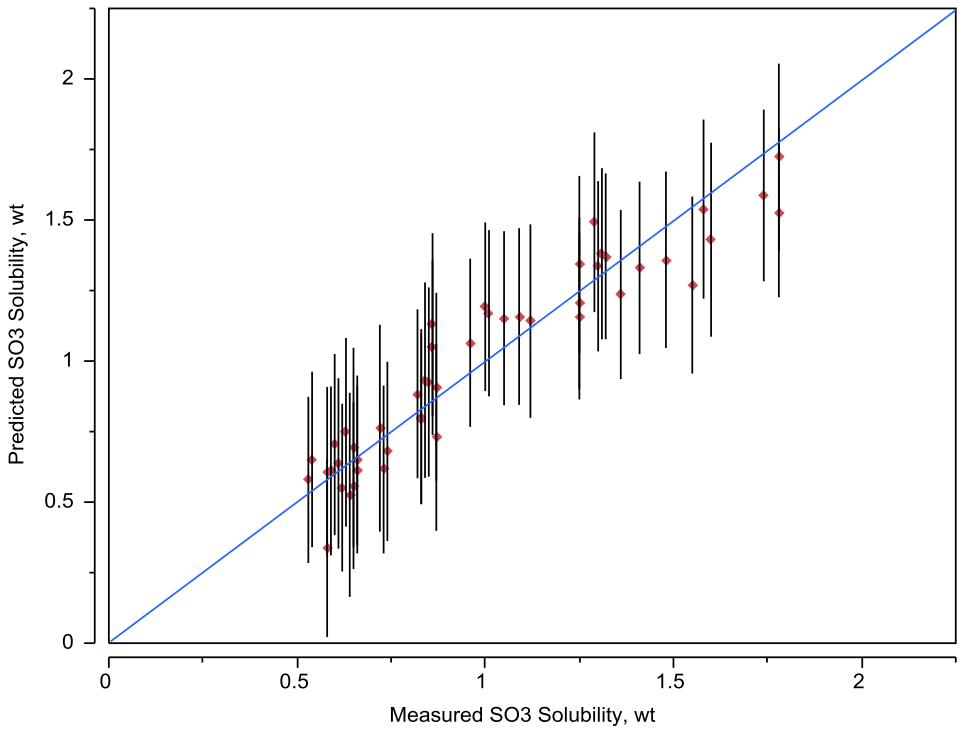

Figure 2.10. Comparison of Predicted and Measured Crucible-Scale w_{SO_3} with 95% Confidence Interval for Individual Prediction, wt%

Table 2.5. Summary of Crucible-Scale HLW $w_{SO_3}^{Limit}$ Model

Components, $_i$	Coefficients, s_i	Summary Statistics	Value
Al_2O_3	-1.8897	R^2	0.8928
B_2O_3	4.74159	R^2_{Adj}	0.8600
CaO	9.152743	R^2_{Press}	0.7851
Cr_2O_3	-27.3782	RMSE	0.139
Fe_2O_3	0.071244	$\text{RMSE}_{\text{Press}}$	0.172
Li_2O	13.65928	-	-
Na_2O	3.528745	-	-
SiO_2	-1.51497	-	-
V_2O_5	6.752861	-	-
ZnO	-3.37833	-	-
ZrO_2	-1.23971	-	-
Others	2.623079	-	-

To validate the model, data not used in model fitting must be obtained. Because all appropriate data within the desired composition region were used in model fitting, subsets of the model data were used to validate the model. The data were sorted by w_{SO_3} value. The data were then numbered 1, 2, 3, 4, 5, 1,

2, … to split them into five representative groups of roughly 20% of the data. The same model form (including the same set of terms) was then refit to subsets 2 to 5 and used to predict data in subset 1. Then the model was fit to each group of four subsets and used to predict the remaining subset in sequence. Table 2.6 summarizes the results of the model validation. The model-fit R^2 values are all close to each other at approximately 0.9. The R^2_{Val} values, however, vary significantly, from 0.72 to 0.95. The R^2_{Press}value of 0.79 is also significantly lower than the model-fit R^2 of 0.89. In addition, 6 of the 12 model coefficients varied by more than a 25% relative standard deviation (RSD) for the validation set, with the largest difference being 788% RSD for Fe_2O_3. This model validation suggests that insufficient data are available to clearly model the composition effects.

Table 2.6. Summary of Crucible-Scale HLW SO_3 Solubility Model Validation

Fit Statistics	Full Model	Grp 1	Grp 2	Grp 3	Grp 4	Grp 5	Average
R^2	0.8928	0.8988	0.8733	0.9157	0.9219	0.9031	0.9025
R^2_{Adj}	0.8600	0.8559	0.8196	0.8800	0.8901	0.8636	0.8619
R^2_{Press}	0.7851	0.7236	0.6405	0.7952	0.8133	0.7958	0.7537
RMSE	0.139	0.140	0.155	0.126	0.126	0.140	0.1375
$\text{RMSE}_{\text{Press}}$	0.172	0.194	0.219	0.165	0.164	0.172	0.1827
Validation							
R^2_{Val}	-	0.7213	0.9498	0.7834	0.9399	0.9550	0.8699

2.2.2 Weighted Crucible- and Melter-Scale w_{SO_3} HLW Model

To focus more on the melter response to SO_3 tolerance, the data set was developed by using the maximum SO_3 in the melter test without salt formation where available (six data points). If no melter data were available, bubbler data were used (33 data points), and if no bubbler data were available, saturation plus offset data were used (nine data points). Equal weighting was given to melter data and crucible data using a weighting factor. The weighting for $w^{Melt}_{SO_3}$ was 48/6/2=4, while the weighting for both $w^{Bubb}_{SO_3}$ and $w^{Sat}_{SO_3}$ was 48/42/2=0.571.

Once properly adjusted, the 48 data were fitted to composition according to Equation 2.5. The results are shown in Figure 2.11 and summarized in Table 2.7.

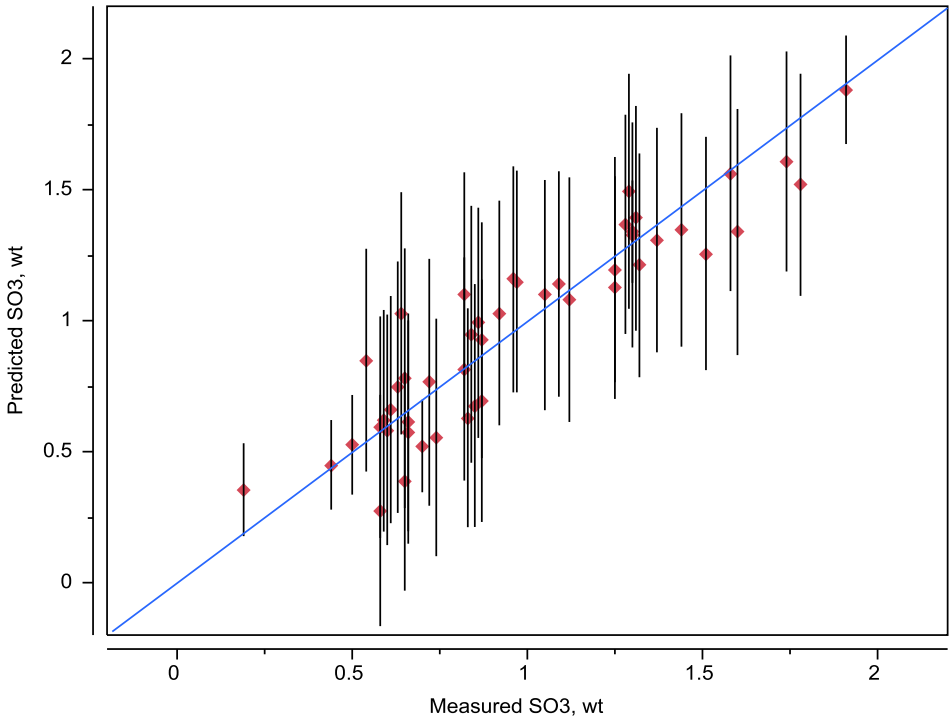

Figure 2.11. Comparison of Predicted and Measured Crucible- and Melter-Scale w_{SO_3} with 95% Confidence Interval for Individual Prediction, wt%

Table 2.7. Summary of Crucible- and Melter-Scale HLW SO_3 Model

Components, i	Coefficients, s_i	Summary Statistics	Value
Al_2O_3	–1.8897	R^2	0.8928
B_2O_3	4.74159	R^2_{Adj}	0.8600
CaO	9.152743	R^2_{Press}	0.7851
Cr_2O_3	–27.3782	RMSE	0.139
Fe_2O_3	0.071244	$\text{RMSE}_{\text{Press}}$	0.172
Li_2O	13.65928	-	-
Na_2O	3.528745	-	-
SiO_2	–1.51497	-	-
V_2O_5	6.752861	-	-
ZnO	–3.37833	-	-
ZrO_2	–1.23971	-	-
Others	2.623079	-	-

To validate the model, data not used in model fitting must be obtained. Because all appropriate data within the desired composition region were used in model fitting, subsets of the model data were used to validate the model. The data were sorted by w_{SO_3} value. The data were then numbered 1, 2, 3, 4, 5, 1, 2, … to split them into five representative groups of roughly 20% of the data. The same model form

(including the same set of terms) was then refit to subsets 2 to 5 and used to predict data in subset 1. Then the model was fit to each group of four subsets and used to predict the remaining subset in sequence. Table 2.8 summarizes the results of the model validation. The model-fit R^2 values are all close to each other at approximately 0.9. The R^2_{Val} values, however, vary significantly, from 0.50 to 0.80. The R^2_{Press}value of 0.79 is also significantly lower than the model-fit R^2 of 0.89. In addition, 6 of the 12 model coefficients varied by more than 25% RSD for the validation set, with the largest difference being 788% RSD for Fe_2O_3. This model validation suggests that insufficient data are available to clearly model the composition effects.

Table 2.8. Summary of Crucible- and Melter-Scale HLW SO_3 Model Validation

Fit Statistics	Full Model	Grp 1	Grp 2	Grp 3	Grp 4	Grp 5	Average
R^2	0.8928	0.8988	0.8733	0.9157	0.9219	0.9031	0.9025
R^2_{Adj}	0.8600	0.8559	0.8196	0.8800	0.8901	0.8636	0.8619
R^2_{Press}	0.7851	0.7236	0.6405	0.7952	0.8133	0.7958	0.7537
RMSE	0.139	0.140	0.155	0.126	0.126	0.140	0.1375
$\text{RMSE}_{\text{Press}}$	0.172	0.194	0.219	0.165	0.164	0.172	0.1827
Validation							
R^2_{Val}	-	0.7343	0.7843	0.7823	0.7950	0.5031	0.7198

2.2.3 Crucible-Scale LAW and HLW w_{SO_3} Model

The difficulties with the HLW SO_3 model validation suggest that LAW and HLW w_{SO_3} should be combined and modeled. To accomplish this, we first compiled all the LAW and HLW w_{SO_3} data. A total of 312 data points were available. The composition region covered by these glasses is summarized in Table 2.9 and shown in a scatterplot matrix in Figure 2.12.

Table 2.9. Component Concentration Ranges for the Combined HLW and LAW w_{SO_3} Database (n_i, in mass fraction)

Comp, *i*	Min	Max	Comp, *i*	Min	Max
Al_2O_3	0.0188	0.2387	SiO_2	0.2703	0.5310
B_2O_3	0.0398	0.2030	SrO	0	0.1032
CaO	0	0.1294	SnO_2	0	0.0501
Cl	0	0.0117	TiO_2	0	0.0411
Cr_2O_3	0	0.0100	V_2O_5	0	0.0439
F	0	0.0306	ZnO	0	0.0586
Fe_2O_3	0	0.1707	ZrO_2	0	0.1150
K_2O	0	0.0834	BaO	0	0.0790
Li_2O	0	0.0607	Bi_2O_3	0	0.0670
MgO	0	0.1010	CdO	0	0.0165
MnO	0	0.0800	ThO_2	0	0.0596
Na_2O	0.0248	0.2605	UO_3	0	0.0652
P_2O_5	0	0.0508	-	-	-

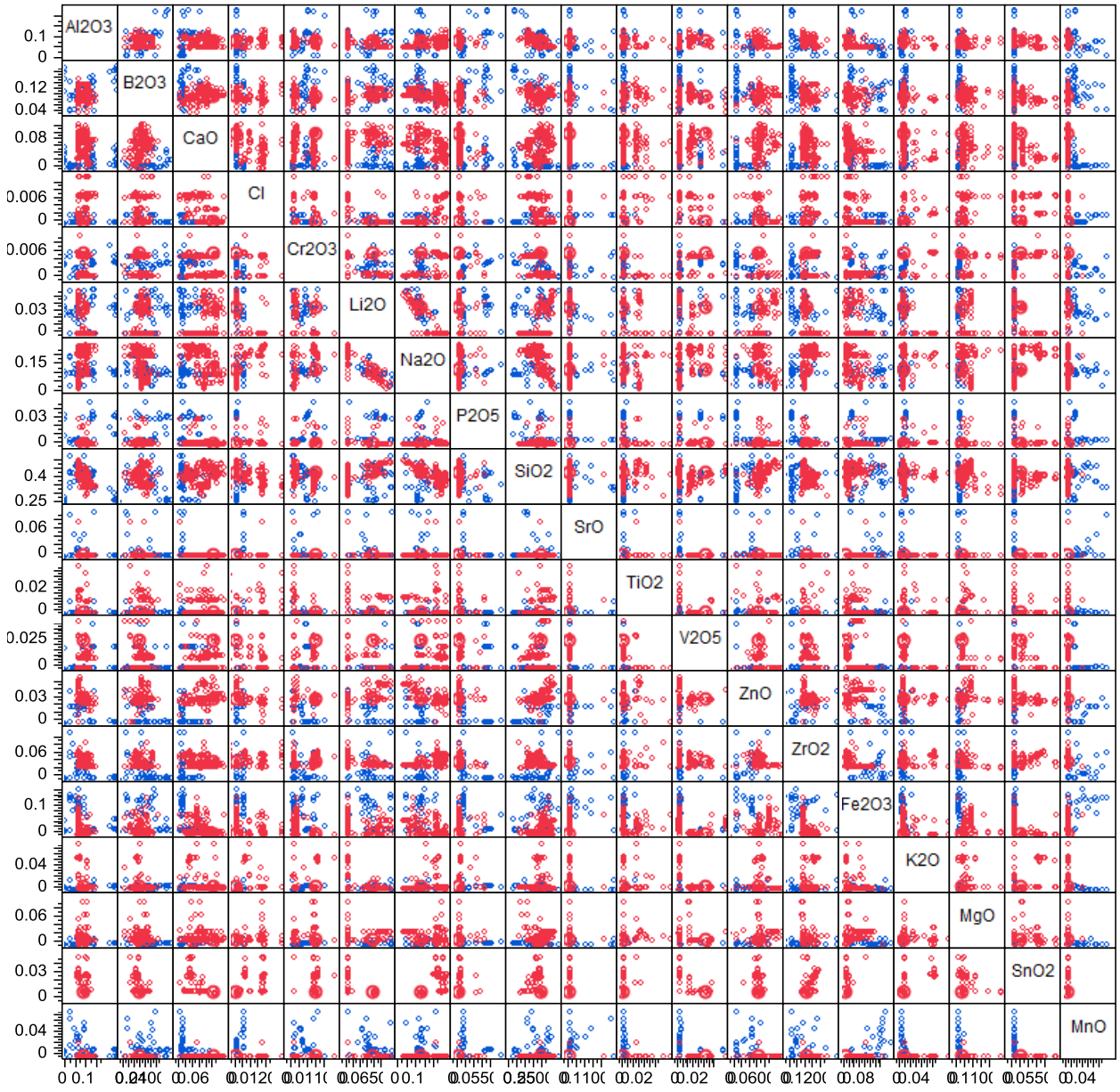

Figure 2.12. Scatterplot Matrix of Component Concentrations in the Combined HLW (blue) and LAW (red) SO_3 Database (n_i in mass fraction)

The few melter-scale data are compared to crucible-scale data in Figure 2.13. It is clear from this plot that, similar to the HLW SO_3 data, the combined data show an excellent correlation between $w_{SO_3}^{Melt}$ and $w_{SO_3}^{Bubb}$ as well as a good correlation with an offset between $w_{SO_3}^{Melt}$ and $w_{SO_3}^{Sat}$. The average offset $w_{SO_3}^{Melt}$ - $w_{SO_3}^{Sat}$ = 0.216 wt%. The final model data set used $w_{SO_3}^{Bubb}$ for any glass with bubbler data available (77 data points) and $w_{SO_3}^{Sat}$ + offset for all other glasses (235 data points).

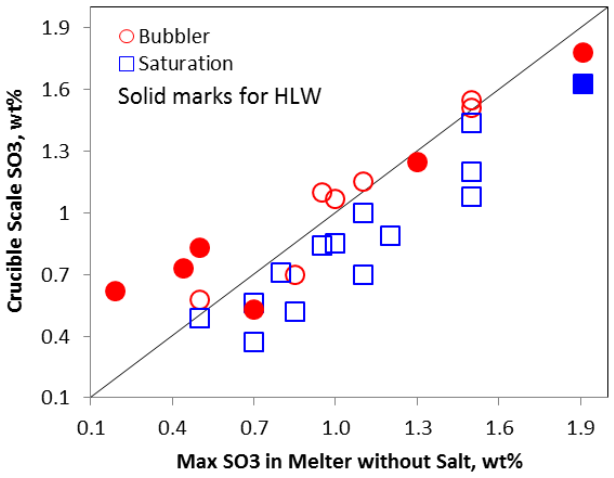

Figure 2.13. Comparison of $w_{SO_3}^{Melt}$ to $w_{SO_3}^{Bubb}$ (red circles) and $w_{SO_3}^{Sat}$ (blue squares) for the Combined HLW (solid) and LAW (open)

Once properly adjusted, the 312 data were fitted to composition according to:

$$w_{SO_3}^{Limit} = \sum_{i=1}^{p} s_i n_i + selected \left\{ \sum_{i=1}^{p-1} \sum_{j=i}^{p} s_{ij} n_i n_j \right\} \tag{2.6}$$

where $w_{SO_3}^{Limit}$ = the sulfur tolerance limit (in wt%),

s_i = the i^{th} component coefficients,

n_i = the i^{th} component normalized (after removing SO_3) mass fraction, and

s_{ij} = the i^{th} time j^{th} component coefficient.

The results are shown in Figure 2.14 and summarized in Table 2.10.

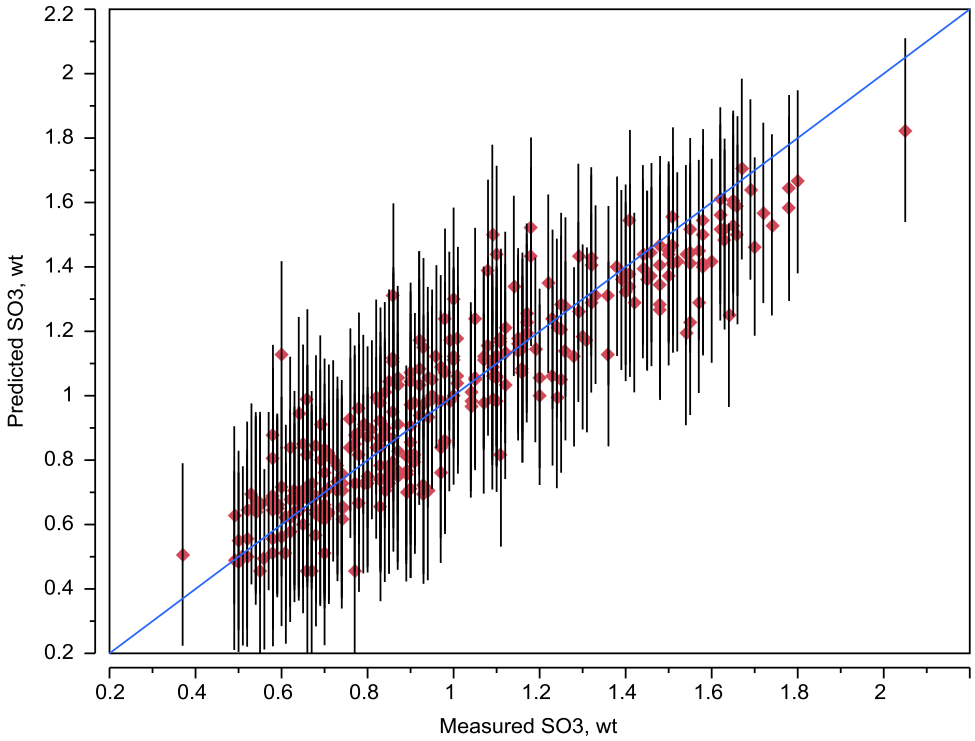

Figure 2.14. Comparison of Predicted and Measured Crucible-Scale HLW and LAW SO_3 Solubility with 95% Confidence Interval for Individual Prediction, wt%

Table 2.10. Summary of Crucible-Scale HLW and LAW SO_3 Model

Components, $_i$	Coefficients, s_i	Summary Statistics	Value
Al_2O_3	-0.803866	R^2	0.8419
B_2O_3	3.0983142	R^2_{Adj}	0.8339
CaO	5.6570336	R^2_{Press}	0.8176
Cl	-29.77093	RMSE	0.139
Cr_2O_3	-7.5784	$RMSE_{Press}$	0.146
Li_2O	3.2746409	R^2 (HLW-only)	0.7619
Na_2O	2.7845163	-	-
P_2O_5	4.4652267	-	-
SiO_2	-0.542488	-	-
SrO	2.6347706	-	-
TiO_2	6.3907736	-	-
V_2O_5	6.2747968	-	-
ZnO	4.2286005	-	-
ZrO_2	-1.291709	-	-
Other	0.1221757	-	-
$Li_2O \times Li_2O$	179.71011	-	-

To validate the model, data not used in model fitting must be obtained. Because all appropriate data within the desired composition region were used in model fitting, subsets of the model data were used to validate the model. The data were sorted by w_{SO_3} value. The data were then numbered 1, 2, 3, 4, 5, 1, 2, … to split them into five representative groups of roughly 20% of the data. The same model form (including the same set of terms) was then refit to subsets 2 to 5 and used to predict data in subset 1. Then the model was fit to each group of four subsets and used to predict the remaining subset in sequence. Table 2.11 summarizes the results of the model validation. The model-fit R^2 values are all close to each other at approximately 0.84. The R^2_{Val} values range from 0.80 to 0.85, which is a significantly lower variation than the HLW-only models. The R^2_{Press}value of 0.82 is also significantly closer to the fit R^2 value of 0.84, and almost identical to the average R^2_{Val} value of 0.82. The coefficients for individual fits also varied less broadly than the HLW-only models. This model is well validated and should give predictions of unknown data within the model-validity region nearly as well as for the model-fit data.

Table 2.11. Summary of Crucible-Scale HLW and LAW SO_3 Model Validation

Fit Statistics	Full Model	Grp 1	Grp 2	Grp 3	Grp 4	Grp 5	Average
R^2	0.8419	0.8481	0.8361	0.8482	0.8431	0.8470	0.8445
R^2_{Adj}	0.8339	0.8383	0.8256	0.8385	0.8331	0.8372	0.8345
R^2_{Press}	0.8176	0.8169	0.8063	0.8157	0.8111	0.8185	0.8137
RMSE	0.139	0.137	0.141	0.138	0.140	0.138	0.1390
$\mathrm{RMSE}_{\mathrm{Press}}$	0.146	0.146	0.149	0.148	0.149	0.146	0.1475
Validation							
R^2_{Val}	-	0.7994	0.8530	0.7980	0.8201	0.8093	0.8160

Applying this model to the HLW data yielded an R^2 value of only 0.76. Although this is lower than the model-fit R^2 value for the HLW-only models in Sections 2.2.1and 2.2.2, it is still on the same order or higher than the HLW-only R^2_{Val} and R^2_{Press} values.

2.2.4 Weighted Crucible- and Melter-Scale LAW and HLW w_{SO_3} Model

To focus more on the melter response to SO_3 tolerance, the data set was developed by using the maximum SO_3 in the melter test without salt formation where available (19 data points). If no melter data were available, bubbler data were used (64 data points), and if no bubbler data were available, saturation plus offset data was used (229 data points). Equal weighting was given to melter data and crucible data using a weighting factor. The weight for $w^{Melt}_{SO_3}$ was 312/19/2=8.21, while the weighting for both $w^{Bubb}_{SO_3}$ and $w^{Sat}_{SO_3}$ was 312/293/2=0.532.

Once properly adjusted, the 312 data points were fitted to composition according to Equation 2.5. Note that second order compositional terms were investigated using Equation 2.6 without yielding a sufficient advantage to be used. The model results are shown in Figure 2.15 and summarized in Table 2.12.

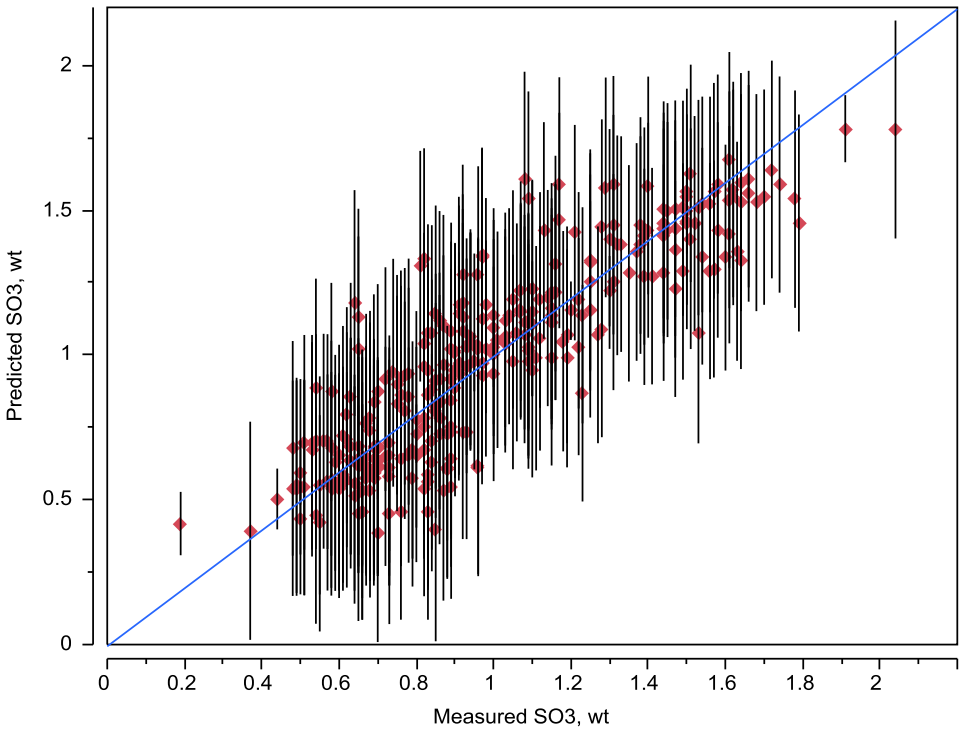

Figure 2.15. Comparison of the Predicted and Measured Crucible- and Melter-Scale HLW and LAW SO_3 with 95% Confidence Interval for Individual Prediction, wt%

Table 2.12. Summary of the Crucible- and Melter-Scale HLW and LAW SO_3 Model

Components, $_i$	Coefficients, s_i	Summary Statistics	Value
Al_2O_3	0.104254	R^2	0.8832
CaO	6.689832	R^2_{Adj}	0.8785
Cl	-21.1286	R^2_{Press}	0.8038
Cr_2O_3	-14.135	RMSE	0.135
Fe_2O_3	-1.40865	$RMSE_{Press}$	0.172
K_2O	-1.05279	R^2 (HLW-only)	0.6917
Li_2O	9.38707	-	-
Na_2O	1.543692	-	-
P_2O_5	8.120125	-	-
SiO_2	-0.55299	-	-
TiO_2	9.818723	-	-
V_2O_5	7.464254	-	-
Others	2.464308	-	-

To validate the model, data not used in model fitting must be obtained. Because all appropriate data within the desired composition region were used in model fitting, subsets of the model data were used to validate the model. The data were sorted by w_{SO_3} value. The data were then numbered 1, 2, 3, 4, 5, 1,

2, … to split them into five representative groups of roughly 20% of the data. The same model form (including the same set of terms) was then refit to subsets 2 to 5 and used to predict data in subset 1. Then the model was fit to each group of four subsets and used to predict the remaining subset in sequence. Table 2.13 summarizes the results of the model validation. The model-fit R^2 values are all close to each other at approximately 0.88. The R^2_{Val} values range from 0.61 to 0.84, which is broader than the combined HLW and LAW crucible-scale-only model, but narrower than the HLW-only models. The R^2_{Press}value of 0.80 is also significantly lower than the fit R^2 value of 0.88 and significantly above the average R^2_{Val} value of 0.74. The coefficients for individual fits also varied significantly, with %RSD values as high as 512. This model validation suggests that composition effects are not well captured by the model.

Table 2.13. Summary of Crucible- and Melter-Scale HLW and LAW SO_3 Model Validation

Fit Statistics	Full Model	Grp 1	Grp 2	Grp 3	Grp 4	Grp 5	Average
R^2	0.8832	0.8957	0.8855	0.8745	0.8966	0.8869	0.8878
R^2_{Adj}	0.8785	0.8885	0.8797	0.8681	0.8914	0.8811	0.8818
R^2_{Press}	0.8038	0.7944	0.7987	0.7828	0.8188	0.8026	0.7995
RMSE	0.135	0.118	0.140	0.141	0.130	0.136	0.1331
$\text{RMSE}_{\text{Press}}$	0.172	0.160	0.181	0.181	0.169	0.176	0.1732
Validation							
R^2_{Val}	-	0.7016	0.8391	0.8171	0.6149	0.7131	0.7372

Applying this model to only the HLW data yielded an R^2 value of 0.69, which is lower than all other modeling approaches attempted.

2.2.5 Recommended w_{SO_3} Model

Four different modeling approaches were attempted to describe the impact of composition on the sulfur tolerance of either HLW glass melts or combined LAW and HLW glass melts. Those models for HLW-only data described the model data well, but they were poorly validated. Likewise, the model used to fit the weighted melter-scale and crucible-scale combined LAW and HLW data did not validate well.

The crucible-scale-only, combined HLW and LAW model performed the best in validation. Applying this model to the melter-scale SO_3 values shows a very good correlation (Figure 2.16). The R^2_{Val} value calculated for melter-scale data predicted by the crucible-scale model is 0.841 for all melter data and 0.769 for HLW data only. The point at a maximum melter SO_3 of 0.19 wt% and the predicted w_{SO_3} of 0.68 (HLW04-07) was found to be an outlier. This data point was identified as an outlier when the initial melter test (DM-100) showed the unexpected formation of salt. After reviewing the data, it was decided to proceed with a DM-1200 melter test with the same composition, which, as expected, did not show any signs of salt. Removing this data point from the validation data set would increase the R^2_{Val} value calculated for melter-scale data predicted by the crucible-scale model to 0.852 for HLW data and 0.908 for LAW and HLW data.

It is therefore recommended that the model described in Section 2.2.3 with coefficients listed in Table 2.10 be used to predict sulfur limits for HLW glasses. As discussed in the LAW sulfur tolerance section of this report (Section 3.2), this combined HLW and LAW, crucible-scale, w_{SO_3} model is also compared favorably to the LAW-only model. It should also be pointed out that at the predicted value of 0.7 wt% SO_3, the data is highly scattered. Additional data needs to be collected in the 0.5 to 1 wt% region to improve the predictions in this critical point of SO_3 concentration.

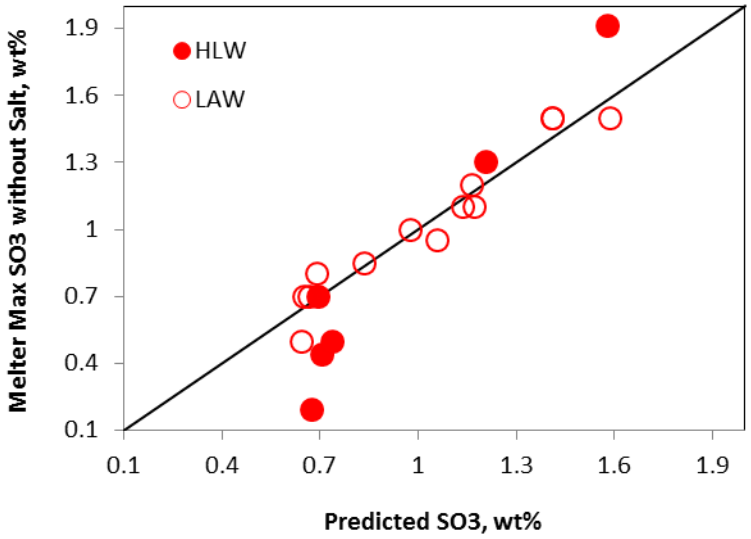

Figure 2.16. Comparison of Crucible-Scale Combined HLW and LAW SO_3 Model Predictions with Measured Melter-Scale SO_3, in wt%

2.3 Nepheline Limit

If nepheline (ideally $NaAlSiO_4$) precipitates from HLW glass during canister cooling, it will likely reduce the chemical durability of the glass by removing Al and Si from the residual glass at a 1:1:1 ratio with Na (Kim et al. 1995). It will also make it difficult to predict the PCT response of the glass. Because PCT response must be controlled and reported to meet current disposal criteria (DOE 1996), nepheline precipitation must either be avoided, or the amount of nepheline formed and its impact on PCT must be predicted. Because canistered waste glass will be subjected to a broad range of thermal histories, a simulated canister centerline cooling (CCC) is used as a bounding thermal history to determine the risk of nepheline formation. A nepheline discriminator (ND) was developed and shown to successfully reduce the risk of nepheline precipitation in CCC heat treated waste glasses (Li et al. 1997). The ND is based on limiting the normalized SiO_2 concentration (*NSi*) as follows:

$$NSi = \frac{g_{SiO_2}}{g_{SiO_2} + g_{Al_2O_3} + g_{Na_2O}} \tag{2.7}$$

to >0.62 in the glass as shown in Figure 2.17. The ND constraint is overly conservative, however. As can be seen in the plot, several glasses with *NSi* <0.62 do not form nepheline on slow cooling, some as low as *NSi* = 0.47. The lower *NSi* glasses are those with the highest waste loadings, and therefore a less

conservative method of limiting nepheline precipitation is needed to both maintain acceptable glasses and allow higher waste loading.

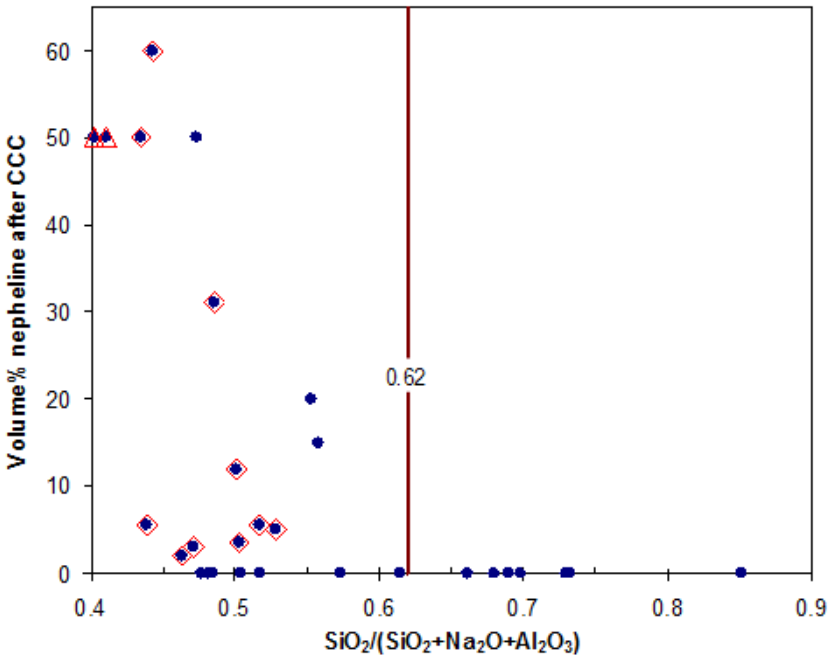

Figure 2.17. Comparison of *NSi* to Nepheline Volume Percent from WTP HLW Glasses Subjected to CCC Heat Treatment (Vienna and Kim 2008). ● – quantitative value, ◊-- less than value, Δ -- greater than value

McCloy et al. proposed a revised constraint whereby glasses with *NSi* < 0.62 would be allowed as long as the optical basicity (OB) of the melt was greater than 0.55 (McCloy et al. 2010; McCloy and Vienna 2010; Rodriguez et al. 2011). This approach did reduce some of the conservatism, but still limited the potential loading of high alumina wastes in glass. A new approach to limiting the nepheline precipitation on CCC is clearly needed to optimize waste loading in glass.

The proposed nepheline prediction model uses a neural network (NN) to model the complex non-linear interactions between the components. The final model comprised a network with a single layer and three nodes, all using the hyperbolic tangent (TanH) activation function. These nodes are classified as the hidden layers of the model. A series of modeling experiments explored the effects of many different glass descriptors, including OB, normalized concentrations of SiO_2 (*NSi*), Na_2O, and Al_2O_3, and the unnormalized mass fractions (g_i) of Al_2O_3, B_2O_3, CaO, Fe_2O_3, K_2O, Li_2O, MgO, Na_2O, and SiO_2. It was determined that the normalized component concentrations and OB were not as effective in predicting nepheline formation as the unnormalized oxide concentrations.

An original set of 20 models was generated using different combinations of predictors (g_i). From this study, two sets were determined to be the most promising: 1) Al_2O_3, B_2O_3, CaO, Li_2O, Na_2O, and SiO_2, and 2) Al_2O_3, B_2O_3, CaO, Fe_2O_3, K_2O, Li_2O, MgO, Na_2O, and SiO_2. It was ultimately determined that model set 1 offered the greatest predictive ability with the lowest complexity and lowest chance of overfitting.

A data set of 629 glasses was used to train and validate the model as summarized in Table 2.14. Ideally, a data set with a single heat treatment method (WTP CCC) is preferred as other heat treatments (e.g., DWPF CCC and 950°C isothermal) may show different nepheline formation results. However, it was determined that there is insufficient data (149 of 629 glasses) to develop the NN model if restricted to only WTP CCC heat treatment data. As this is a preliminary model, it was decided to include all three heat treatments to develop the model and collect additional data with the single WTP CCC heat treatment for final model fitting in the future. The compositional ranges for these glasses are described in Table 2.15 and are shown graphically in Figure 2.18. In an effort to create the most predictive model possible, K-fold cross validation was used. This method splits the data set into k subsets. Each of these subsets contains 1/(1-*k*) of the data for modeling as well as a unique 1/*k* of the data for validation. Each of these subsets is modeled and the best model based on validation performance is presented. With K-fold validation, it is possible to evaluate the predictive properties of the model by retaining a portion of the data during the modeling of each subset. This allows maximum use of the data while maintaining a validation set. Studies were performed on the data varying k from 5 to 628.

Table 2.14. Summary of Data Used in Nepheline Model Development and Validation

Glass Family[(a)]	#	Lab	Heat Treatment[(b)]	Ref for Glass Compositions	Ref for Crystal Measurement
EM	30	SRNL	DWPF CCC	(Johnson and Edwards 2009)	unpublished
SRNL-JB	18	SRNL	DWPF CCC	unpublished	unpublished
SRNL-JB02	20	SRNL	DWPF CCC	unpublished	unpublished
HWI-ALS	13	VSL	DWPF CCC	(Matlack et al. 2010b)	(Matlack et al. 2010b)
HWI-Al	8	VSL	WTP CCC	(Matlack et al. 2010a)	(Matlack et al. 2010a)
IWL-SLC	7	PNNL	WTP CCC	(Kim et al. 2011)	(Kim et al. 2011)
IWL-HAC	10	PNNL	WTP CCC	(Kim et al. 2011)	(Kim et al. 2011)
NE3	29	SRNL	DWPF CCC	(Fox and Edwards 2009)	(Rodriguez et al. 2011)
NP2	25	SRNL	DWPF CCC	(Fox and Edwards 2008)	(Rodriguez et al. 2011)
HWI-Al	15	VSL	WTP CCC	(Matlack et al. 2008)	(Rodriguez et al. 2011)
HLW-E-Al	14	VSL	WTP CCC	(Matlack et al. 2007a)	(Rodriguez et al. 2011)
PNNL-Al-24-X	13	PNNL	WTP CCC	(Rodriguez et al. 2011)	(Rodriguez et al. 2011)
HLW-E-ANa	13	VSL/PNNL	WTP CCC	(Matlack et al. 2007a)	(Rodriguez et al. 2011)
HLW-E-ANa-X	24	PNNL	WTP CCC	(Rodriguez et al. 2011)	(Rodriguez et al. 2011)
A	6	PNNL	WTP CCC	(Hrma et al. 2010)	(Rodriguez et al. 2011)
HAL	19	PNNL/SRNL	WTP CCC	(Kim et al. 2008)	(Rodriguez et al. 2011)
NP	20	PNNL	WTP CCC	(Li et al. 1997)	(Li et al. 1997)
NEPH	12	SRNL	DWPF CCC	(Peeler et al. 2005)	(Rodriguez et al. 2011)
NEPH2	27	SRNL	DWPF CCC	(Peeler et al. 2006)	(Rodriguez et al. 2011)
NEPH3	16	SRNL	DWPF CCC	(Fox et al. 2006)	(Rodriguez et al. 2011)
DZr	24	PNNL/SRNL	INEEL CCC	(Crum et al. 2002)	(Riley et al. 2001)
US	44	PNNL/SRNL	DWPF CCC	(Fox et al. 2008)	(Fox et al. 2008)
CVS1, CVS2	121	PNNL	HWVP CCC	(Hrma et al. 1994)	(Hrma et al. 1994)
CVS3	39	PNNL	HTM CCC	(Vienna et al. 1996b)	(Vienna et al. 1996b)
EM09-	22	PNNL	950°C, 24h	(McCloy et al. 2010)	(McCloy et al. 2010)
SB5NEPH	40	SRNL	950°C, 24h	(Fox et al. 2007)	(Rodriguez et al. 2011)

(a) See original citations for glass family nomenclature.
(b) INEEL = Idaho National Engineering and Environmental Laboratory, HTM = high temperature melter.

Table 2.15. Component Concentration Ranges for Nepheline Model Data, wt%

Component	Min	Max
Al_2O_3	0	39.00
B_2O_3	0	28.65
Bi_2O_3	0	16.37
CaO	0	18.20
Cr_2O_3	0	2.97
Fe_2O_3	0	19.95
F	0	6.50
K_2O	0	24.07
Li_2O	0	9.14
MnO	0	5.59
Na_2O	2.00	39.00
NiO	0	2.91
P_2O_5	0	9.00
SiO_2	17.44	60.00
SO_3	0	1.50
SrO	0	3.00
TiO_2	0	2.12
ZnO	0	2.00
ZrO_2	0	16.00

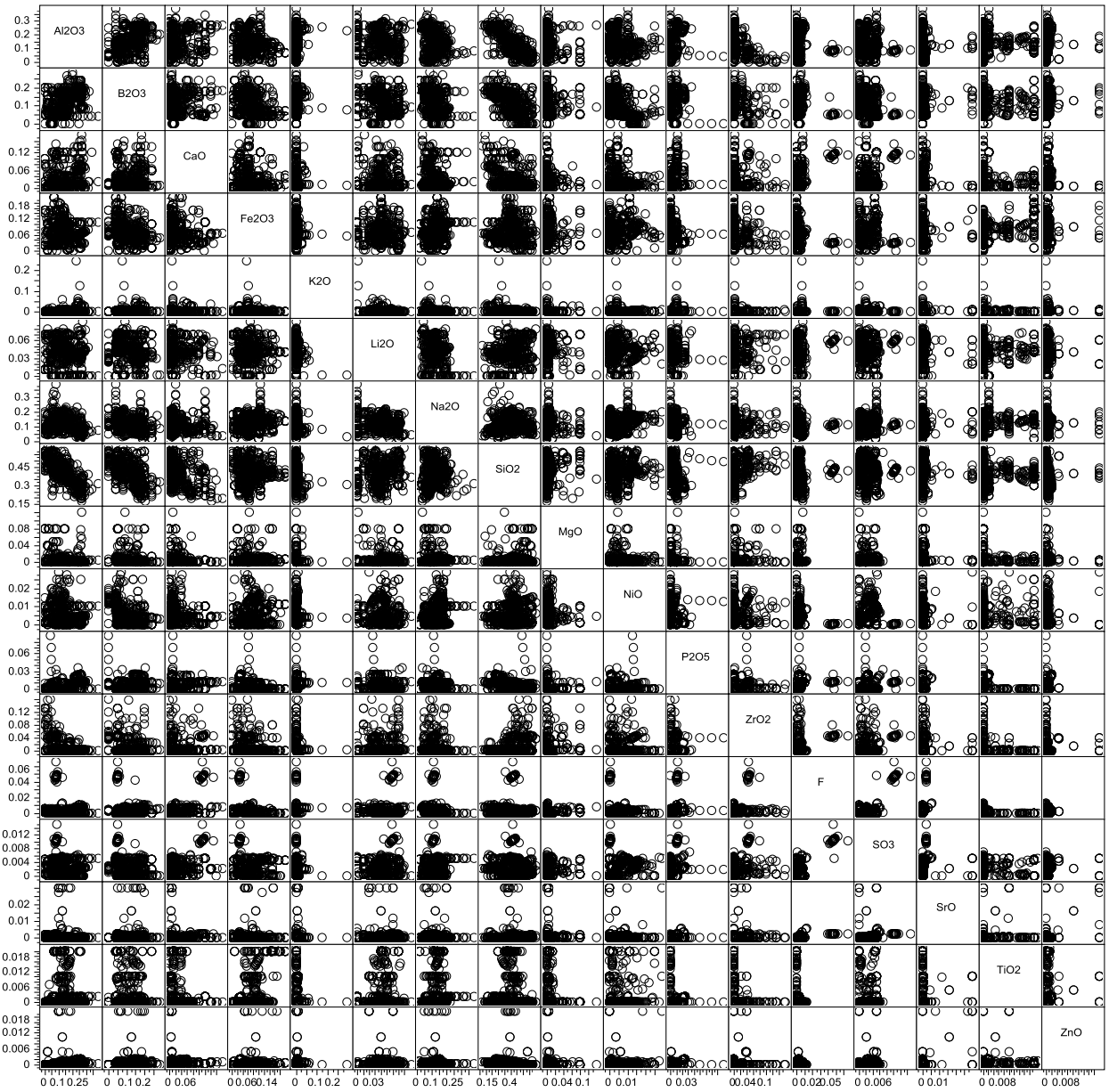

Figure 2.18. Scatterplot Matrix of Nepheline Model Data, Mass Fractions

A graphical representation of the NN used for this model is presented in Figure 2.19. Each of the inputs to the model is listed on the left. The values from these inputs are fed into the three circular nodes immediately after the input. These nodes (called the hidden layer of the model) are composed of an intercept and a transfer function to create an understandable output from the inputs. A detail of an example node from the diagram is shown in Figure 2.20.

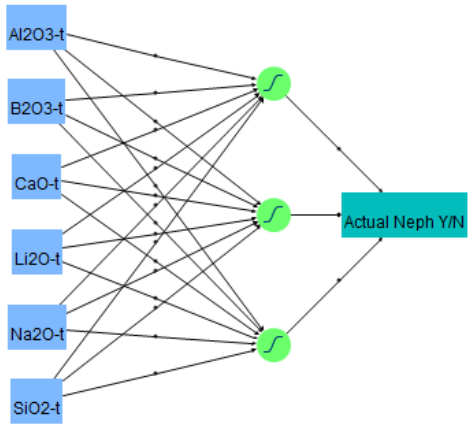

Figure 2.19. Block Diagram of the Neural Network Nepheline Formation Models

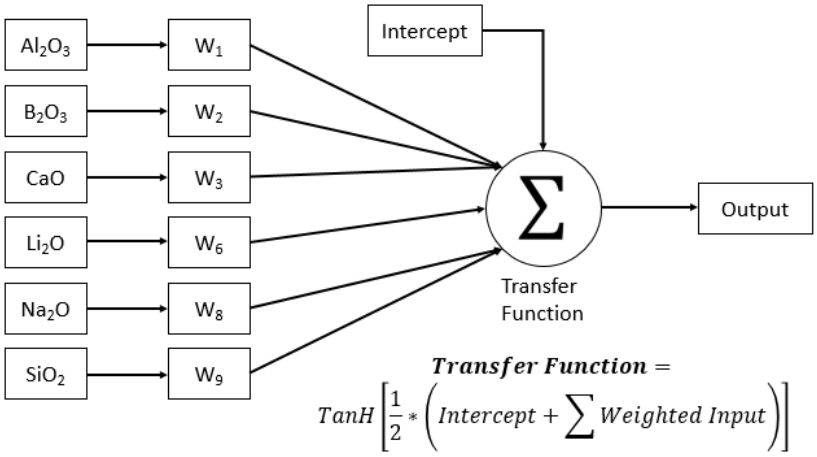

Figure 2.20. Detailed Node Diagram From Neural Network

Efforts were made to create a quantitative prediction model for the nepheline fraction in glass, but there were not a sufficient number of data points to create an accurate model. As a result, a binary response (i.e., nepheline forms or not) was modeled and the misclassification rate, as well as a weighted model score, were used to qualify the model. These results rely on classifying each glass into one of four categories. The test result is classified as positive or negative. Based on a comparison of the actual nepheline response to the predicted nepheline response, if they match, the data point is classified as true. Therefore, a glass that is predicted to form nepheline is a positive, and it becomes a true positive if the composition actually forms nepheline. The model scoring nomenclature is graphically presented in Figure 2.21.

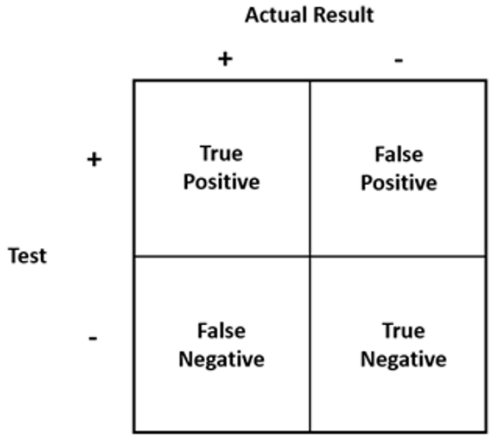

Figure 2.21. Model Scoring Nomenclature

The misclassification percentage is defined by:

$$Misclassification\ \% = \frac{Number\ of\ incorrect\ predictions}{Total\ number\ of\ predictions} \tag{2.8}$$

and the weighted model score is defined as follows:

$$Weighted\ Model\ Score = \frac{True\ Positives * 2.7142 + True\ Negatives}{Positives * 2.7142 + Negatives} \tag{2.9}$$

These two metrics were combined with the false negative percentage, which examines the percentage of data that formed nepheline but were not correctly predicted by the model. In general, a balanced data set would simply use the misclassification rate as the other scoring metric, but this data set is highly biased towards non-forming compositions. As a result, low misclassification rates can be obtained with a model that has a bias towards a non-forming prediction. The weighted model score normalizes this bias and ensures the model is valid for both forming and non-forming glasses.

As the data being modeled is a binary response, the final output is the probability that the composition will form nepheline. This slight difference offers a number of benefits for the analyst; primarily, a percentage can be chosen to match the desired risk threshold. This percentage cutoff can be set in many different ways, all of which affect the resulting model metrics. The initial selection is made at a simple 50% probability. This value was rarely the optimal value based on risk thresholds or weighted scores. As a result, new probability cutoffs were chosen that maximized the weighted score of the model or that matched the false negative threshold from previous models.

The predictive ability of a model is not necessarily a function of the original fit on data points used to train the model; therefore, validation sets of data were used to select the most predictive model. This portion of data is never used to train the data and is only used at the completion of model creation.

Original sensitivity studies were performed using 50%, 75%, and 98% of the data, as well as different K-fold values. Three models were created at each of the subsets, and the resulting accuracies were averaged together. Based on these studies, a *k* value of 10 was chosen for cross validation.

Further studies were performed by fitting models to each of five randomly selected data subsets. The results were processed to select an optimal cutoff value based on a maximum false negative rate of 3%. After a cutoff value was determined, the validation set was used to evaluate the predictive performance of the model. The cutoff values and the performance of the validation models are shown in Table 2.16.

Table 2.16. Validation Model Set Comparison Targeting False Negative Percentage

	Test Data			Validation Data	
	Probability Cutoff	Weighted Misclassification Rate	False Negative	Weighted Misclassification Rate	False Negative
Group 1	11%	7.8%	2.4%	9.5%	3.1%
Group 2	9%	8.9%	2.4%	10.5%	6.3%
Group 3	15%	7.4%	2.4%	13.2%	6.3%
Group 4	20%	5.4%	2.4%	10.1%	12.9%
Group 5	9%	8.2%	2.4%	15.5%	12.9%
Average	12.8%	7.6%	2.4%	11.8%	8.3%

In the final model, 90% of the data was used to train the model and the remaining 10% was used as a validation set. This corresponded to 10 K-fold cross validation. Based on the results of 200 model trials, the model with the best validation metrics was chosen. The model was evaluated across the 10 folds from cross validation and 2 probability of formation cutoffs were determined, one for the minimum weighted misclassification rate and one for the targeted false negative rate. This is similar to the two levels of OB in previous models (McCloy and Vienna 2010). The final metrics of the model are shown in Table 2.17.

Table 2.17. Probability Cutoff Comparison for Neural Network

	Test Data			Validation Data	
	Probability Cutoff	Weighted Misclassification Rate	False Negative	Weighted Misclassification Rate	False Negative
Optimal Score	27%	6.6%	5.6%	6.3%	5.1%
Minimum Risk	10%	10.1%	2.2%	9.4%	2.6%

A probability cutoff of 27% was selected for the optimal model. It is clear from the table that the optimal model score allows for more false negatives. With a false negative rate similar to previous models, the overall weighted misclassification rate of the model is 10%. Neither the probability cutoff or misclassification rate should be misinterpreted as the prediction uncertainties used in waste form qualification efforts. The graphical effect of varying the cutoff probability can be observed in Figure 2.22. As the graph shows, increasing the probability cutoff will result in a higher percentage of

true negatives and a lower percentage of true positives. The location on the graph where the two lines cross corresponds to the maximum weighted model score.

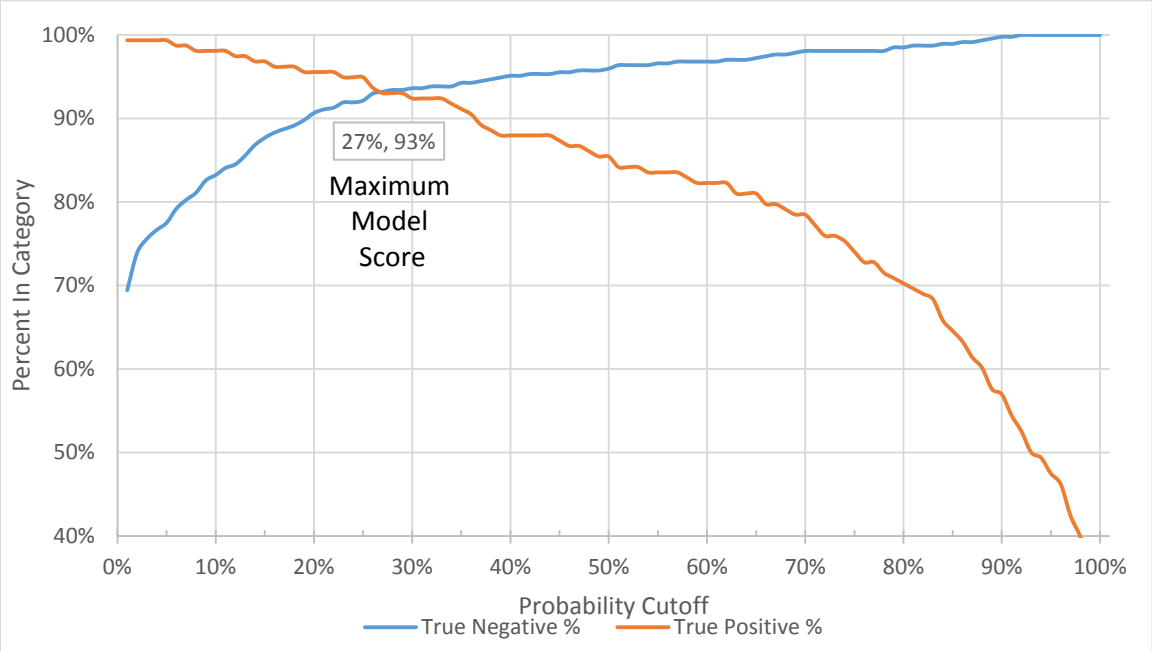

Figure 2.22. Effect of Varying Probability Cutoffs on the True Positive and True Negative Performance

Previous models have described the nepheline formation region using ND and OB cutoffs. The model presented by McCloy et al. (2011) is used as a comparison to benchmark the performance of the NN model. This comparison shows a significant reduction in both the absolute and the weighted misclassification rates at similar or lower false negative rates. A full table of comparisons is shown in Table 2.18. To summarize this data, the outcome of each of the 629 glass data set is described in Figure 2.23.

Table 2.18. Comparison of Neural Network and Previous Model Performance

	ND/OB		NN
	OB = 0.55	OB = 0.575	P(Y) = 27%
True Positive	155	137	147
False Positive	209	125	32
True Negative	262	346	439
False Negative	3	21	11
Standard Misclassification Rate	33.7%	23.2%	6.8%
Weighted Misclassification Rate	24.1%	26.5%	6.8%

		Experimentally Formed Nepheline: Yes	Experimentally Formed Nepheline: No
Predicted to Form Nepheline	Yes	True Positive 147 (23%)	False Positive 32 (5.1%)
	No	False Negative 11 (1.7%)	True Negative 439 (70%)

Figure 2.23. Model Scoring Summary for the Selected Nepheline Neural Network Model

The components of the NN have an effect that is aligned with previous research aimed at predicting nepheline formation. As expected, increased SiO_2 decreases the probability of formation, while both Al_2O_3 and Na_2O increase the probability of formation. These results can be seen in the main effects plot presented in Figure 2.24.

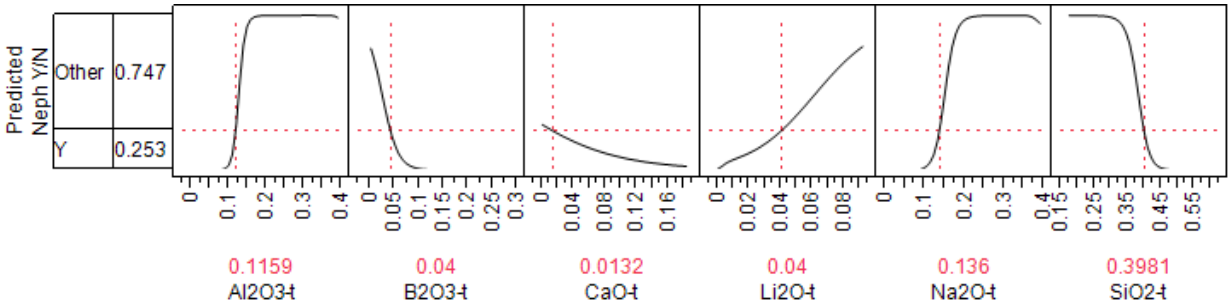

Figure 2.24. Effect of Component Concentration on Probability of Nepheline Formation

A full interaction plot of the components of the model is presented in Figure 2.25. Each plot shows how varying one component (bottom scale) will affect the probability of formation at the high- and low-level for the second component (right axis). As an example, higher Al_2O_3 values will generally increase the probability of formation, but as more Na_2O is added, this effect is seen at lower Al_2O_3 levels. This can be seen in the plot in column one, row five. Plots that overlap, such as the Li_2O and CaO, show no interaction between components.

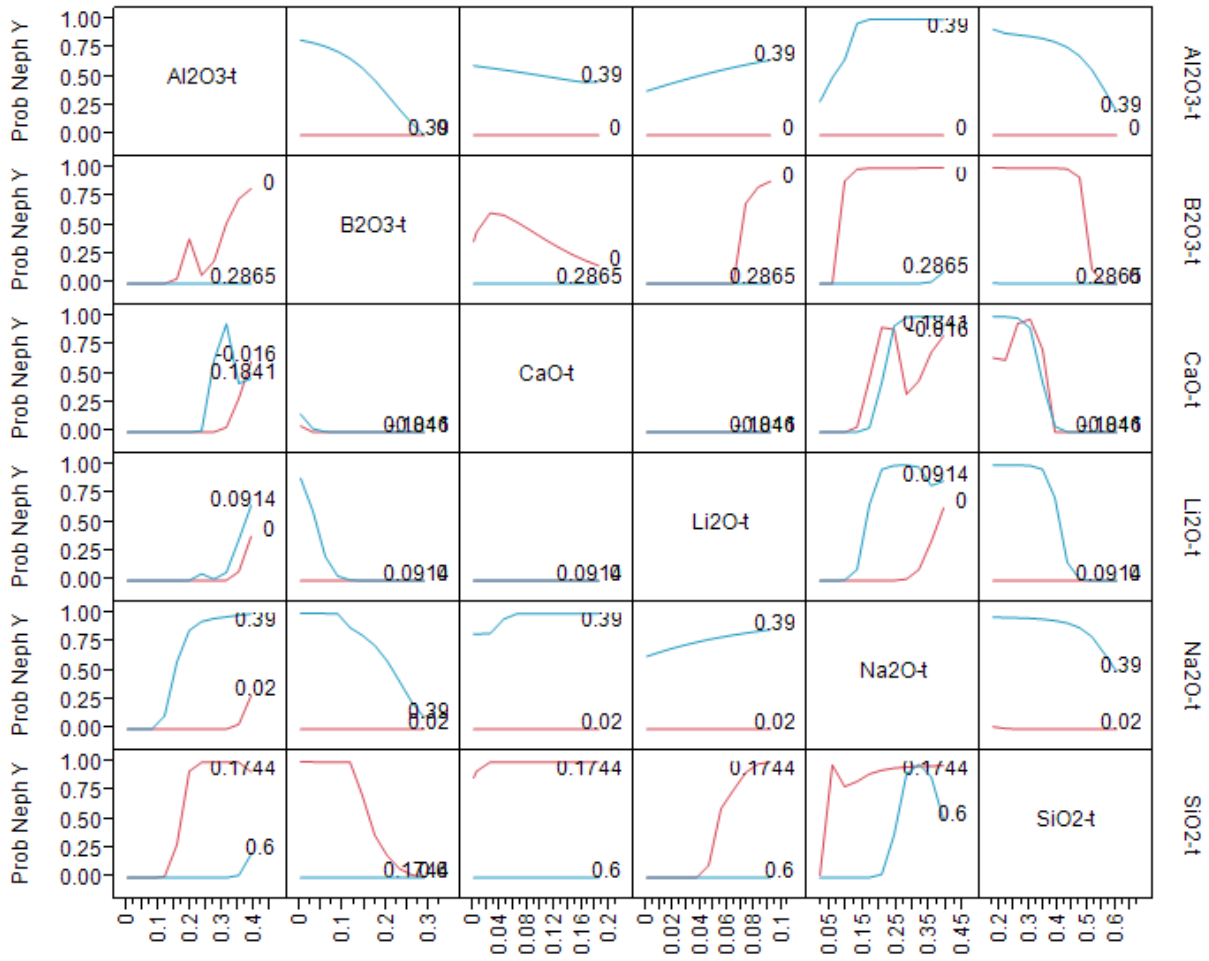

Figure 2.25. Interaction Profile Plot for the Six Components of the Neural Network Nepheline Model. The blue and red lines are the maximum and minimum value for the secondary components.

The inclusion of the six compositional inputs in the model also allows for profiling to determine regions with a higher probability of formation. An example of the composition effects is shown for an earlier version of the model that uses normalized SiO_2, Al_2O_3, and Na_2O (N_{Si}, N_{Al}, and N_{Na}, respectively) concentrations for illustration purposes. This model was found to be less predictive than the final model discussed in this report, but is similar in component effects, and allows for direct visualizations of the nepheline formation regions on Na_2O-SiO_2-Al_2O_3 ternary plots as shown in Figure 2.26. These regions generally agree with observations made in previous work (McCloy et al. 2011). These ternary plots illustrate the effects of B_2O_3, CaO, and Li_2O on the probability of the nepheline formation region in the SiO_2, Al_2O_3, and Na_2O submixture.

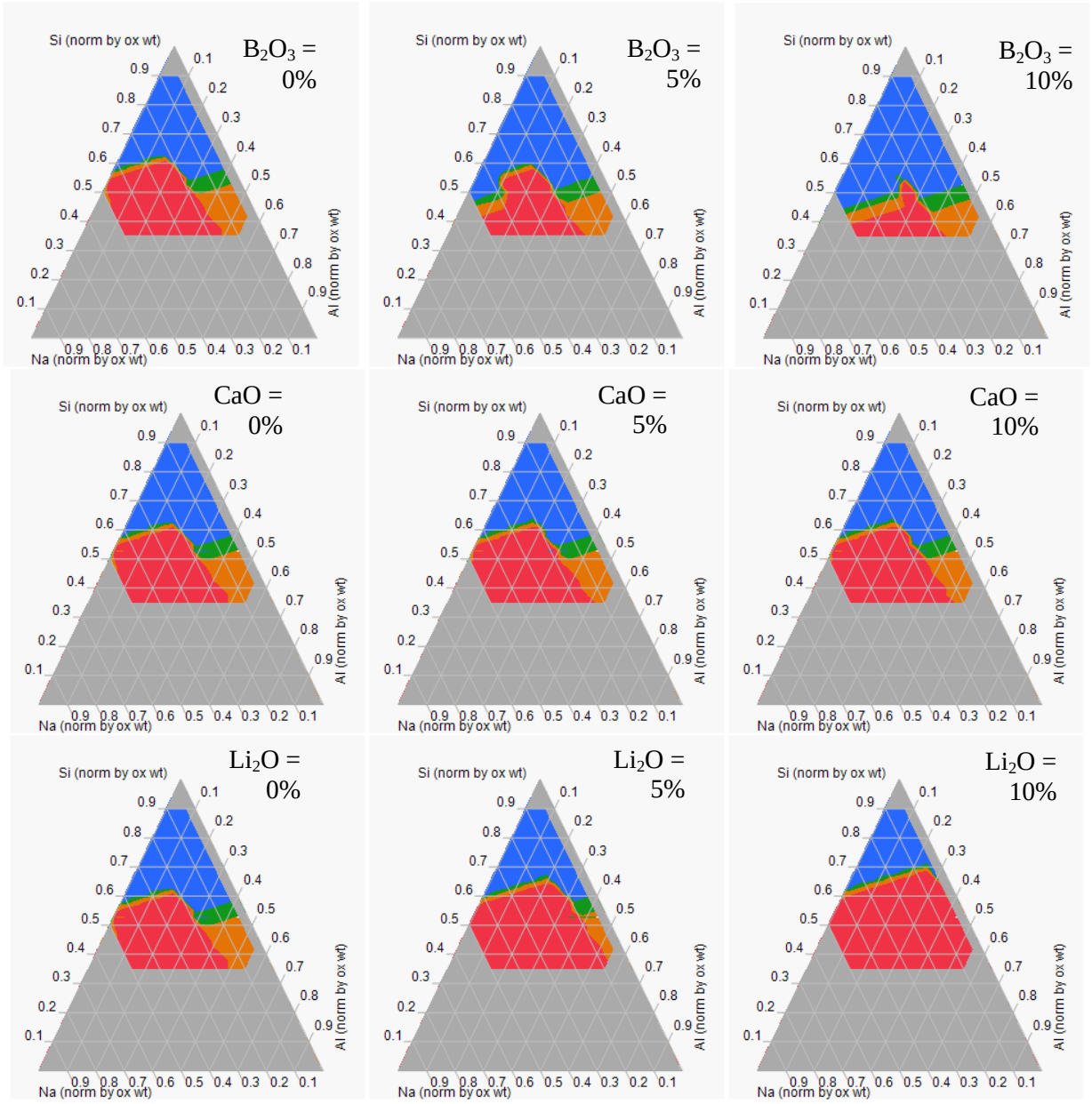

Figure 2.26. Nepheline Formation Regions at Different Concentrations of B_2O_3, CaO, and Li_2O [blue – low probability (0-5%), red – high probability (50+%), and orange (27-50%) and green (6-27%) are intermediate probabilities]

As described earlier, the NN comprises three hidden nodes with six inputs. The complete set of equations for the NN is described in Figure 2.27. This model determines the probability that the glass composition will form nepheline.

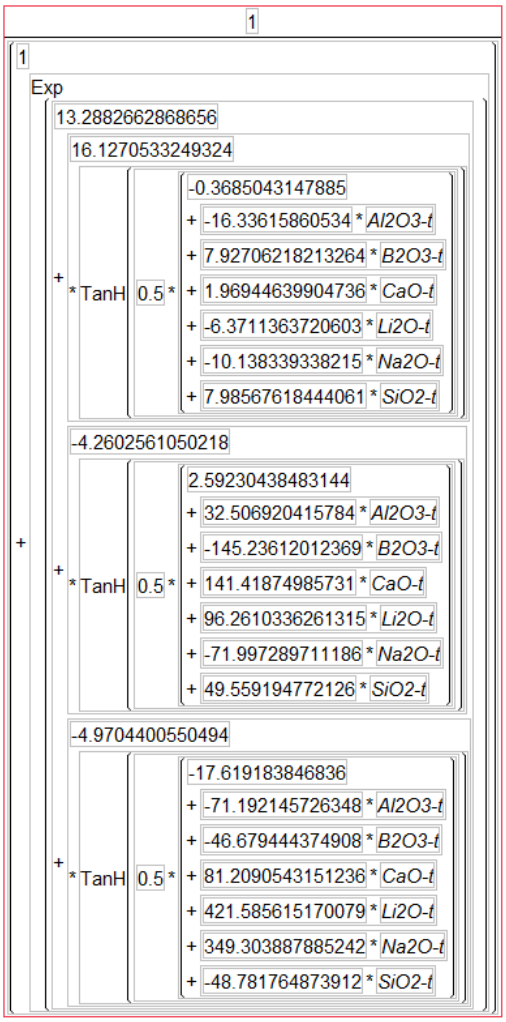

Figure 2.27. Equation Representing the Probability of a Nepheline Formation (oxide-t values represent mass fraction of those oxides in glass or g_i)

The NN model described above gives a reasonable first step in defining a composition region in which nepheline is likely to form. However, it is far from a final solution to the nepheline management problem. The next steps include development of a method for quantifying the prediction uncertainties of such a model as well as the expansion of the data set so that the prediction can be based on a single representative heat treatment method (i.e., WTP CCC). Additional data is required in the pertinent, high-alumina, glass composition region to reduce the prediction uncertainties within that region (e.g., the orange and green regions in Figure 2.26).

2.4 Chromium Content

If the content of chromium in the melter feed is too high, one of three things will most likely occur (Hrma 2006):

1. A chromate- (and sulfate-) containing salt will accumulate on the melt surface. This typically, but not always, occurs in melts high in sulfate and other salt-forming compounds.

2. Transition metal spinel, $(Fe,Ni,Mn,Zn)(Fe,Cr)_2O_4$, will form. This typically occurs in melts with relatively high concentrations of iron, nickel, manganese, and/or zinc.

3. Eskolaite, Cr_2O_3, will form. This typically occurs only in melts that are relatively low in sulfur, iron, nickel, manganese, and/or zinc.

Additionally, chromate species such as $Na_2Cr_2O_7$, are semi-volatile and partition to some extent to the off-gas system, where they are captured and eventually recycled back to the melter (e.g., Jantzen 1991b). This is partially offset by the addition of small amounts of chromium from corrosion/erosion of high chromium melter materials such as K-3 and Inconel 690.

The formation of salt in waste glasses is clearly influenced by the chromium content of the feed, as seen in the salt models described in Section 2.2. The Cr_2O_3 content of the melt also strongly increases the amount of spinel formed at a given temperature as seen in the spinel models described in Section 2.1.

A series of high Cr_2O_3 glasses were formulated and tested in the DM-100 melter (Matlack et al. 2009b). The Cr_2O_3 content of these glasses extended up to 6 wt%. Crucible-scale testing of these glasses showed that for the glasses specifically formulated to have low sulfur and transition metals (e.g., those prone to eskolaite formation), the fraction of eskolaite in the melt after 70-hour heat treatments at 950°C roughly corresponded to the total Cr_2O_3 content of the glass. This is shown in Figure 2.28, where the blue data points ("ES series" glasses) form eskolaite concentrations roughly equal to the maximum amount of all Cr_2O_3 precipitated in the form of eskolaite. There is a slightly higher eskolaite fraction for the glasses with >3 wt% Cr_2O_3, which is likely caused by the inclusion of some Al_2O_3 and/or Fe_2O_3 in the eskolaite, because they are known to form solid solutions. Also shown in the plot is a single "M-series" glass that precipitated both spinel and eskolaite—only the eskolaite fraction is shown on the plot.

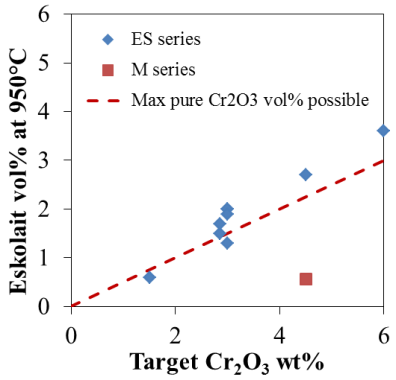

Figure 2.28. Eskolaite vol% in High-Cr_2O_3 Crucible-Scale Glasses Heat Treated at 950°C for 70 hours (data from Matlack et al. 2009b)

Eskolaite crystals are typically small, plate-like crystals that do not settle readily in glass melts. An example is shown in Figure 2.29. It is thus theorized that on an equal volume basis, eskolaite is less likely to cause melter operation problems than spinel.

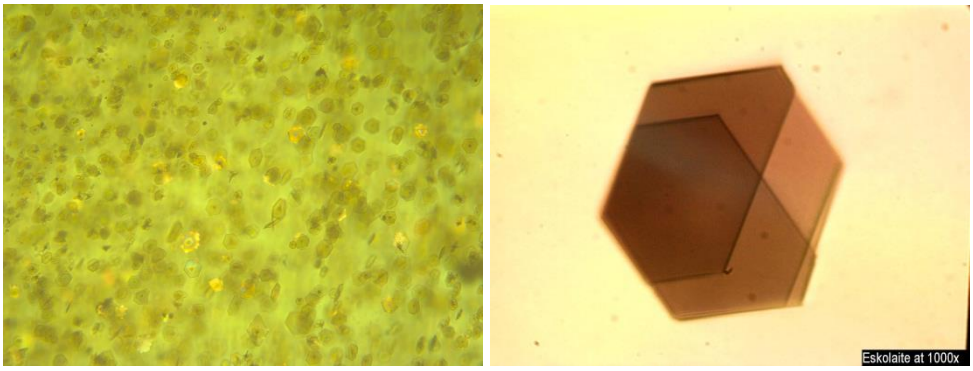

Figure 2.29. Optical Micrographs of Eskolaite in High Cr_2O_3 Glasses

Two tests were performed to develop an initial indication of the eskolaite behavior in the melter (Matlack et al. 2009b). In the first test, a glass with 2 vol% eskolaite was fabricated (measured in crucible-scale glass heat treated at 950°C). In the second test a glass with 4.2 vol% combined eskolaite and spinel was fabricated (measured in crucible-scale glass heat treated at 950°C). These tests were operated for roughly 50 hours each of continuous feeding in the DM-100 melter. The melter was then idled for 181 to 299 hours. The results, although too limited to clearly define if this amount of crystals could be processed over extended time periods, did not indicate any potential problems with this amount of crystals. Additionally, it was shown that during idling, the spinel settled significantly faster than either eskolaite or hematite crystals.

By assuming that eskolaite and spinel can be tolerated equally well in the melter, preliminary limits for Cr_2O_3 in glass can be postulated. The predicted impacts of changes in $g_{Cr_2O_3}$ on c_{Sp} for a typical high Cr_2O_3 Hanford HLW glass are shown in Figure 2.30. Taking a conservative assumption that all of the Cr_2O_3 precipitates in the form of either high chromium spinel ([Fe,Mn,Ni,Zn]Cr_2O_4) or eskolaite (Cr_2O_3), the maximum amount of crystal formed for each mass fraction increase in Cr_2O_3 would range between 0.46 and 0.77 vol% (assuming densities of 2.5, 5.2, and 4.6 for melt, eskolaite, and spinel, respectively). This maximum value represents 72 to 120% of the effect of Cr_2O_3 shown in Figure 2.30 (0.555). This suggests that using the c_{Sp} model will give a reasonable estimate of the maximum fraction of crystal to form in high Cr_2O_3 glasses. This also gives a reasonable justification for extrapolation of the c_{Sp} model to higher Cr_2O_3 concentrations that were found in the data used to fit the model (max Cr_2O_3 in the model data was 2 wt%). If all Cr_2O_3 crystallized as eskolaite and there was a 2 vol% limit on eskolaite at 950°C, then the maximum $w_{Cr_2O_3}$ would be 4 wt%.

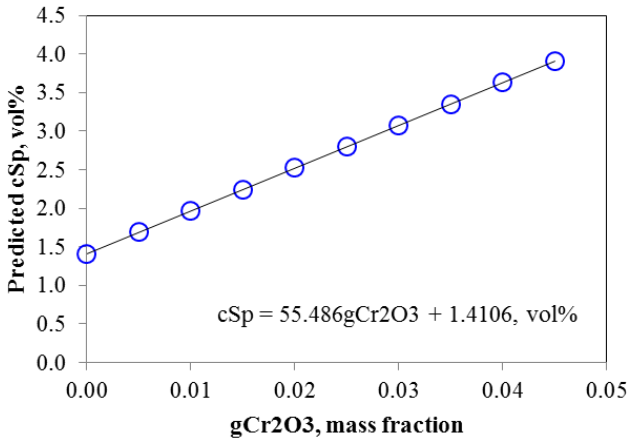

Figure 2.30. Impact of Cr_2O_3 Mass Fraction on Predicted c_{Sp}

No similar, simple approach is possible to evaluate the impacts of high Cr_2O_3 concentrations on salt formation. However, it is interesting to note that aside from Cl, Cr_2O_3 has the highest impact on the allowable sulfur concentration in melter feed. Using component effects on the same high Cr_2O_3 Hanford HLW glass discussed above, the most impactful components on salt formation are (with their effects relative to SO_3): SO_3 (1) > Cl (0.30) > Cr_2O_3 (0.083). Until sufficient additional data becomes available, it must be assumed that this model (Table 2.10) adequately represents the impacts of Cr_2O_3 on salt formation.

2.5 Viscosity

The viscosity of waste glass melts should be maintained between roughly 20 and 80 P (2 to 8 Pa·s) at the melting temperature (nominally 1150°C). It is not appropriate to fit new viscosity models for advanced HLW glass formulations at this time, because:

- the current models can be extrapolated to the new composition region quite reliably (as shown in Figure 2.31), and
- the viscosity of glass must be maintained in the correct range to estimate glass composition, but has little influence on the ultimate waste loading of the HLW glasses.

There is a somewhat consistent offset in the predicted values of roughly 0.32 on a Ln[η_{1150}, Pa·s] basis. This roughly translates to measured values of 2.75 and 11.0 for predicted values of 2 and 8 Pa·s, respectively. The correction can be added to the predictions when comparing to viscosity limits, if desired. For the purposes of the example calculations, no correction was used.

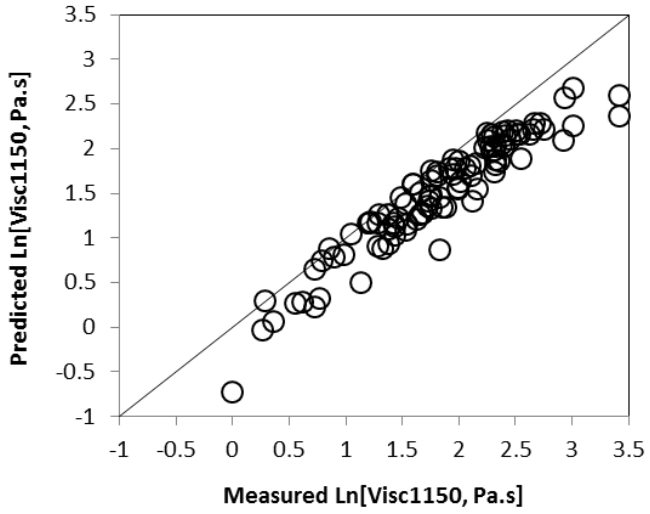

Figure 2.31. Comparison of Predicted and Measured Ln(viscosity) Data for ORP Advanced HLW Glasses Using the 2009 Viscosity Model (Vienna et al. 2009)

It is therefore recommended that the 2009 viscosity Ln[η_{1150}] model be applied to estimate reasonable glass compositions. This model is of the following form:

$$Ln[\eta_{1150}] = \sum_{i=1}^{p} h_i g_i + selected \left\{ \sum_{i=1}^{p-1} \sum_{j=i}^{p} h_{ij} g_i g_j \right\} \qquad (2.10)$$

where η_{1150} = the viscosity at 1150°C (in Pa·s)
h_i = the i^{th} component coefficient,
g_i = the i^{th} component mass fraction, and
h_{ij} = the i^{th} times j^{th} component coefficient.

This model is summarized in Table 2.19. Like the other models, composition is in mass fraction. Alternative models for viscosity as a function of temperature, such as that recently published by Hrma et al. (2009) based on the Arrhenius relationship.

Table 2.19. Viscosity-Composition Model Coefficients and Selected Statistical Parameters

Model Term	Coefficient, Ln(η_{1150}, Pa·s)	Statistic	Value
Al_2O_3	10.6085	R^2	0.962
B_2O_3	-9.37529	R^2_{Adj}	0.961
BaO	-3.41816	R^2_{Press}	0.959
CaO	-6.9328	R^2_{Val}	0.962
F	-12.3445	RMSE, Ln(Pa·s)	0.163
K_2O	-3.82491	# of glasses	967
La_2O_3	-4.96954	-	-
Li_2O	-39.0249	-	-
MgO	-3.23141	-	-
MnO	-6.88677	-	-
Na_2O	-9.63275	-	-
P_2O_5	5.305007	-	-
PbO	-23.1436	-	-
SiO_2	9.368089	-	-
SrO	-4.35052	-	-
UO_3	2.151455	-	-
ZnO	-2.69626	-	-
ZrO_2	7.14044	-	-
Others	-0.09027	-	-
$B_2O_3 \times B_2O_3$	24.59262	-	-
$Na_2O \times B_2O_3$	-26.9571	-	-
$Li_2O \times Li_2O$	47.35918	-	-
$Na_2O \times Al_2O_3$	17.51718	-	-
$CaO \times Al_2O_3$	-8.13474	-	-

2.6 Product Consistency Test

The WTP contract (DOE 2000), the Waste Acceptance Product Specifications (DOE 1996), and the Waste Acceptance System Requirements Document (OCRWM 2008) all require the PCT responses of HLW glasses to meet the standard, with sufficient confidence, and be reported during production. The standard is that the PCT responses of B, Li, and Na, normalized to their concentration in the glass, be below those of the DWPF Environmental Assessment (EA) glass (Jantzen et al. 1993).

Existing PCT models (Piepel et al. 2008; Vienna et al. 2009) were first evaluated to determine if they adequately predicted the PCT responses of advanced HLW glasses. However, it was clear that they did not accurately predict the responses of the newer glasses and they were not generally conservative (as seen in Figure 2.32 and reported by Muller et al. [2012]). The significantly underpredicted PCT responses shown in the plot are primarily from higher alumina glasses. It has long been known that the impact of Al_2O_3 on PCT response is highly non-linear (Vienna et al. 1996a). At low concentrations ($g_{Al_2O_3} \lesssim 0.05$), additions of Al_2O_3 significantly reduce the PCT response of a glass. At higher concentrations, additions of Al_2O_3 have little impact on the PCT response of glass. With the advanced HLW glass formulations, unprecedented high concentrations of Al_2O_3 are added to glass, and we theorize

that at these higher concentrations, Al_2O_3 additions may increase PCT response. It was therefore decided that a new PCT model must be used to help bound the response of advanced HLW glass formulations.

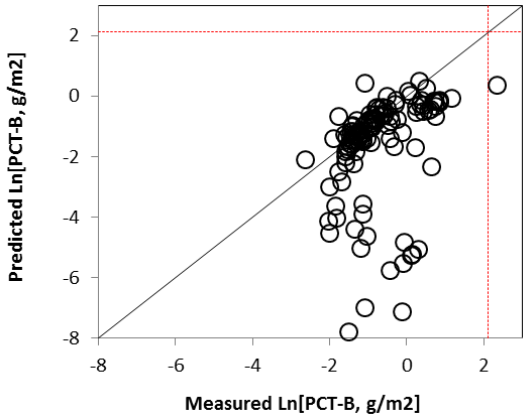

Figure 2.32. Comparison of Normalized PCT-B Response of Advanced HLW Glasses to HTWOS 2009 Model Predictions

A database of HLW glasses was compiled to model their PCT responses. These data include the data used in the development of the HTWOS 2009 PCT models (1115 data points tabulated and described by (Vienna et al. 2009), excluding the 31 data points found to be outliers in that report) and the advanced HLW glass data (111 data points tabulated and described by Muller et al. [2012]). The data concentration ranges are summarized in Table 2.20 and shown graphically in a scatterplot matrix in Figure 2.33. It should be noted that these glasses are a combination of quenched crucible melts and melter test glasses. They do not include CCC glasses that in some cases precipitate nepheline as described and modeled in Section 2.3.

Table 2.20. Component Concentration Ranges for HLW PCT Model Data, wt%

Component,	HTWOS		ORP Adv		Total	
i	*Min*	*Max*	*Min*	*Max*	*Min*	*Max*
Al_2O_3	1.6	20.0	1.9	26.6	1.6	26.6
B_2O_3	4.0	20.0	4.3	20.2	4.0	20.2
BaO	0.0	4.7	0.0	0.2	0.0	4.7
CaO	0.0	10.4	0.2	14.2	0.0	14.2
CdO	0.0	1.5	0.0	0.9	0.0	1.5
F	0.0	2.5	0.0	1.1	0.0	2.5
Fe_2O_3	0.0	17.4	2.7	21.3	0.0	21.3
K_2O	0.0	6.9	0.0	15.3	0.0	15.3
Li2O	0.0	9.0	0.0	5.8	0.0	9.0
MgO	0.0	8.0	0.0	3.1	0.0	8.0
MnO	0.0	7.0	0.0	8.0	0.0	8.0
Na_2O	4.1	23.0	3.6	20.0	3.6	23.0
Nd_2O_3	0.0	5.9	0.0	0.3	0.0	5.9
P_2O_5	0.0	5.0	0.0	6.0	0.0	6.0
SiO_2	30.3	62.8	17.4	53.1	17.4	62.8
SO_3	0.0	2.5	0.0	0.8	0.0	2.5
SrO	0.0	10.1	0.0	9.3	0.0	10.1
ThO_2	0.0	6.0	0.0	3.6	0.0	6.0
TiO_2	0.0	4.0	0.0	1.6	0.0	4.0
UO_3	0.0	6.5	0.0	5.6	0.0	6.5
ZnO	0.0	5.8	0.0	4.5	0.0	5.8
ZrO_2	0.0	13.5	0.0	10.6	0.0	13.5
Others[(a)]	0.0	9.4	0.5	11.3	0.0	11.3

(a) Others equals the sum of all components not specifically listed here.

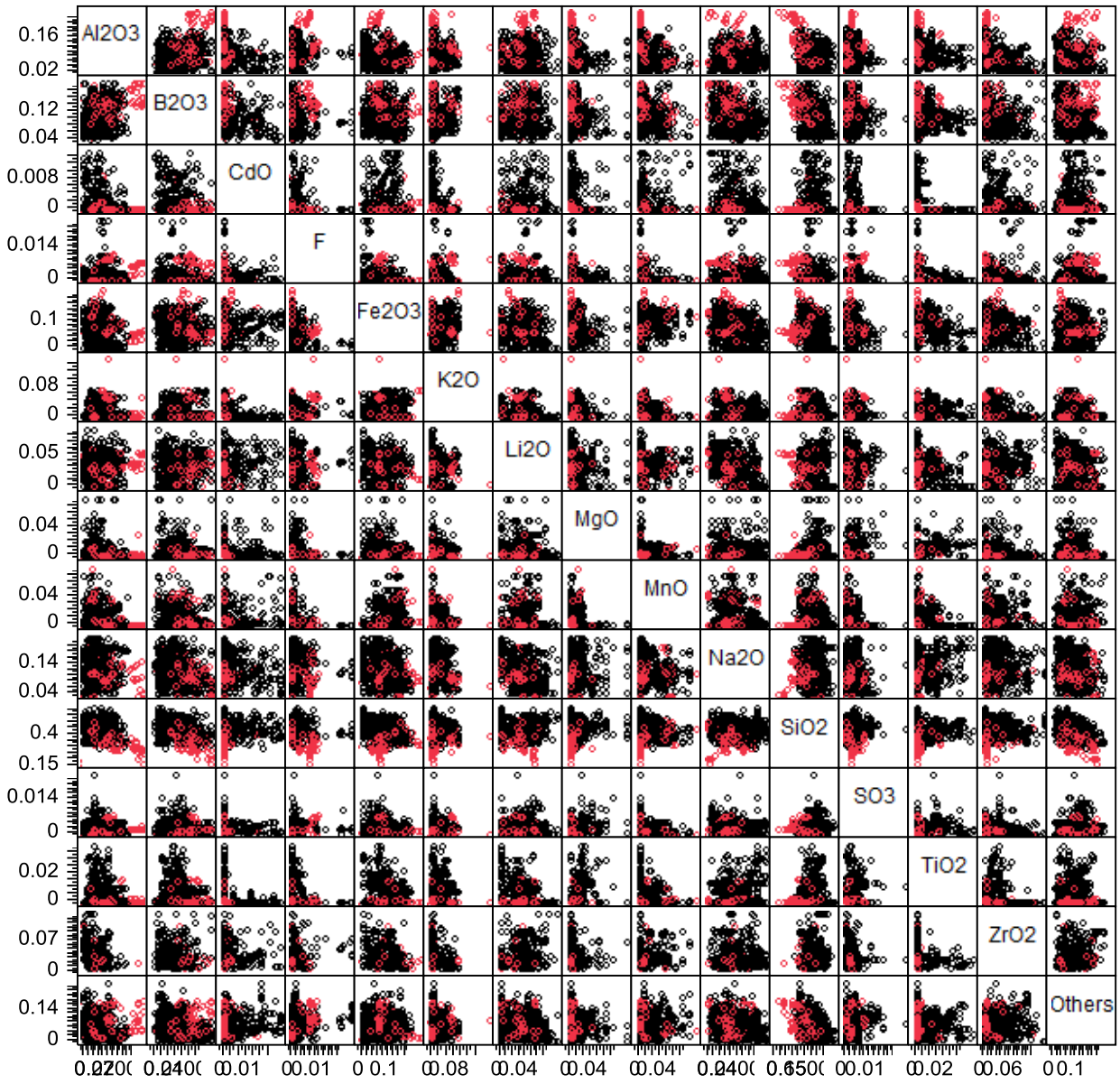

Figure 2.33. Scatterplot Matrix of HLW PCT Model Data (red points for ORP advanced HLW glasses).

Repeated analyses show that, in general, normalized boron, lithium, and sodium responses are nearly the same. This is confirmed to be the case with our data set in Figure 2.34. Therefore, there is no need to model or control the composition for each elemental PCT response. Rather than fit PCT(B), PCT(Li), and PCT(Na) separately, it was decided to average the natural logarithm (Ln) of the three values for each glass, and fit the average (Ln[PCT(B), g/m^2], Ln[PCT(Li), g/m^2], and Ln[PCT(Na), g/m^2]) value as a measure of PCT response of these glasses.

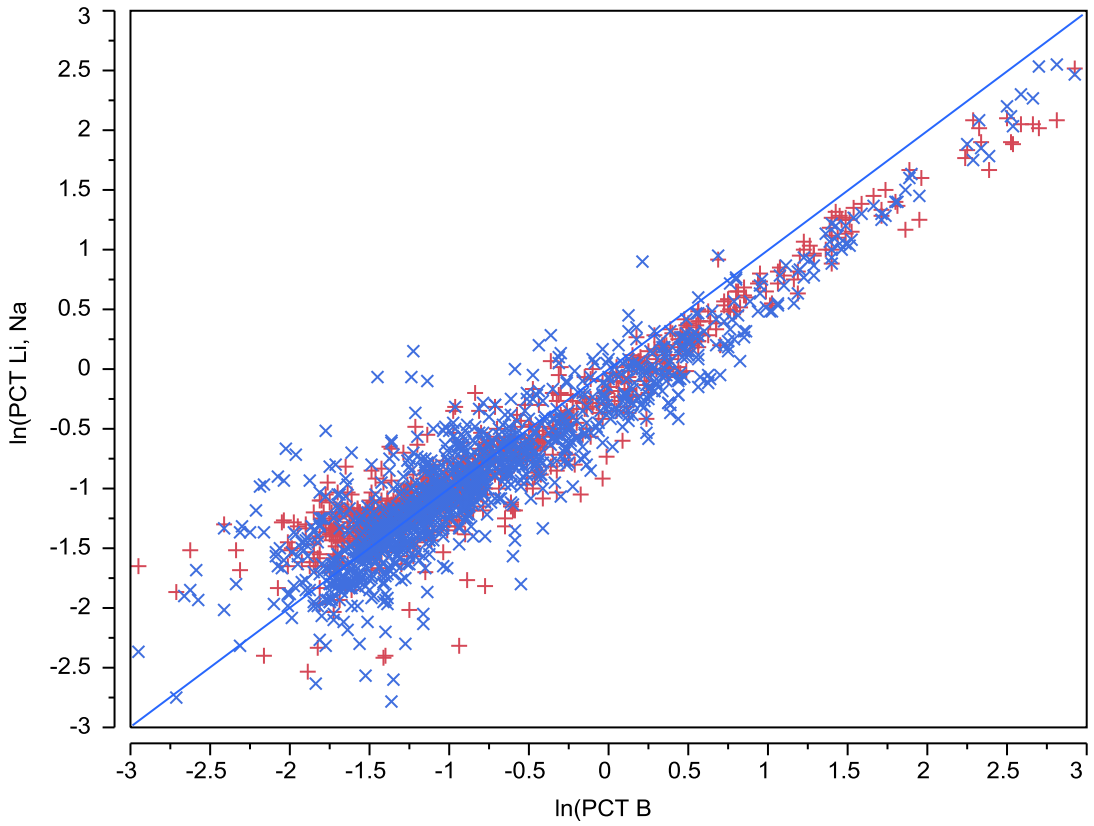

Figure 2.34. Comparison of PCT(B), PCT(Na), and PCT(Li) (red + is Li, blue × is Na)

Only one model form was attempted to model the HLW glass PCT response—the partial quadratic model:

$$\mathrm{Ln}\left[PCT\right] = \sum_{i=1}^{p} b_i g_i + selected\left\{\sum_{i=1}^{p-1}\sum_{j=i}^{p} b_{ij} g_i g_j\right\} + b2_{Al_2O_3} g_{Al_2O_3}^2 + b3_{Al_2O_3} g_{Al_2O_3}^3 + b4_{Al_2O_3} g_{Al_2O_3}^4 + \ldots \quad (2.11)$$

where Ln[PCT] is the mean response (Ln[PCT(B), g/m^2], Ln[PCT(Li), g/m^2], Ln[PCT(Na), g/m^2], b_i is the i^{th} component coefficient, g_i is the i^{th} component mass fraction in glass, and $b2_{Al_2O_3}$, $b3_{Al_2O_3}$, $b4_{Al_2O_3}$ … are the coefficients for higher order Al_2O_3 mass fraction terms. During the modeling effort, both the model-fit and validation statistics improved with the higher order Al_2O_3 terms, as was expected. No other cross product or higher order term was found to be significant in comparison to the first-order terms and higher order Al_2O_3 terms. Ultimately, validation statistics were used to decide which first-order terms and how many higher order Al_2O_3 terms to include. The final model terms are summarized in Table 2.21 and the model-fit is shown graphically as a predicted vs. measured plot in Figure 2.35.

Table 2.21. Summary of HLW PCT Response Model Coefficients and Fit Statistics

Term	Coefficient	Statistic	Value
Al_2O_3	-103.76	R^2	0.7629
B_2O_3	10.75627	R^2_{Adj}	0.7595
CdO	15.74204	R^2_{Press}	0.7547
F	26.97387	RMSE	0.397
Fe_2O_3	-2.574697	$RMSE_{Press}$	0.401
K_2O	11.64107	Mean of response	-0.799
Li_2O	23.52778	# of data points	1,226
MgO	10.4331	-	-
MnO	4.028527	-	-
Na_2O	15.27193	-	-
SiO_2	-2.827361	-	-
SO_3	20.6466	-	-
TiO_2	-11.8236	-	-
ZrO_2	-6.265786	-	-
Others	-0.595703	-	-
$(Al_2O_3)^2$	1166.629	-	-
$(Al_2O_3)^3$	-5871.868	-	-
$(Al_2O_3)^4$	10289.47	-	-

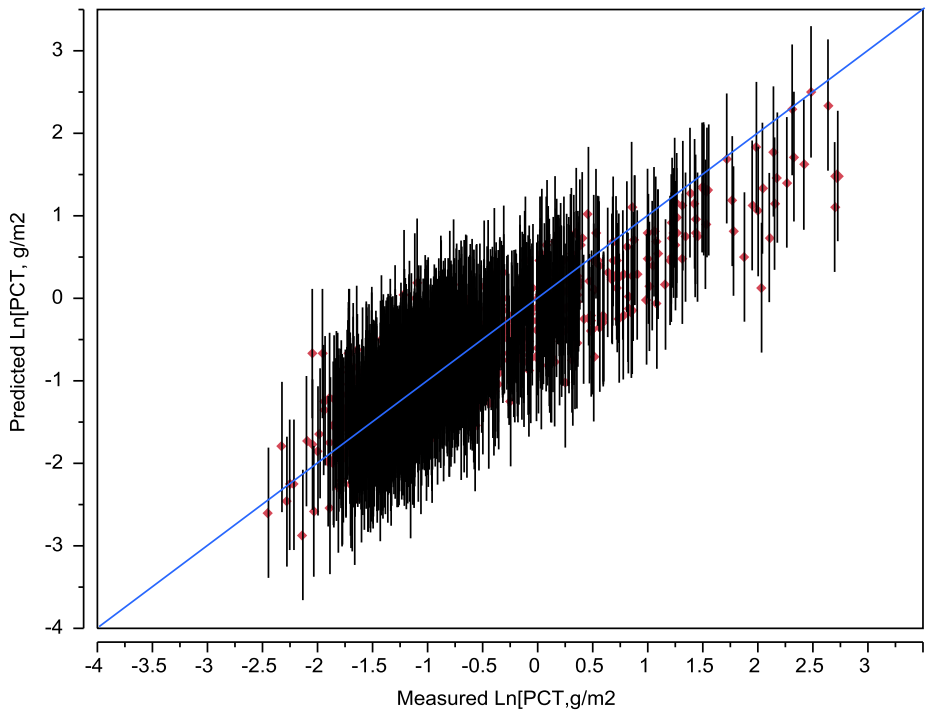

Figure 2.35. Predicted vs. Measured Average (Ln[PCT]) with 95% Confidence Interval for Individual Prediction

Because such high order terms for any component are unusual in waste glass property-composition models, we must first evaluate the predicted impacts of components on the Ln[PCT] response. Figure 2.36 shows the impacts of changing each component, one at a time, from an average glass on the predicted Ln[PCT] response. The impact of Al_2O_3 change, the only non-linear impact, is zoomed in on for further consideration. The general trends are as expected, including the non-linear effect of Al_2O_3, which dramatically reduces the response at low concentrations, levels off in intermediate concentrations, and dramatically increases the response at the highest concentrations. This, along with the validation statistics, adds comfort to an unprecedented non-linear model.

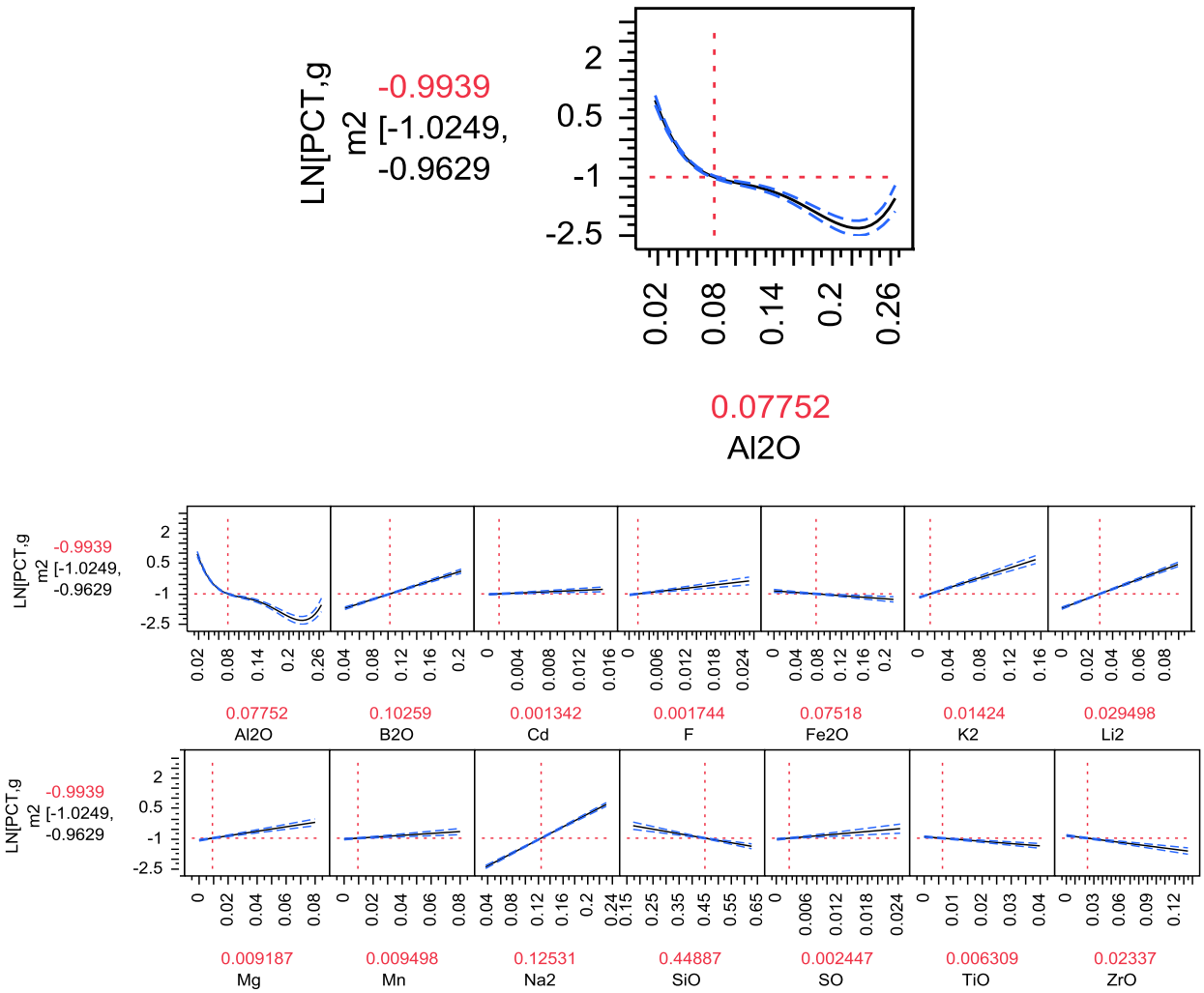

Figure 2.36. Component Effects "Profiler" for HLW PCT Model

To validate the model, data not used in model fitting must be obtained. Because all appropriate data within the desired composition region were used in model fitting, subsets of the model data were used to validate the model. The data were first divided into the set used to fit the HTWOS 2009 model and those from the ORP advanced glasses. Then each set was sorted by average (Ln[PCT]) response value. The data were then numbered 1, 2, 3, 4, 5, 1, 2, … to split them into five representative groups of roughly 20% of the data, each set containing roughly equal portions of glasses from the two data sets. The model was then refit to subsets 2 to 5 and used to predict data in subset 1. Then the model was fit to each group

of four subsets and used to predict the remaining subset in sequence. Table 2.22 summarizes the results of the model validation. The coefficients are reasonably close, having an RSD of less than 25% for all components. The model-fit R^2 values are all close to each other at approximately 0.76. The R^2_{val} values are also close to 0.75. The average R^2_{val} value is almost identical to the R^2_{Press}value of 0.75. This model is well validated, and should give predictions of unknown data within the model-validity region nearly as well as for the model-fit data.

Table 2.22. Summary of PCT Model Validation Data

Components	Full Model	Grp 1	Grp 2	Grp 3	Grp 4	Grp 5	%RSD
Al_2O_3	-103.76	-102.4011	-106.4965	-103.1341	-103.89	-104.0309	-1%
B_2O_3	10.75627	11.15146	10.69746	10.74049	10.62057	10.62811	2%
CdO	15.74204	16.44303	16.9026	12.18981	17.86679	15.1351	14%
F	26.97387	26.65909	25.58735	29.66286	27.11623	25.77008	6%
Fe_2O_3	-2.574697	-3.302401	-2.665192	-2.293572	-2.023997	-2.58754	-19%
K_2O	11.64107	12.09041	12.11811	11.26681	11.4803	11.14698	4%
Li_2O	23.52778	23.18214	23.49416	23.75547	23.17885	24.06747	2%
MgO	10.4331	11.24244	11.37676	10.39039	9.8022	9.534219	8%
MnO	4.028527	4.636964	4.999633	2.691618	3.406623	4.493336	24%
Na_2O	15.27193	15.18371	15.37501	15.47002	14.94776	15.36367	1%
SiO_2	-2.827361	-2.83753	-2.782461	-2.892939	-2.777461	-2.820917	-2%
SO_3	20.6466	21.27637	21.11248	18.60138	21.88151	20.50533	6%
TiO_2	-11.8236	-11.32367	-12.11721	-12.95733	-11.08802	-11.42091	-6%
ZrO_2	-6.265786	-6.590919	-6.876644	-6.493511	-5.35194	-6.021701	-10%
Others	-0.595703	-0.580153	-0.58186	-0.443082	-0.64686	-0.672792	-15%
$(Al_2O_3)^2$	1166.629	1146.06	1,226.44	1157.207	1158.115	1163.735	3%
$(Al_2O_3)^3$	-5871.868	-5774.142	-6309.478	-5815.044	-5751.041	-5820.943	-4%
$(Al_2O_3)^4$	10289.47	10151	11247.87	10166.06	9955.12	10142.39	5%
Fit Statistics							
R^2	0.7629	0.7617	0.7689	0.7577	0.7728	0.7595	0.7641
R^2_{Adj}	0.7595	0.7575	0.7648	0.7534	0.7687	0.7553	0.7599
R^2_{Press}	0.7547	0.7516	0.7588	0.7471	0.7627	0.7493	0.7539
RMSE	0.397	0.398	0.394	0.403	0.389	0.400	0.3969
$RMSE_{\text{Press}}$	0.401	0.403	0.399	0.408	0.394	0.405	0.4019
Validation							
R^2_{Val}	-	0.7592	0.7311	0.7789	0.7165	0.7711	0.7513

2.7 Zirconium Containing Phases

Advanced glass formulation efforts have not yet focused on expanding the range of glasses containing significant concentrations of zirconium; therefore, there is little basis for changing the zirconium-containing phase T_L model or limit. It is recommended that the HTWOS 2009 model and constraint be used for advanced glass formulations until additional data are developed (Vienna et al. 2009).

This model is of the following form:

$$T_L = \sum_{i=1}^{p} t_i g_i \tag{2.12}$$

where T_L is the liquidus temperature (in °C), t_i is the i^{th} component coefficient, and g_i is the i^{th} component mass fraction. This model is summarized in Table 2.23. Similar to the other models the composition is in mass fraction. This model was shown to validate well and be predictive as long as the glasses were sufficiently high in ZrO_2 concentration (Vienna et al. 2009). The minimum g_{ZrO_2} for which the model is valid is 0.04 (i.e., 4 wt%). This model should not be applied to glasses with lower g_{ZrO_2}.

Table 2.23. T_L-Zs Composition Model Coefficients and Selected Statistical Parameters

Component, *i*	Coefficient, °C		Statistic	Value
Al_2O_3	3193.3628		R^2	0.9069
B_2O_3	651.39721		R^2_{Adj}	0.8962
LN_2O_3[(a)]	2156.4074		R^2_{Press}	0.8693
Li_2O	-1904.417		R^2_{Val}	0.8718
Na_2O	-1947.711		RMSE	26.2
SrO	13011.909		Mean	1079
ZrO_2	3747.4241		*n*	69
Others	1259.2233		-	-

(a) $g_{LN_2O_3} = g_{Y_2O_3} + g_{Ce_2O_3} + g_{Pr_2O_3} + g_{Nd_2O_3} + g_{Pm_2O_3} + g_{Sm_2O_3} + g_{Eu_2O_3} + g_{Gd_2O_3} + \ldots$

2.8 Phosphate Limits

Vienna and Kim (2008) evaluated a broad range of high phosphate glasses ($1 \leq w_{P_2O_5} \leq 6.49$ wt%) and found that the following rules effectively excluded glasses that showed deleterious effects of phosphorous on glass processing and product-quality-related properties:

$$g_{P_2O_5} \leq 0.045 \tag{2.13}$$

$$g_{CaO} \times g_{P_2O_5} < 6.5 \times 10^{-4} \tag{2.14}$$

$$g_{Li_2O} \leq 0.06 \tag{2.15}$$

where g_i is the *i*-th oxide mass fraction in glass. However, the model-validity constraints for some properties were found to be lower than this limit because of a lack of data coverage at higher concentrations of P_2O_5. McCloy and Vienna (2010) further evaluated the impact of P_2O_5 concentrations on various key properties of HLW glasses and recommended:

…that additional data with P_2O_5 concentrations extending to 4.5 wt% and above be collected and used to revise glass property models, including T_L, $T_{1\%}$, PCT-Li, and N_{TCLP}. While these data are being developed, there is a low risk of using the existing models, reported by Vienna et al. (2009), for glasses with phosphate concentrations up to 4.5 wt%.

We recommend adopting the same set of P_2O_5 limits for this effort; additional study of high phosphate (e.g., >1 wt%) glasses should also be conducted to refine the limits and ensure that phase separated glasses are avoided.

2.9 Limits and Constraints Summary

Table 2.24 lists the commonly applied limits for HLW glass and melt properties. Table 2.24 also compares the limits and models used in the WTP formulation algorithm (Vienna and Kim 2008), the HTWOS model (Vienna et al. 2009), the updated HTWOS model (McCloy and Vienna 2010), and those recommended for advanced HLW glass volume estimation. These constraints have evolved in consecutive steps; changed constraints from the previous step are highlighted in red in Table 2.24.

Table 2.24. Comparison of HLW Melt and Glass Constraints Used in HLW Glass Volume Estimation

	WTP		HTWOS 2009		HTWOS 2010		Advanced	
	Model	Value	Model	Value	Model	Value	Model	Value
PCT-B	WTP	<16.7 g/L[(b)]	**2009 rpt**	**<4 g/m^2**	2009 rpt	<4 g/m^2		
PCT-Na	WTP	<13.35 g/L	**2009 rpt**	**<4 g/m^2**	2009 rpt	<4 g/m^2	**New PCT**	<4 g/m^2
PCT-Li	WTP	<9.57 g/L	**2009 rpt**	**<4 g/m^2**	2009 rpt	<4 g/m^2		
Nepheline	*NSi*	>0.62	*NSi*	>0.62	*NSi* **OB**	>0.62 **<0.575**	**New**	**<27% prob**
TCLP [(a)]	WTP	<0.48 mg/L	**not used**	**not used**	not used	not used	not used	not used
$T_{1\%}$ Spinel	WTP	<950°C	**2009 rpt**	<950°C	2009 rpt	<950°C	**New**	**2vol%, 950°C**
Nonspinel	Al+Th+Zr Th+Zr Zr	<18% <13% <9.5%	**T_L-Zr, 2009 rpt**	**<1050°C if ZrO_2>4%**	T_L-Zr, 2009 rpt	<1050°C if ZrO_2>4%	T_L-Zr, 2009 rpt	<1050°C if ZrO_2>4%
Low η_{1150}	WTP	>2 Pa·s	**2009 rpt**	**>4 Pa·s**	2009 rpt	>4 Pa·s	2009 rpt	>4 Pa·s
High η_{1150}	WTP	<8 Pa·s	**2009 rpt**	**<6 Pa·s**	2009 rpt	<6 Pa·s	2009 rpt	<6 Pa·s
High η_{1100}	WTP	<15 Pa·s	**not used**	**not used**	not used	not used	not used	not used
Low ε_{1100}	WTP	>0.1 S/cm	**not used**	**not used**	not used	not used	not used	not used
High ε_{1200}	WTP	<0.7 S/cm	**not used**	**not used**	not used	not used	not used	not used
$CaO \times P_2O_5$	$CaO \times P_2O_5$	<6.5 wt%^{2}	$CaO \times P_2O_5$	<6.5 wt%^{2}	$CaO \times P_2O_5$	<6.5 wt%^{2}	$CaO \times P_2O_5$	<6.5 wt%^{2}
Salt	SO_3	<0.44 wt%	SO_3	**<0.5 wt%**	SO_3	**<0.6 wt%**	**New**	**SO_3 limit**
Noble Metal	Pd+Ru+Rh	<0.25 wt%	Pd+Ru+Rh	<0.25 wt%	Pd+Ru+Rh	<0.25 wt%	Pd+Ru+Rh	<0.25 wt%

(a) TCLP = Toxicity Characteristic Leaching Procedure. This constraint is only active for one waste tank with high CdO concentrations and it has been repeatedly shown not to significantly influence glass volumes.

(b) PCT responses may be normalized to component concentration in glass and reported in units of $g_{glass}/L_{solution}$ or normalized to both component concentration in glass and glass surface area and reported in units of g_{glass}/m^2_{glass} surface. If the glass has a density of roughly 2.65 g/cm^3 (as these glasses do) and a surface area to solution volume of 2000 m^{-1} is used for the test (as it was) then the 1 g/L is equivalent to 0.5 g/m^2.

With new models come new model-validity constraints. Table 2.25 summarizes the single component constraints, primarily due to model-validity ranges. Between the HTWOS 2010 constraints and the advanced constraints, there have been a number of changes (listed below).

- **Maximum $g_{Al_2O_3}$ was increased to 29 wt%.** This value represents the range of data used in the nepheline and spinel models. The viscosity, SO_3, and T_L-Zr models will need to be extrapolated. This extrapolation is not expected to be a problem because the high alumina wastes are typically limited by spinel and nepheline in the glass, not by the other properties. The PCT model ranges to 27 wt% Al_2O_3, which is close to the maximum and, based on the strong upward effect of Al_2O_3 at higher concentrations, is likely to be conservative. The viscosity model was tested against advanced glasses with Al_2O_3 concentrations as high as 29 wt%, and other than a small offset, was found to predict quite well.
- **Maximum $g_{Cr_2O_3}$ was increased to 4 wt%.** This value represents the crystal fraction of 2 vol% if all the Cr_2O_3 precipitates as eskolaite. The viscosity, PCT, SO_3, nepheline, and spinel models will all need to be extrapolated. This extrapolation poses a substantive risk for both the SO_3 (with a 1 wt% validity range) and spinel (with a 2 wt% validity range) models. Both models indicate strong negative impacts of Cr_2O_3. Chromia concentrations greater than ~ 1 wt% are expected to precipitate either as spinel (high transition metal wastes) or eskolaite (low transition metal wastes). Additional work is required to validate these models in the future.
- **Maximum g_F was increased to 2.5 wt%.** This value represents the range of data used in the HTWOS 2009 PCT and viscosity models; the nepheline model contained data with up to 6.5 wt%, the spinel model up to 2 wt%, and the SO_3 model up to 3 wt%. The HTWOS 2009 T_L-Zr model does not report an F concentration range, but lists "others" ranging up to 3.3 wt%.
- **The $g_{Fe_2O_3}$ lower bound was decreased to 0 and upper bound increased to 20 wt**%. The upper limit represents the range of data used in the HTWOS 2009 viscosity model, the nepheline model, and the spinel model. The lower limit represents the data in the SO_3, nepheline, and HTWOS 2009 viscosity model. Spinel generally does not form in glasses with less than the 2.6 wt% lower limit for that model, so the model (and associated constraint) becomes moot at the low concentrations. HTWOS 2009 PCT models must be extrapolated from 17.4 wt% to the new 20 wt% maximum.
- **Maximum g_{Na_2O} was increased to 23 wt%.** This value represents the range of data used in the HTWOS 2009 PCT-B and PCT-Na, and is below the maximum values in the HTWOS 2009 viscosity, nepheline, SO_3, and spinel models. The viscosity, PCT, SO_3, and T_L-Zr models will need to be extrapolated.

Table 2.25. Summary of Single Component Constraints, wt%

	WTP[(a)]		HTWOS 2009		HTWOS 2010		Advanced	
Comp, *i*	Min	Max	Min	Max	Min	Max	Min	Max
Al_2O_3	1.8 [1.9]	13 [8.5]	1.9	**20**	1.9	20	1.9	**29**
B_2O_3	4.5	15	4	**20**	4	20	4	20
BaO	0	"O"	0	4.7	0	4.7	0	4.7
Bi_2O_3	0	"O"	0	3.2	0	**7**	0	7
CaO	0	1	0	**7**	0	7	0	7
CdO	0	0.1 [1.6]	0	1.5	0	1.5	0	1.5
Cr_2O_3	0	0.6 [0.5]	0	**1.2**	0	1.2	0	**4**
F	0	0.44	0	**2**	0	2	0	**2.5**
Fe_2O_3	1.4 [1.9]	15 [14]	**4**	**17.4**	4	17.4	**0**	**20**
K_2O	0	1.6	0	**6**	0	6	0	6
Li_2O	0 [1.9]	6	0	6	0	6	0	6
MgO	0	1.2	0	**6**	0	6	0	6
MnO	0	8 [7]	0	7	0	7	0	7
Na_2O	3.9	20 [15]	4.1	**21.4**	4.1	21.4	4.1	**23**
Nd_2O_3	0	"O"	0	**5.9**	0	5.9	0	5.9
NiO	0	1	0	**3**	0	3	0	3
P_2O_5	0	4.5	0	**2.5**	0	**4.5**	0	4.5
PbO	0	1	0	-	0	-	0	-
SiO_2	35	53	**30.3**	53	30.3	53	30.3	53
SrO	0	10	0	10.1	0	10.1	0	10.1
ThO_2	0	6	0	6	0	6	0	6
TiO_2	0	1	0	**3.1**	0	3.1	0	3.1
UO_3	0	6.5 [6.3]	0	6.3	0	6.3	0	6.3
ZnO	0	4	0	4	0	4	0	4
ZrO_2	0	9.6 [9.1]	0	**13.5**	0	13.5	0	13.5
Others	0	5.19 [4.26]	0	-	0	-	0	-

(a) WTP model-validity constraints are different depending on if the Toxicity Characteristic Leaching Procedure (TCLP) model is used. TCLP model-validity constraints are given in square brackets for those components with differences. This model is used for glasses with $g_{CdO} > 0.1$ wt%.

This revised set of constraints and models is recommended for assessing the potential impact of continuing advanced HLW glass formulation efforts on the likely volume of HLW glass to be produced at Hanford.

2.10 Calculation Examples

Two examples are given for use in determining if application and coding of the HLW models are correct. To make these examples, two hypothetical wastes, based loosely on real projected Hanford HLW feeds, were used in glass optimization calculations. The glass formulations were optimized for maximum waste loading while maintaining component concentrations and property values within the limits described in Section 2.9. Additives, including those currently available in the WTP design (Al_2O_3, B_2O_3, CaO, Fe_2O_3, Li_2O, MgO, Na_2O, SiO_2, ZnO, and ZrO_2 as pure oxides without impurities) were selected,

and their concentrations adjusted along with waste loading until a maximum waste loading was obtained. Only B_2O_3, Li_2O, Na_2O, and SiO_2 were selected for inclusion. The details are summarized in Table 2.26.

Example 1 is a high alumina waste. It was optimized until it met four constraints with four additives (all the degrees of freedom being used up): Li_2O=6.0 wt%, SiO_2=30.3 wt%, η_{1150} = 6 Pa·s, and a probability of nepheline formation = 27%. The resulting waste loading of 47.06 wt% was obtained.

Example 2 is a high iron waste. It was optimized until it met three constraints with three additives (all the degrees of freedom being used up): η_{1150} = 4 Pa·s, spinel vol% at 950°C = 2, and a probability of nepheline formation = 27%. The resulting waste loading of 56.99 wt% was obtained.

Table 2.26. Summary of Example Calculation Results

	Limits		Example 1			Example 2		
Oxide	LL	UL	Waste	Add	Glass	Waste	Add	Glass
Al_2O_3	1.9	29	60.00	-	28.24	17.00	-	9.70
B_2O_3	4	20	-	33.73	17.86	-	13.12	5.63
Bi_2O_3	0	7	2.00	-	0.94	2.00	-	1.14
CaO	0	7	1.00	-	0.47	3.00	-	1.71
Cr_2O_3	0	4	2.00	-	0.94	1.00	-	0.57
Fe_2O_3	0	20	4.00	-	1.88	30.00	-	17.12
Li_2O	0	6	-	11.33	6.00	-	0.00	0.00
MnO	0	7	2.00	-	0.94	3.00	-	1.71
Na_2O	4.1	23	19.00	1.70	9.84	22.00	24.12	22.91
NiO	0	3	0.50	-	0.24	2.00	-	1.14
P_2O_5	0	4.5	1.00	-	0.47	1.50	-	0.86
SiO_2	30.3	53	4.50	53.24	30.30	8.00	62.77	31.52
UO_3	0	6.3	4.00	-	1.88	6.50	-	3.71
ZrO_2	0	13.5		-	0.00	4.00	-	2.28
Loading	-	-	47.06	52.94	100.00	57.06	42.94	100.00
Property								
η_{1150}, Pa·s	4	6	-	-	6.00	-	-	4.00
T_L-Zrs, °C	-	1050, if ZrO_2>4%			1192	-	-	735
$CaO \times P_2O_5$, wt%^{2}	-	6.5	-	-	2.2	-	-	1.5
Crystal fraction, vol%	-	2	-	-	1.45	-	-	2.00
Nepheline Probability	-	27	-	-	27	-	-	27
SO_3 limit, wt%	-	-	-	-	1.26	-	-	0.66
PCT Response, g/m^2	-	4	-	-	2.39	-	-	0.41

To demonstrate the application of these models to the Hanford mission and document the current expectations for increased waste loadings across the estimated HLW types, a study was performed and documented in Appendix A. The results of the calculations in Appendix A can also be used as examples to verify correct application of the models and constraints.

3.0 Low-Activity Waste Glass Constraints Set

This section summarizes the recent advances in LAW glass formulation, and recommends constraints that can be applied to estimate the amount of LAW glass that may be produced at Hanford. Alkali, sulfur, and halide loading rules, sulfur tolerance model, PCT response, VHT response, and viscosity are discussed in the following subsections. The recommended constraints are then summarized and example waste loading estimates are shown.

3.1 Loading Rules

The WTP baseline LAW glass formulation method is based on setting a waste loading and initial glass composition based on a correlation that interpolates between successful (up to pilot scale) formulations for wastes with different normalized alkali ($NAlk = g_{Na_2O} + 0.66 g_{K_2O} + 2 g_{Li_2O}$)-to-sulfur ratios of the waste. This method is summarized in Section 3.1.1. A similar approach can be used to identify the loading of advanced LAW glasses (as described in Section 3.1.2). However, the resulting glass compositions are less amenable to interpolation, as the component concentrations in glass are not smooth functions of *NAlk* from the waste. Therefore, the glass compositions (and waste loadings) will be estimated based on a combination of the rules in Section 3.1.2 and key waste glass properties constraints (sulfur tolerance, PCT response, VHT response, and viscosity) implemented by the use of property-composition models.

3.1.1 WTP Baseline Formulation Correlation

LAW glasses were formulated for a series of wastes spanning the range of waste compositions expected during the initial phase of WTP operation. Following the results of Gimpel (2002), Muller et al. (2004) fit functions between glass component concentrations and the concentrations of Na_2O, K_2O, and SO_3 in the LAW. The original waste loading was determined as the minimum of four rules:

$$w_{Na_2O} \le 21 \text{ wt\%}, \tag{3.1}$$

$$w_{Na_2O} + 0.66\ w_{K_2O} \le 21.5 \text{ wt\%}, \tag{3.2}$$

$$w_{Na_2O} + 42.5\, w_{SO_3} \le 35.9 \text{ wt\%, and} \tag{3.3}$$

$$w_{SO_3} \le 0.77 \text{ wt\%}. \tag{3.4}$$

These constraints are shown schematically in Figure 1.2. However, later analysis showed the need to add loading rules related to the concentrations of halogens, chromium, and phosphorous in the waste (Kim and Vienna 2012):

$$NH \le 1.4656 - 2.1111 \times w_{SO_3} \text{ wt\% for } w_{SO_3} \le 0.59 \text{ wt\%} \tag{3.5}$$

$$NH \le 0.22 \text{ wt\% for } w_{SO_3} > 0.59 \text{ wt\%} \tag{3.6}$$

$$w_{Cr_2O_3} \le 0.63 \text{ wt\% for } w_{P_2O_5} \ge 2.79 \text{ wt\%} \tag{3.7}$$

$$w_{K_2O} \le 5 \text{ wt\% for } w_{P_2O_5} \ge 2.79 \text{ wt\%} \tag{3.8}$$

$$w_{Cr_2O_3} \le 0.63 \text{ wt\% for } w_{P_2O_5} < 2.79 \text{ wt\% and } w_{K_2O} \le 0.54 \text{ wt\%} \tag{3.9}$$

$$w_{Cr_2O_3} \le 0.08 \text{ wt\% for } w_{P_2O_5} < 2.79 \text{ wt\% and } 0.54 < w_{K_2O} \le 5 \text{ wt\%} \tag{3.10}$$

where *NH* is normalized halogen (= w_{Cl} + 0.3 w_F). These rules are shown schematically in Figure 1.2 and Figure 1.4.

3.1.1.1 Glass Composition Determination

With the waste loading determined, the concentration of other components in glass are either held constant or are based on the waste alkali concentration d = Na_2O + 0.66 K_2O wt%. Constant concentrations (wt%) of Al_2O_3 (6.1), B_2O_3 (10), Fe_2O_3 (5.5), TiO_2 (1.4), ZnO (3.5), and ZrO_2 (3) are targeted. The concentrations of CaO, MgO, and Li_2O are determined from fitted smooth functions of d (Muller et al. 2004):

$$w_{CaO} = 1.5 + 5.5\left\{1 + \exp\left[\frac{d-17}{2}\right]\right\}^{-1} \tag{3.11}$$

$$w_{Li_2O} = 4.3\left\{1 - \frac{[d-5.4]^2}{12.75^2}\right\}^{0.7} \text{ wt\% for } d < 18.15\%$$

$$= 0 \text{ wt\% for } d \ge 18.15 \text{ wt\%} \tag{3.12}$$

$$w_{MgO} = 1.48 + 1.49\{1 + \exp[d-9]\}^{-1} \text{ wt\%.} \tag{3.13}$$

Finally, the SiO_2 concentration is then adjusted so that the glass composition sums to 100%:

$$w_{SiO_2} = 100 - w_{Waste} - w_{Al_2O_3} - w_{B_2O_3} - w_{Fe_2O_3} - w_{TiO_2} - w_{ZrO_2} - w_{CaO} - w_{Li_2O} - w_{MgO} \tag{3.14}$$

3.1.2 Advanced Formulation Loading Rules

A similar approach to determining advanced glass waste loading was developed by Muller et al. (2010) as shown schematically in Figure 3.1. The data used to develop this plot are summarized in Table 3.1.

This correlation leads to the following rules:

$$w_{Na_2O} + 0.66\, w_{K_2O} \le 24, \text{ wt\%} \tag{3.15}$$

$$w_{Na_2O} + 0.66\ w_{K_2O} \le 33.94 - 11.69\ w_{SO_3}, \text{ wt\%} \tag{3.16}$$

$$w_{SO_3} \le 1.5, \text{ wt\%} \tag{3.17}$$

These rules are compared in Figure 3.1.

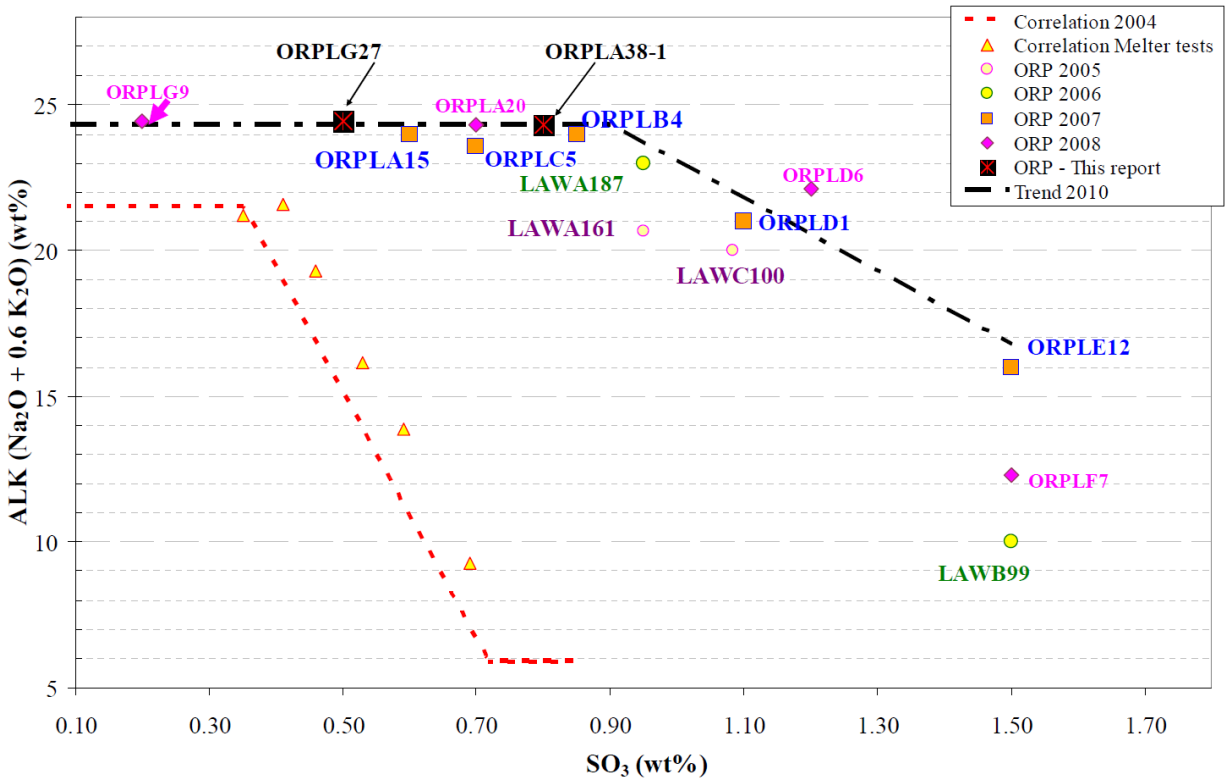

Figure 3.1. Overview of Waste Alkali Concentration (*d*) and SO_3 Loadings for Advanced LAW Glasses (Muller et al. 2010)

Table 3.1. Summary of Advanced LAW Correlation Glasses

Glass ID	Target w_{SO_3}	Measured w_{SO_3}	Target w_{Na_2O}	Target w_{K_2O}	*d*
ORPLG9	0.2	0.21	21.08	5.77	24.89
ORPLG27	0.5	-	21.08	5.77	24.89
ORPLA20	0.7	0.63	24.04	0.54	24.40
ORPLC5	0.7	0.61	23.69	0.54	24.05
ORPLA38-1	0.8	-	24.24	0.54	24.60
ORPLB4	0.85	0.81	24.12	0.11	24.20
LAWA187	0.95	0.77	23.17	0.51	23.51
LAWA161	1	-	20.70	0.44	20.99
LAWC100	1.1	1.05	20.24	0.15	20.34
ORPLD1	1.1	0.89	21.21	0.16	21.31
ORPLD6	1.2	1.25	22.22	0.17	22.34
LAWB99	1.5	1.14	10.08	0.41	10.35
ORPLE12	1.5	1.38	16.20	0.56	16.57
ORPLF7	1.5	1.35	12.24	0.51	12.57

The impacts of halogen and chromium concentrations on the *d*-SO_3 loading limits need to be evaluated. Two methods were used to estimate these impacts:

1. Conservative method: Plot the concentrations of SO_3-Cl-F-Cr_2O_3 in melter tests and divide the compositions with salt from those without salt. This is the same approach used for the WTP baseline formulation correlation waste loading rules (Section 3.1.1).
2. Optimistic method: Compile both the successful melter test and crucible-scale SO_3 solubility data and identify the maximum SO_3 solubility as a function of Cl, F, and Cr_2O_3 in the feed. This would give an optimistic upper bound on Cl, F, and Cr_2O_3 tolerance without salt separation. Note that Section 3.2 discusses the correlation between SO_3 solubility and salt accumulation during melter tests.

To define the conservative approach, the melter tests with salt accumulation and without salt accumulation are plotted in Figure 3.2. A range of component ratios were considered to better separate the salt-forming from the non-salt-forming compositions using the general functional form:

$$NH = \sum_{i=1}^{p} b_i g_i \tag{3.18}$$

where *NH* is the modified normalized halogen concentration, b_i is the i^{th} component coefficient, and g_i is the i^{th} component mass fraction.

The number of "false-positives" (the number of tests predicted to form salt while not forming salt) was minimized while maintaining no "false negatives" by adjusting the coefficients b_i and using no more than three line segments. It was found that when i = Cl, F, Cr_2O_3, and K_2O, b_i values were 1.000, 0.607, 0.542, and 1.000, respectively. The results are shown in Figure 3.2 with the two fitted line segments with equations:

$$g_{Cl} + 0.607 g_F + 0.542\, g_{Cr_2O_3} + g_{K_2O} \le 3.746 - 4.694\, w_{SO_3} \text{ for } w_{SO_3} < 0.59 \text{ wt\%} \tag{3.19}$$

$$g_{Cl} + 0.607 g_F + 0.542\, g_{Cr_2O_3} + g_{K_2O} \le 1.243 - 0.4506\, w_{SO_3} \text{ for } w_{SO_3} \ge 0.59 \text{ wt\%} \tag{3.20}$$

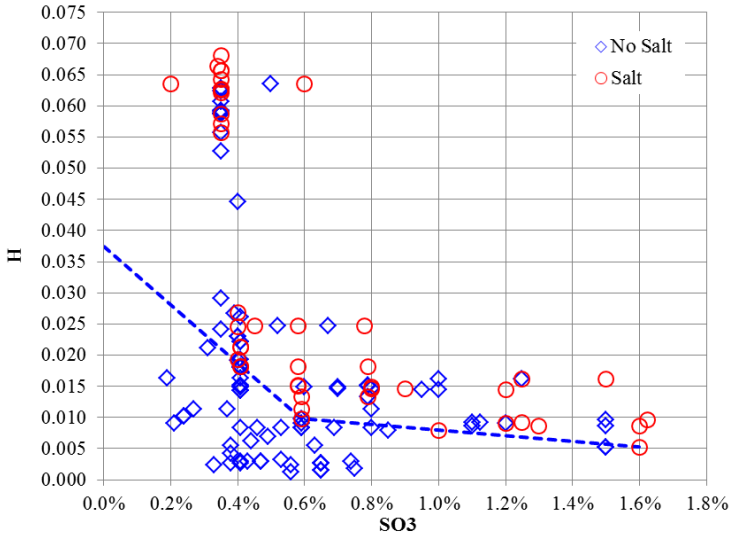

Figure 3.2. Plot of w_{SO_3} vs. $NH = g_{Cl} + 0.607g_F + 0.542\, g_{Cr_2O_3} + g_{K_2O}$ from Melter Tests With and Without Salt Accumulation

For an optimistic halide rule, the crucible-scale SO_3 saturation and maximum SO_3 in melter tests without salt accumulation are plotted against NH ($g_{Cl} + 0.3g_F + 0.4\, g_{Cr_2O_3}$). The following equation of a line roughly represents the maximum concentrations of SO_3, Cl, F, and Cr_2O_3 that do not form a salt (see related plot in Figure 3.3):

$$w_{SO_3} \leq 1.65\text{-}0.725(g_{Cl} + 0.3g_F + 0.4\, g_{Cr_2O_3}) \tag{3.21}$$

This "optimistic" method describes the maximum concentrations of halides and chromium for which glasses have been formulated and tested without salt formation. Therefore, applying it will give an estimate of the maximum that could be formulated for each given waste.

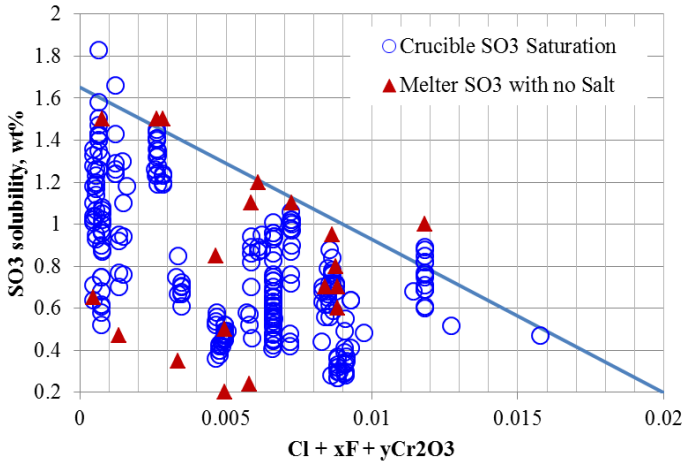

Figure 3.3. Plot of w_{SO_3} vs. $g_{Cl} + 0.3g_F + 0.4\, g_{Cr_2O_3}$

To summarize the "halide" rules, two options are considered. The first approach is a conservative limit that avoids salt formation for all the melter tests performed. The second approach is optimistic and represents the maximum loadings that have been successfully demonstrated at the crucible or melter-scale. Real "halide" limits likely lie between the two approaches. Figure 3.4 summarize these rules.

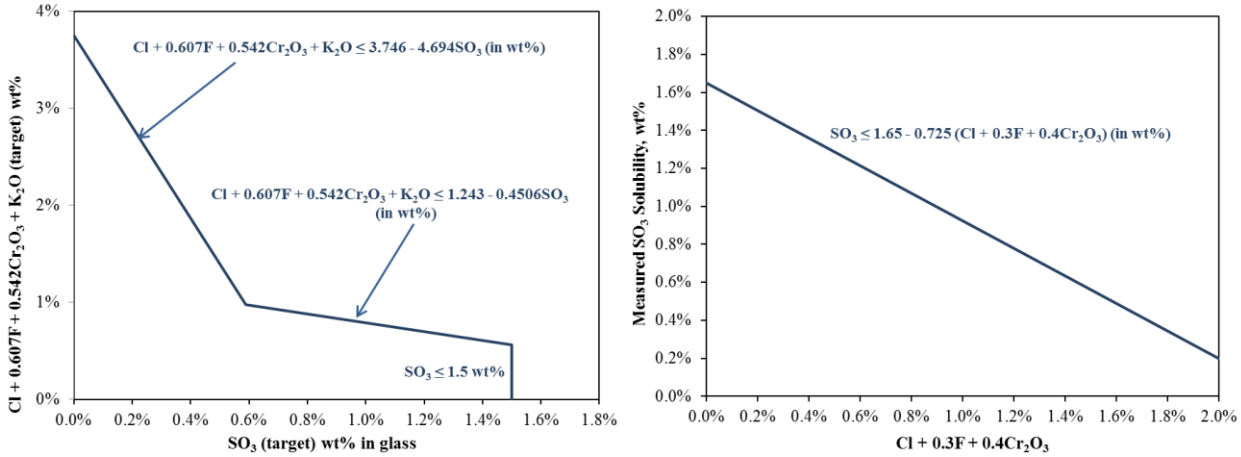

(a) Conservative (b) Optimistic

Figure 3.4. Proposed Cl-F-Cr_2O_3-SO_3-K_2O Loading Rules

3.1.2.1 Glass Composition Determination

The glass compositions used to define the loading rules for advanced LAW formulations were plotted (Figure 3.5) as functions of d, w_{SO_3}, and w_{SO_3} / d to try to develop a correlation similar to the one used for the WTP baseline formulations. Trends are apparent for some additive components—CaO, Li_2O, MgO, SnO_2, and ZrO_2—but not apparent for other additive components—Al_2O_3, B_2O_3, Fe_2O_3, and V_2O_5. In the case of the WTP baseline formulations, concentration trends (as a function of d) were apparent for every additive component. Therefore, determining the compositions of advanced LAW glasses will not be as simple as applying a correlation to interpolate between successful, optimized data points.

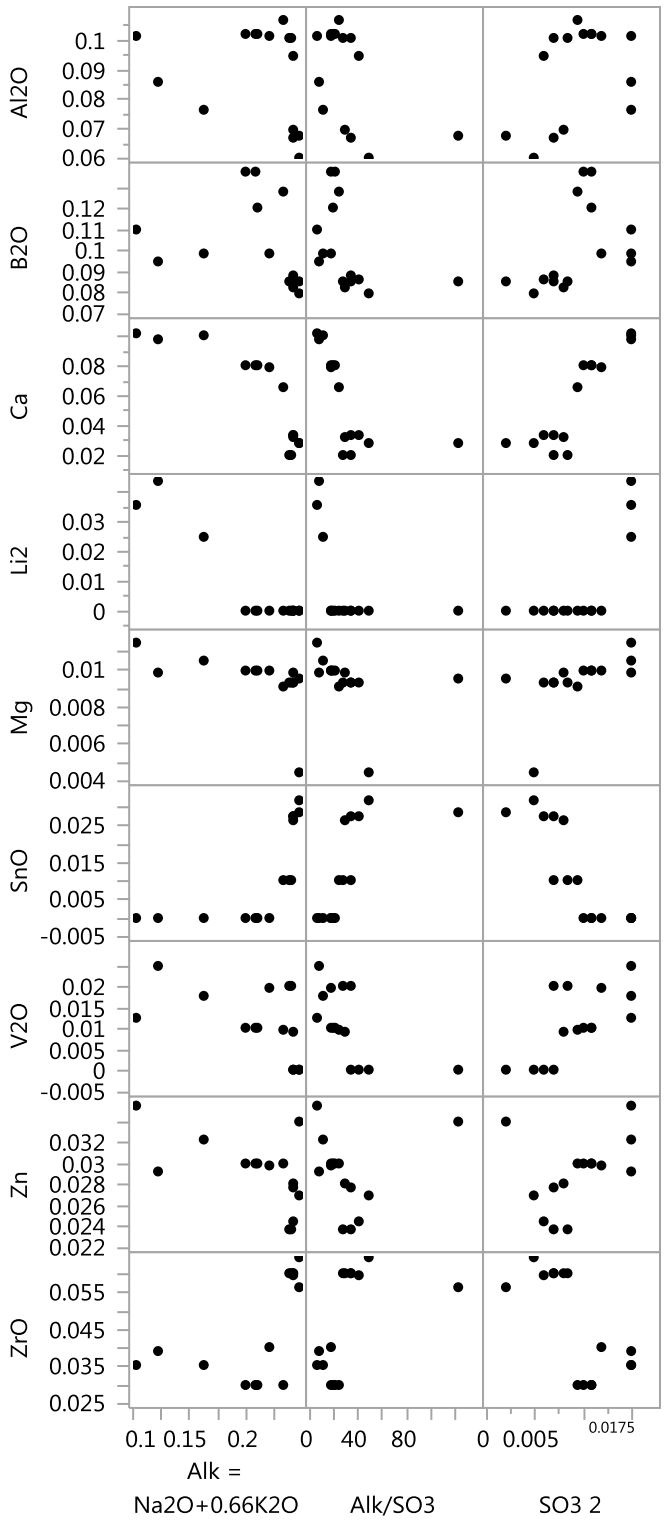

Figure 3.5. Pairwise Plots of Glass Components vs. *d* and SO_3 for Glasses Used to Define the Waste Loading Limits

It is therefore recommended that once the loading is determined based on the rules defined in Section 3.1.2, the glass property models and constraints discussed in Sections 3.2 through 3.6 be used to develop an optimized glass formulation meeting all the constraints. To assist in this formulation, the trends in CaO, Li_2O, MgO, SnO_2, and ZrO_2 concentrations can be used in obtaining a starting point for the optimization.

3.2 Sulfur Tolerance

Salt accumulation in the melter will increase the corrosion rates of melter components in contact with the salt, increase volatility, and potentially supersaturate the melt with salt that will separate into a water-soluble phase when the glass is canister-cooled. Therefore, constraints must be put in place to avoid the accumulation of salt in the melter. SO_3 tolerance models were developed for HLW glasses and combined the data sets of HLW and LAW glasses in Section 2.2. It was concluded in Section 2.2.5 that a combined HLW and LAW SO_3 model was the preferred option for predicting the salt accumulation in the HLW glasses. Here, a model is developed with the crucible-scale LAW-only data as described in Section 2.2 for comparison purposes.

A database of crucible-scale SO_3 saturation data was compiled for modeling. The crucible-scale saturation test included the melting of a target glass composition with excess Na_2SO_4. This forms a two-phase mixture—a glass melt and a Na_2SO_4-based molten salt. The melt is quenched and ground. The resulting powders are acid leached to remove the excess salt. The remaining glass is dissolved and analyzed for concentration of SO_3, which is reported as the crucible saturation concentration of SO_3. Note that the physical/chemical form of sulfur in the glass is not determined and tracked for each glass. Therefore, the concentration is listed as SO_3 only as a mass accounting method for glass composition. Nine data sets are combined to generate the SO_3 concentration model data. These data are listed in Appendix B and summarized in Table 3.2. The compositions listed are normalized after removing the SO_3 concentration. Figure 3.6 shows a scatterplot matrix of the compositions associated with the model data. It was determined through modeling efforts that the halogen impacts the salt separation in a ratio of Cl + 0.3 F, or normalized halogen (*NH*). With the exceptions of the following pairs, the data appear to cover the composition space well: K_2O-Li_2O, Fe_2O_3-SnO_2, Li_2O-SnO_2, and K_2O-V_2O_5. The ranges of component concentrations for the data are listed in Table 3.3.

Table 3.2. Summary of $w_{SO_3}^{Sat}$ Model Data

Data Set	Group	Number of Data Points	Reference Document	Comments
TWRS Part A LAW	WTP	1	(Muller et al. 1998)	-
2001 WTP LAW	WTP	42	(Muller et al. 2001)	-
WTP Baseline	WTP	58 (55)	(Muller and Pegg 2003)	3 data points did not use acid leaching and so were excluded
SO_3 Improvement	ORP	14	(Matlack et al. 2005)	-
Env. C Improvement	ORP	4	(Matlack et al. 2006b)	-
Env. A, B Improvement	ORP	36	(Matlack et al. 2006a)	-
Enhanced LAW	ORP	41	(Matlack et al. 2007b)	-

Data Set	Group	Number of Data Points	Reference Document	Comments
LAW DM-10	ORP	41	(Matlack et al. 2009a)	-
LAW Loading	ORP	30	(Muller et al. 2010)	-

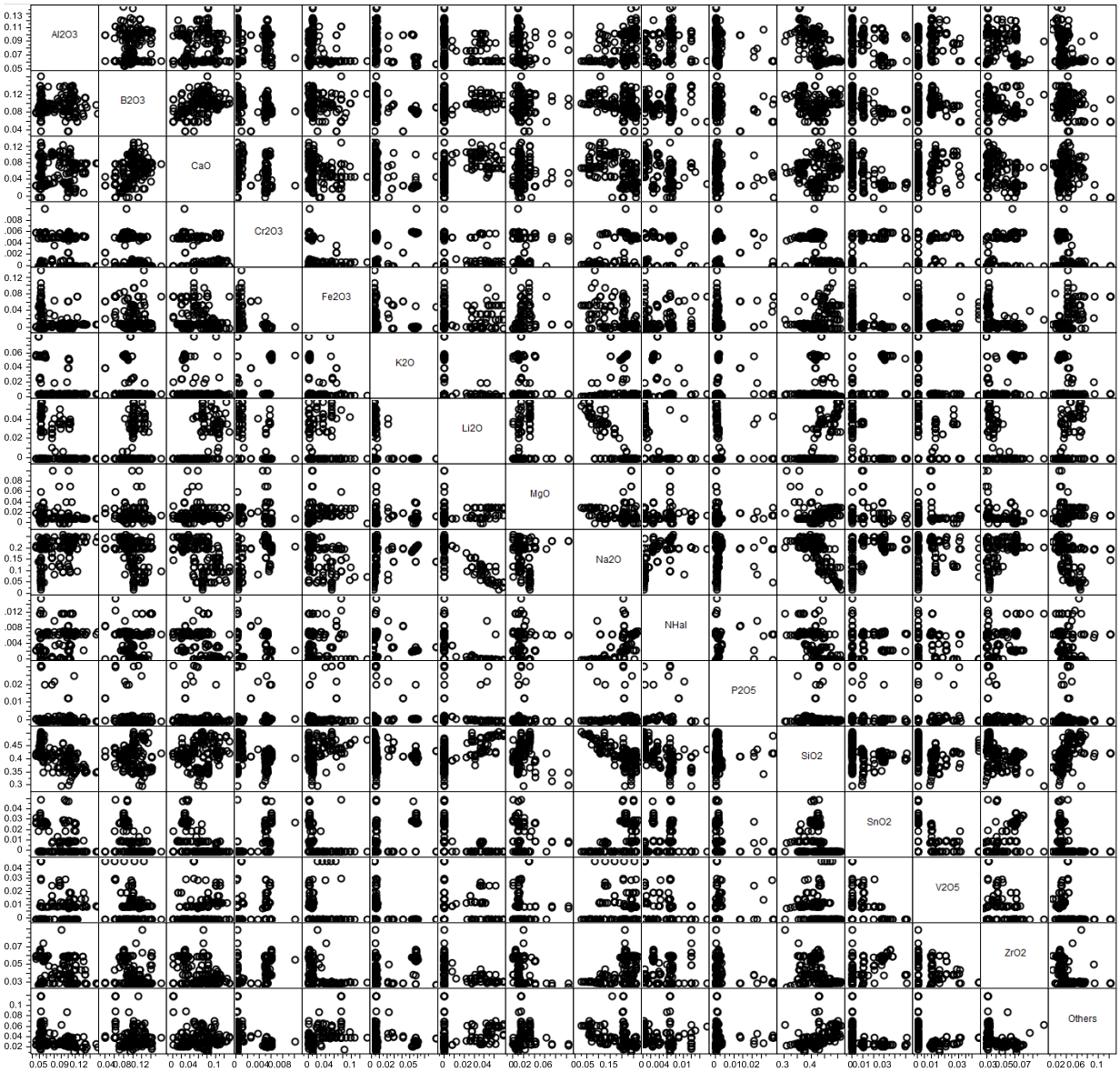

Figure 3.6. Scatterplot Matrix of $w_{SO_3}^{Sat}$ Model Data

Table 3.3. $w_{SO_3}^{Sat}$ Model Data Component Concentration Ranges

Oxide	Min	Max
Al_2O_3	5.53	13.95
B_2O_3	3.98	16.06
CaO	0.00	12.94
Cl	0.00	1.17
Cr_2O_3	0.01	1.00
F	0.00	3.06
Fe_2O_3	0.00	13.54
K_2O	0.11	8.34
Li_2O	0.00	5.86
MgO	0.00	10.10
Na_2O	2.48	26.05
P_2O_5	0.00	3.08
SiO_2	30.05	50.64
SnO_2	0.00	5.01
TiO_2	0.00	4.11
V_2O_5	0.00	4.39
ZnO	0.00	5.86
ZrO_2	2.62	9.02
Minor[(a)]	0.00	7.91

(a) Minor equals all other components not specifically listed. Only BaO, Bi_2O_3, CoO, CuO, Gd_2O_3, La_2O_3, MnO, Sb_2O_3, and SrO are in more than one wt% in the minor components. SrO, La_2O_3, and Gd_2O_3 are >1 wt% for two glasses each, while BaO, Bi_2O_3, CoO, CuO, MnO, and Sb_2O_3 are >1 wt% for only one glass each.

Only one model form was attempted to model the SO_3 saturation data—the partial quadratic model in Equation 2.6. Initial attempts were to include only linear terms (first term in the model form above). However, it was quickly determined that the addition of a second order term ($Li_2O \times Li_2O$) improved both the model-fit statistics and the model validation statistics. The final model terms are summarized in Table 3.4, and the model-fit is shown graphically as a predicted vs. measured plot in Figure 3.7.

Table 3.4. Summary of $w_{SO_3}^{Sat}$ Model Coefficients and Fit Statistics

Term	Coefficient	Statistic	Value
Al_2O_3	-2.228782	R^2	0.8871
B_2O_3	2.7402042	R^2_{Adj}	0.8797
CaO	3.8795344	R^2_{Press}	0.8668
Cr_2O_3	-12.93979	RMSE	0.114
Fe_2O_3	-0.24149	$RMSE_{Press}$	0.120
K_2O	0.900221	Mean of response	0.7865
Li_2O	2.9000608	# of data points	263
MgO	-1.270796	-	-
Na_2O	3.0095451	-	-
NH	-22.20178	-	-
P_2O_5	4.3573512	-	-
SiO_2	-0.233355	-	-
SnO_2	-2.503471	-	-
V_2O_5	8.0476827	-	-
ZrO_2	-2.117697	-	-
Others	1.5505865	-	-
$Li_2O \times Li_2O$	262.04827	-	-

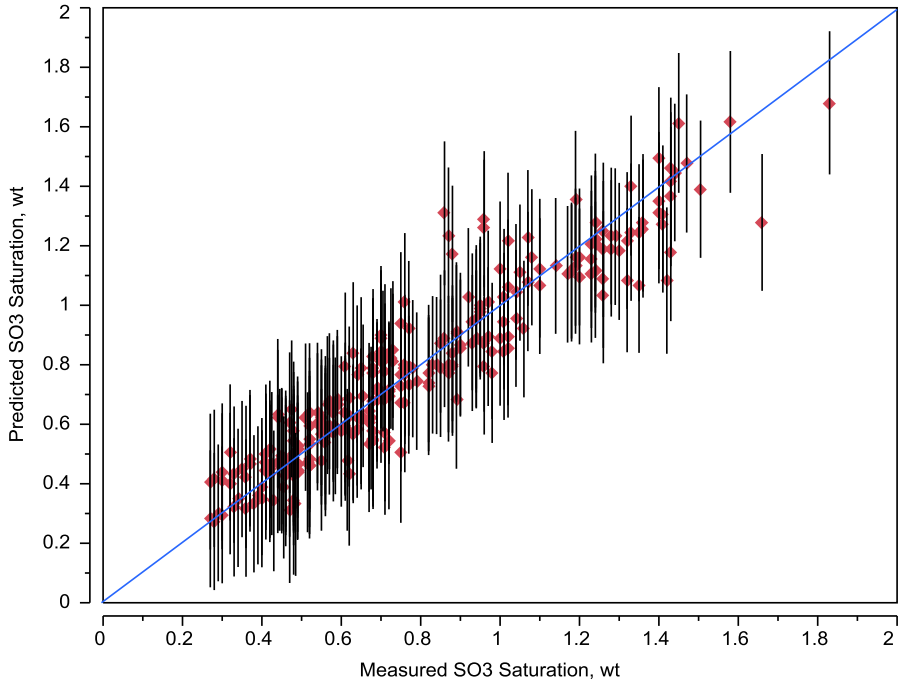

Figure 3.7. Comparison of Predicted and Measured Crucible-Scale $w_{SO_3}^{Sat}$ With 95% Confidence Interval for Individual Prediction, wt%

To validate the model, data not used in model fitting must be obtained. Because all appropriate data within the desired composition region were used in model fitting, subsets of the model data were used to

validate the model. The data were sorted by SO_3 saturation value. The data were then numbered 1, 2, 3, 4, 5, 1, 2, … to split them into five representative groups of roughly 20% of the data. The same model form (including the same set of terms) was then refit to subsets 2 to 5 and used to predict data in subset 1. Then the model was fit to each group of four subsets and used to predict the remaining subset in sequence. Table 3.5 summarizes the results of the model validation. The coefficients are reasonably close, having RSDs of less than 25%, with the exceptions of Fe_2O_3, MgO, P_2O_5, and SiO_2. Only the Fe_2O_3 and SiO_2 coefficients show >50% RSD, and those coefficients are very close to 0. The model-fit R^2 values are all close to each other at approximately 0.89. The R^2_{val} values are all between 0.82 and 0.90. The average R^2_{val} value is almost identical to the R^2_{Press}value of 0.86. This model is well validated, and should give predictions of unknown data within the model-validity region nearly as well as for the model-fit data.

Table 3.5. Summary of $w^{Sat}_{SO_3}$ Model Validation Data

Fit Statistics	Full Model	Grp 1	Grp 2	Grp 3	Grp 4	Grp 5	Average
R^2	0.8871	0.8971	0.8910	0.8820	0.8913	0.8856	0.8894
R^2_{Adj}	0.8797	0.8886	0.8820	0.8722	0.8823	0.8762	0.8803
R^2_{Press}	0.8668	0.8756	0.8667	0.8541	0.8628	0.8596	0.8638
RMSE	0.114	0.110	0.113	0.116	0.114	0.117	0.114
$\mathrm{RMSE_{Press}}$	0.120	0.116	0.120	0.124	0.123	0.124	0.122
Validation							
R^2_{Val}	-	0.8272	0.8587	0.8960	0.8525	0.8819	0.8633

To apply this model (based on crucible-scale SO_3 saturation data) to the consistently higher melter-scale data, an offset must be added. There is a roughly constant offset between the melter data and the crucible-scale saturation data (Figure 2.13). Taking the data listed in Table 3.2, we subtracted the crucible-scale SO_3 saturation from the maximum concentration of SO_3 in melter tests without salt formation. The average difference (melter-saturation) is 0.2115 wt%, with a standard deviation of 0.1398 wt%. Using this offset, we can estimate the sulfur tolerance of a feed by adding 0.2115 wt% to the predicted crucible-scale SO_3 saturation value.

Comparing this model to that described in Section 2.2.3, both models fit the data and are well validated with data not used in their fitting. However, the slightly improved fit statistics of the LAW-only model does not, in our opinion, outweigh the advantage of the additional data, broader composition region, and more general applicability of the combined LAW and HLW model. We therefore recommend that the combined LAW and HLW crucible-scale model described in Section 2.2.3 and recommended in Section 2.2.5 be used to determine LAW SO_3 tolerance.

3.3 Product Consistency Test Response

The WTP contract requires glasses to have 7-d normalized PCT Na, B, and Si responses below 2 g/m^2 (DOE 2000):

2.2.2.17.2 Product Consistency Test: The normalized mass loss of sodium, silicon, and boron shall be measured using a seven day product consistency test run at 90°C as defined in ASTM C1285-98. The test shall be conducted with a glass to water ratio of 1 gram of glass (-100 +200 mesh) per 10 milliliters of water. The normalized mass loss shall be less than 2.0 grams/m^2. Qualification testing shall include glass samples subjected to representative waste form cooling curves. The product consistency test shall be conducted on waste form samples that are statistically representative of the production glass.

For glasses with typical densities near the reference value of 2.65 g/cm^3, this translates to normalized losses of 4.0 g/L.

Glasses with high alkali content tend to challenge this constraint (Figure 3.8). PCT responses of all glasses fall far below the limit when the *NAlk* is below 18 wt%. However, above a *NAlk* of 18 wt%, some glasses exceed the contract limit PCT response while others do not. In fact, glasses with *NAlk* as high as 26 wt% (ORPLA25) still meet the contract limits. A model is needed to predict PCT responses of high alkali glasses to avoid failing the contract PCT constraint.

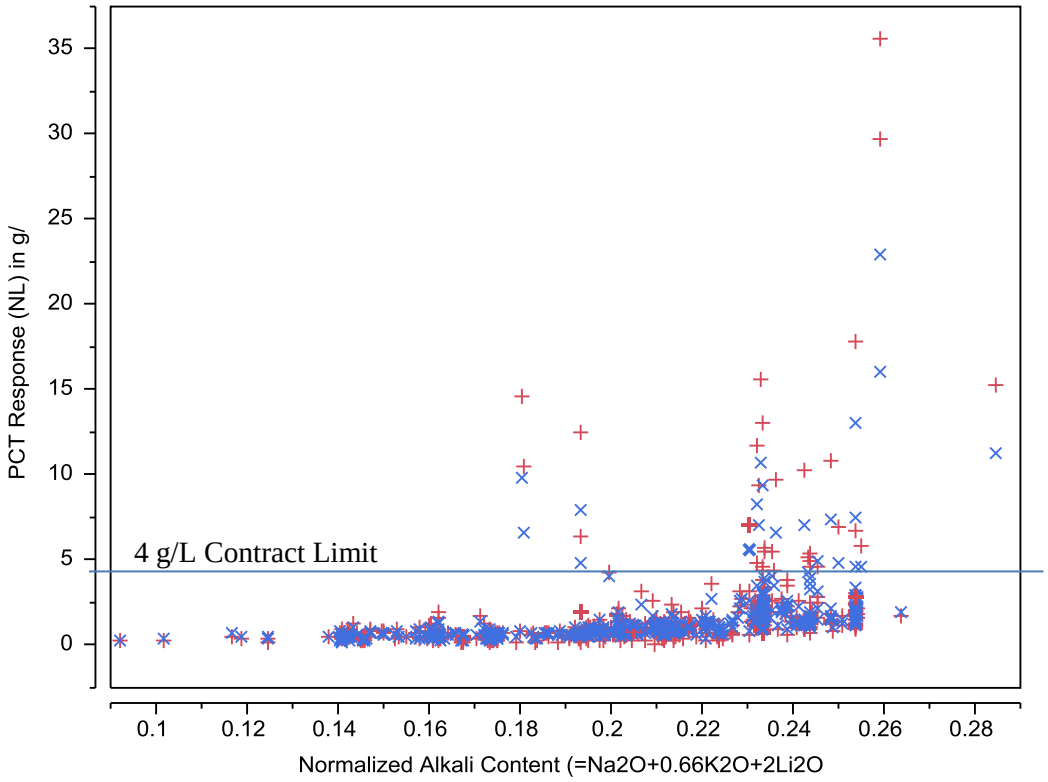

Figure 3.8. Comparison of PCT Normalized Na and B Responses to *NAlk* of LAW Glasses (NL in g/L, alkali content in mass fraction, × for NL[Na], + for NL[B])

A database of LAW glasses was compiled to model their PCT responses. These data include crucible-scale tests with simulants, melter tests with simulants, and crucible-scale tests with actual LAW. The data, summarized in Table 3.6, were compiled for modeling, and are listed in Appendix B. It should

be noted that two additional LAW glass datasets were considered for inclusion in the model data set: 1) the in-container vitrification set (Kim et al. 2003), which was excluded because it was based on boron free glasses, and 2) the Tank Waste Remediation System (TWRS) low-level waste glass set (Feng et al. 1996), which was excluded because of the large fraction of data points falling outside the target composition region. The data set was evaluated for composition coverage and appropriateness to use in models. Five data points (Table 3.7) with relatively extreme compositions were excluded from the fit, leaving a relatively even coverage of the remaining composition space. Note that Fe_2O_3 and V_2O_5 plus K_2O and V_2O_5 are almost mutually exclusive in the data set; V_2O_5 is found in significant concentrations only in glasses with very low Fe_2O_3 and K_2O contents (Figure 3.9). The final PCT model component concentration ranges are listed in Table 3.8.

Table 3.6. Summary of LAW PCT Data Sets

Data Set	# of Data Points	Reference	Comments
ORP	174	(Muller et al. 2012)	Advanced glass formulations with high waste loading
WTP	264	(Piepel et al. 2007)	Data used to develop WTP LAW glass models
HLP	63	(Vienna et al. 2001a)	Study glasses used to set the contract limits for LAW glass performance

Table 3.7. Glasses Excluded from PCT Model Fitting

Excluded Component Concentration Region	Glasses Removed
$B_2O_3 < 2$ wt%	HLP-52
$Cr_2O_3 > 1$ wt%	LAWECr2CCC
Fe^{II}/Fe total > 10%	HLP-44, HLP-45
$La_2O_3 > 0.5$ wt%	HLP-51

Table 3.8. Component Concentration Ranges for PCT Model Data

Component	Min	Max
Al_2O_3	3.50	13.85
B_2O_3	5.00	15.15
CaO	0.00	12.81
Cl	0.00	1.17
Cr_2O_3	0.00	0.63
Cs_2O	0.00	0.19
F	0.00	1.00
Fe_2O_3	0.00	15.77
K_2O	0.00	8.08
Li_2O	0.00	6.29
MgO	0.00	9.94
Na_2O	2.46	26.01
P_2O_5	0.00	4.75
SiO_2	29.82	59.80
SnO_2	0.00	5.00
SO_3	0.06	2.17
TiO_2	0.00	8.59
V_2O_5	0.00	3.00
ZnO	0.00	5.82
ZrO_2	0.00	6.75
Minors[(a)]	0.07	2.17

(a) Minors equal the sum of all components not specifically listed here.

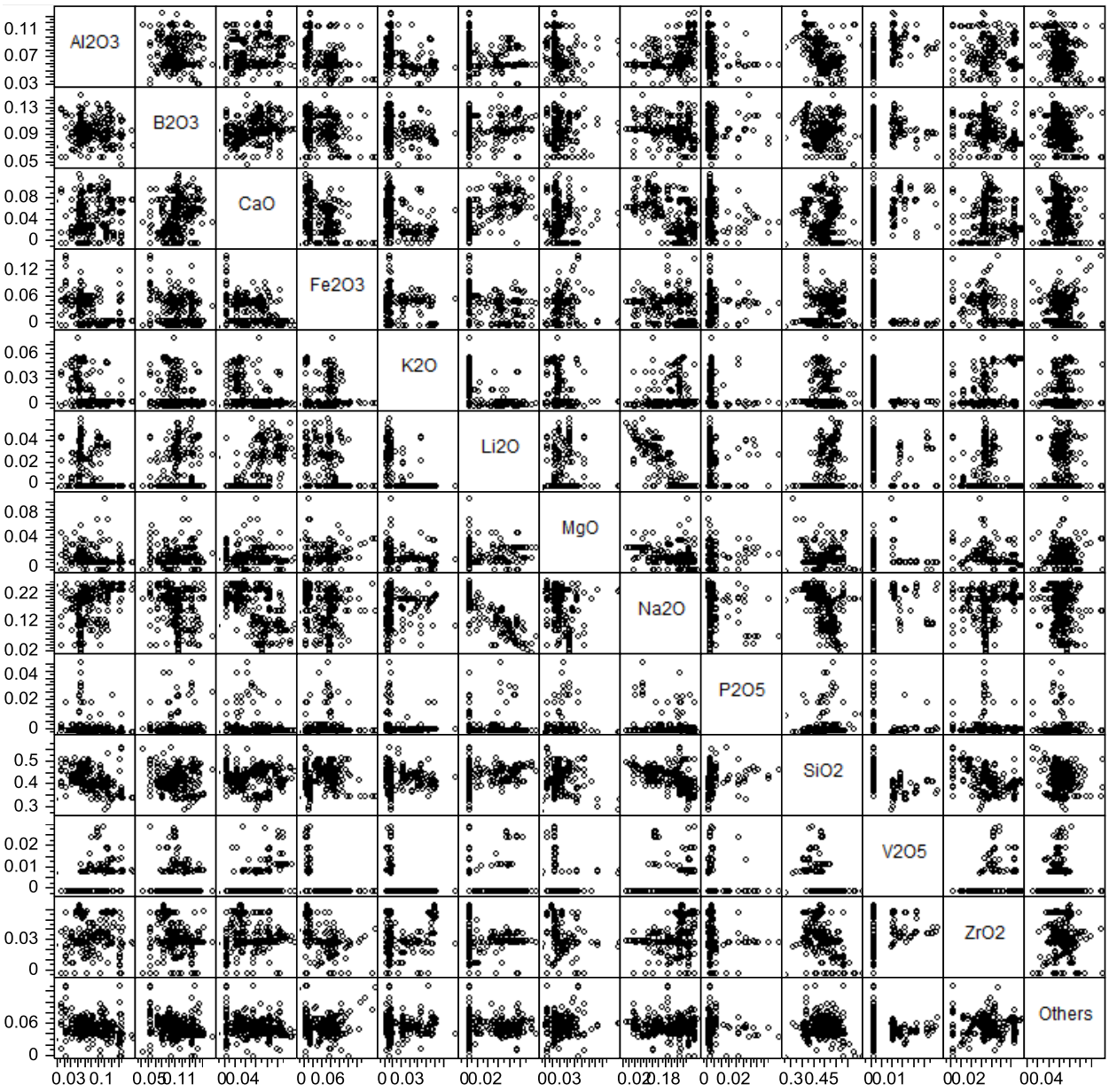

Figure 3.9. Scatterplot Matrix of PCT Model Data

Repeated analyses show that the PCT normalized silicon responses fall well below those of sodium and boron; generally sodium and boron responses are nearly the same. With the exception of one outlier (HLP-46, LD6-5412), NL(Si) are below NL(B), and generally NL(B) ≅ NL(Na) as shown in Figure 3.10. Therefore, there is no need to model or control composition for NL(Si). Rather than fit NL(B) and NL(Na) separately, it was decided to average the natural logarithm (Ln) of the two values for each glass and fit the average (Ln[NL(B)], Ln[NL(Na)]) value as a measure of PCT response of these glasses.

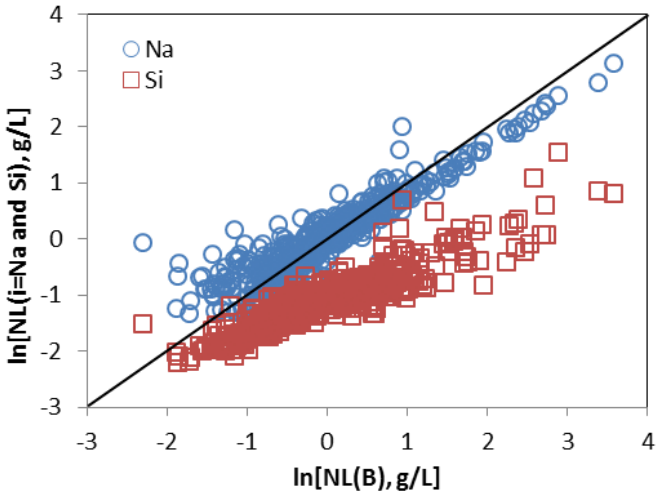

Figure 3.10. Comparison of NL(B), NL(Na), and NL(Si)

Only one model form was attempted to model the LAW glass PCT response—the partial quadratic model:

$$\text{Ln}[\text{NL, g/L}] = \sum_{i=1}^{p} b_i g_i + selected\left\{\sum_{i=1}^{p-1}\sum_{j=i+1}^{p} b_{ij} g_i g_j\right\} \quad (3.22)$$

Initial attempts were to include only linear terms (first term in the model form above). However, it was quickly determined that the addition of second order terms improved both the model-fit statistics and the model validation statistics. The final model terms are summarized in Table 3.9, and the model-fit is shown graphically as a predicted vs. measured plot in Figure 3.11.

Table 3.9. Summary of PCT Response Model Coefficients and Fit Statistics, in g/L

Term	Estimate	Statistic	Value
Al_2O_3	-69.07589	R^2	0.8229
B_2O_3	13.020929	R^2_{Adj}	0.8174
CaO	-7.234449	R^2_{Press}	0.8022
Fe_2O_3	-6.318672	RMSE	0.334
K_2O	10.099748	$RMSE_{Press}$	0.348
Li_2O	27.748976	Mean of Response	0.011
MgO	7.1092189	# of data points	496
Na_2O	16.667725	-	-
P_2O_5	-9.063384	-	-
SiO_2	-3.07673	-	-
V_2O_5	9.3277525	-	-
ZrO_2	-8.556034	-	-
Others	-1.157161	-	-
$Al_2O_3 \times Al_2O_3$	361.93083	-	-
$CaO \times Fe_2O_3$	163.17256	-	-
$MgO \times ZrO_2$	592.93753	-	-

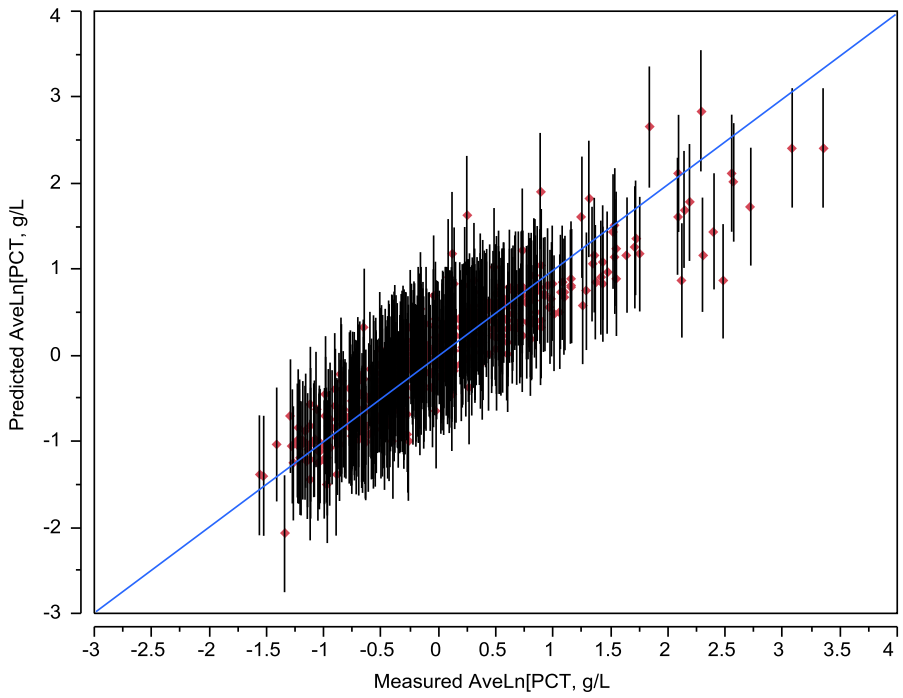

Figure 3.11. Predicted vs. Measured Average (Ln[NL]) with 95% Confidence Interval for Individual Prediction

To validate the model, data not used in model fitting must be obtained. Because all appropriate data within the desired composition region were used in model fitting, subsets of the model data were used to validate the model. The data were sorted by average (Ln[NL]) value. The data were then numbered 1, 2, 3, 4, 5, 1, 2, … to split them into five representative groups of roughly 20% of the data. The model was then refit to subsets 2 to 5 and used to predict data in subset 1. Then the model was fit to each group of four subsets and used to predict the remaining subset in sequence. Table 3.10 summarizes the results of the model validation. The coefficients are reasonably close; they had an RSD of less than 25%, with the exceptions of MgO and Others. Only the "Others" coefficients show >40% RSD. The model-fit R^2 values are all close to each other at approximately 0.82. The R^2_{Val} values are also close to 0.82, with the exception of group 4, which has an R^2_{val} of 0.75 and an MgO coefficient roughly double all the other groups. It is not clear why the fit for group 4 is different from the rest. The average R^2_{val} value is almost identical to the R^2_{Press}value of 0.80. This model is well validated and should give predictions of unknown data within the model-validity region nearly as well as for the model-fit data.

Table 3.10. Summary of PCT Model Validation Data

Components	Full Model	Grp 1	Grp 2	Grp 3	Grp 4	Grp 5	%RSD
Al_2O_3	-69.07589	-67.969	-69.2049	-71.1411	-67.6869	-68.8492	-2.0
B_2O_3	13.020929	12.197258	14.045565	13.22309	13.17081	12.67552	5.3
CaO	-7.234449	-6.956006	-7.640977	-6.97383	-7.40321	-7.20958	-4.0
Fe_2O_3	-6.318672	-5.164495	-7.457974	-6.49346	-7.22671	-5.52111	-16.0
K_2O	10.099748	9.9833717	9.7882282	10.72099	9.299774	10.65577	6.0
Li_2O	27.748976	26.665821	26.461763	28.20851	26.77714	30.20904	5.7
MgO	7.1092189	6.4462014	5.1138895	5.889306	11.95775	6.67606	38.2
Na_2O	16.667725	16.131029	16.51355	17.07661	16.50862	17.01485	2.4
P_2O_5	-9.063384	-7.696309	-8.870755	-9.9238	-9.86013	-8.8276	-10.1
SiO_2	-3.07673	-2.839805	-2.922018	-2.98631	-3.38361	-3.31255	-7.9
V_2O_5	9.3277525	10.143102	8.5526628	10.16775	9.774255	7.815441	11.3
ZrO_2	-8.556034	-7.953202	-8.623589	-9.26938	-7.79964	-8.65066	-6.9
Others	-1.157161	-1.8559	-1.151154	-2.36069	1.147849	-1.49196	-117
$Al_2O_3 \times Al_2O_3$	361.93083	361.12859	357.04268	373.223	348.7296	364.6893	2.5
$CaO \times Fe_2O_3$	163.17256	144.79261	173.52954	172.3198	168.3196	159.5469	7.3
$MgO \times ZrO_2$	592.93753	586.23343	627.85814	672.4307	443.8195	622.4125	14.8
Fit Statistics							
R^2	0.8229	0.8143	0.8220	0.8235	0.8354	0.8309	0.8252
R^2_{Adj}	0.8174	0.8069	0.8150	0.8165	0.8289	0.8242	0.8183
R^2_{Press}	0.8022	0.7875	0.7947	0.7975	0.8107	0.8043	0.7989
RMSE	0.348	0.340	0.339	0.337	0.324	0.327	0.333
$RMSE_{Press}$	0.334	0.356	0.357	0.354	0.341	0.345	0.351
Validation							
R^2_{Val}	-	0.8436	0.8127	0.8124	0.7450	0.7854	0.7998

3.4 Vapor Hydration Test Response

The WTP contract requires glasses to have VHT responses below 50 g/m^2 (DOE 2000):

> *2.2.2.17.3 Vapor Hydration Test: The glass corrosion rate shall be measured using at least a seven (7)-day vapor hydration test run at 200°C as defined in the DOE-concurred upon ILAW Product Compliance Plan. The measured glass alteration rate shall be less than 50 grams/(m^2 day). Qualification testing shall include glass samples subjected to representative waste form cooling curves. The vapor hydration test shall be conducted on waste form samples that are representative of the production glass.*

Glasses with high alkali content tend to challenge this constraint, as shown in Figure 3.12. Below a *NAlk* of roughly 16 wt%, the VHT responses of all glasses fall far below the limit. However, above a *NAlk* of 16 wt%, some glasses exceed the contract limit VHT response while others do not. In fact,

glasses with *NAlk* as high as 26 wt% (ORPLA25) still meet the contract limits. A model is needed to predict VHT responses of high *NAlk* glasses to avoid failing the contract VHT constraint while at the same time allowing for the formulation of high *NAlk* glasses.

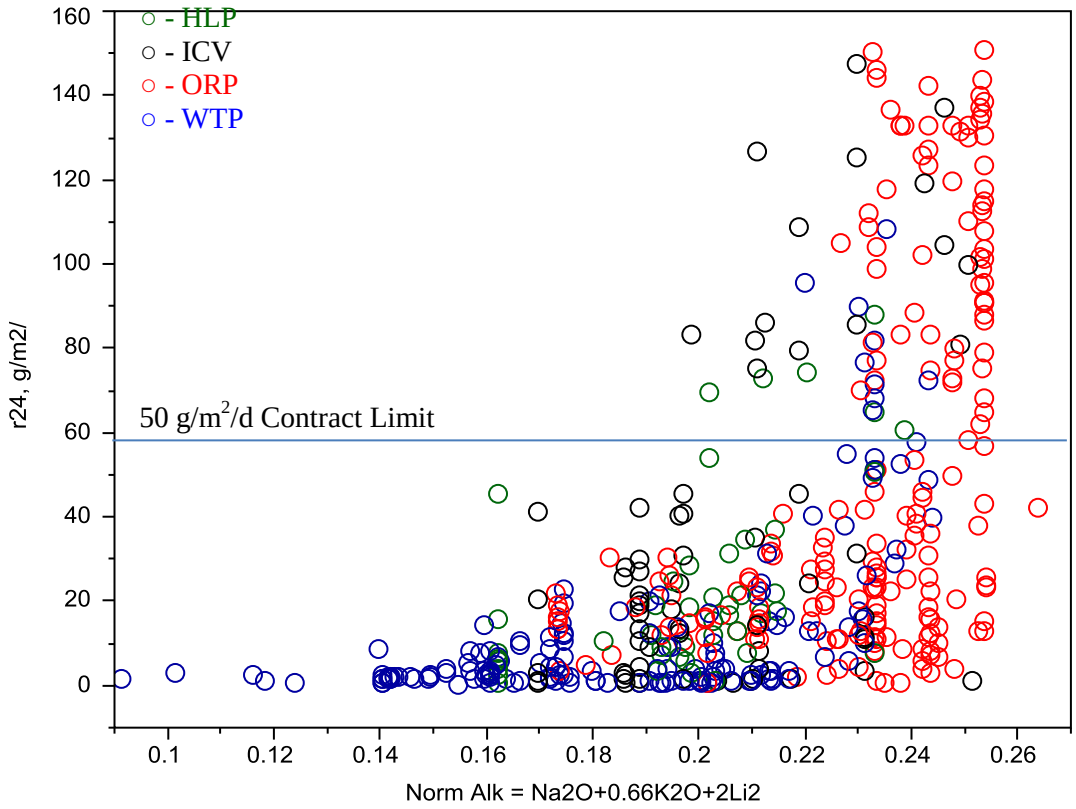

Figure 3.12. Comparison of 200°C VHT Rates, Normalized to 24 d Test, to *NAlk* of LAW Glasses

A database of LAW glasses was compiled to model their VHT responses. These data include crucible-scale tests with simulants, melter tests with simulants, and crucible-scale tests with actual LAW. The data, summarized in Table 3.11, were compiled for modeling, and are listed in Appendix B. The data set was evaluated for composition coverage of the single component concentration ranges (Table 3.12) and appropriateness for use in models. The data generally cover the concentration ranges well, as shown in Figure 3.13.

Table 3.11. Summary of LAW VHT Data Sets

Data Set	Number of Data Points	Reference
HLP	72	Vienna et al. 2001b
ICV	93	Kim et al. 2003 plus previously unpublished data
ORP	203	Muller et al. 2012
WTP	177	Piepel et al. 2007

Table 3.12. Component Concentration Ranges for VHT Model Data

Component	Min	Max
Al_2O_3	3.5	16.79
B_2O_3	0	13.73
CaO	0	12.81
Fe_2O_3	0	15.77
K_2O	0	5.88
Li_2O	0	5.79
MgO	0	9.94
Na_2O	2.45	28.74
SiO_2	29.82	60.01
ZrO_2	0	10

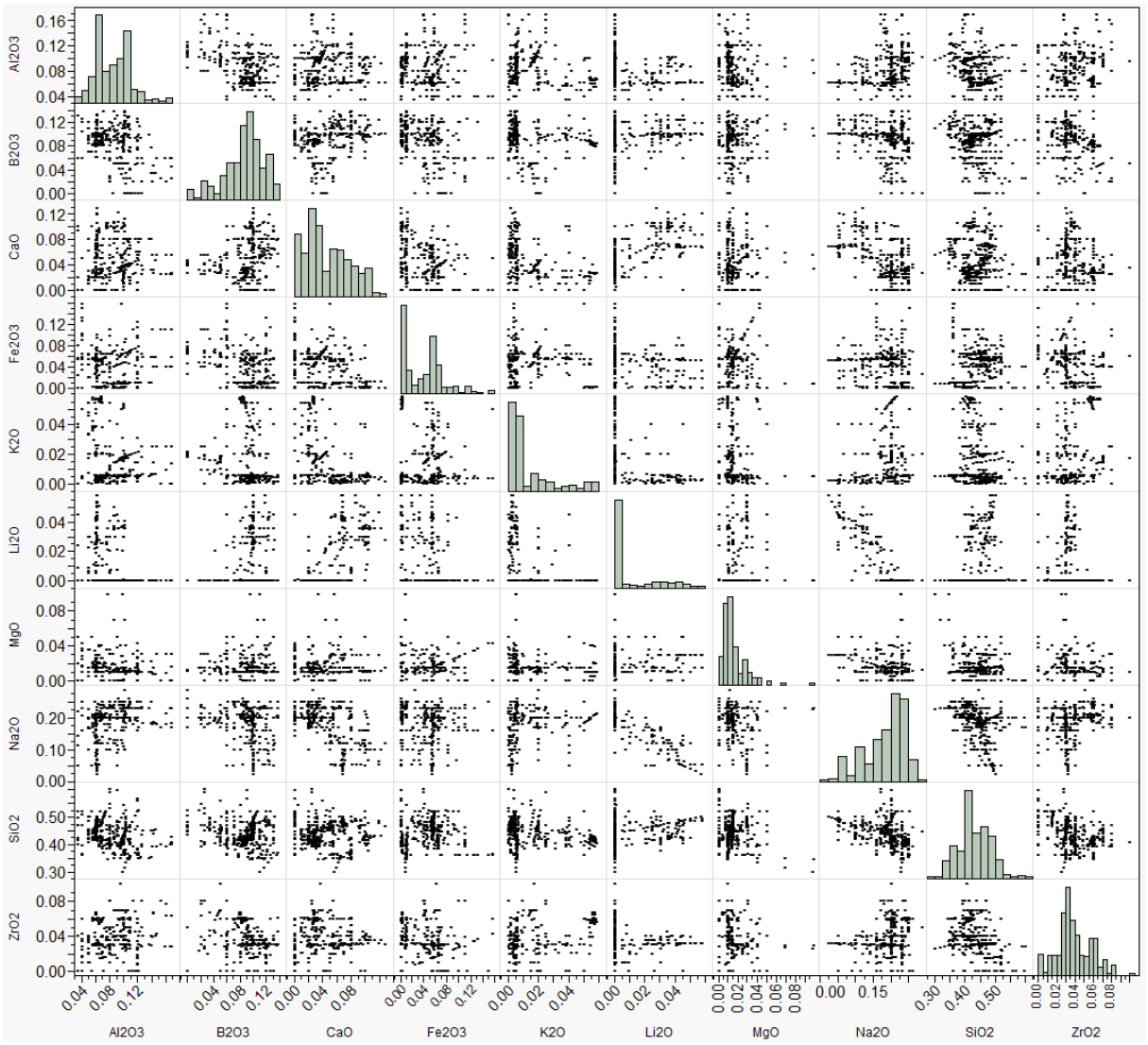

Figure 3.13. Scatterplot Matrix of VHT Model Data

There are two primary ways of estimating the alteration rate by VHT: 1) a single time test is run and the amount of glass altered in the test is divided by the test time to give an average rate, and 2) multiple tests are run at different times and an alteration rate is determined by the slope of the linear portion of the alteration vs. time relationship (Vienna et al. 2001b). Because there is a significant positive intercept for most VHT alteration vs. time relationship lines, the two options will necessarily yield different results, with option 1 being generally higher than option 2. Further, the time at which the test is run will also influence the option 1 rate. Therefore, to make the data from the different studies compatible, an attempt was made to put the data on the same time basis. Because a vast majority of the model data was measured for a single time at 24 days, that was the basis chosen. For glasses with multiple time measurements, the amount of alteration was interpolated to 24 days, and that number was divided by 24 to put the rate in terms of grams per square meter per day ($g/m^2/d$). In this report, this rate is referred to as r24. For the glasses with a different, single time measurement, we could find no basis for adjusting the rate, so we took the mass of glass altered during the test duration and divided by the test duration.

Attempts to fit partial quadratic models to the VHT data (r24) were unsuccessful; the fit R^2 values were below 70% even for many-term models, and the validation statistics were well below the model-fit statistics (lower R^2s and higher RMSEs). In addition, the range residuals were very high (Figure 3.14). Glasses with measured VHT responses of roughly 50 g/m^2/d were predicted to have responses ranging from 2 to 90 g/m^2/d with model-fit data. Therefore, other modeling approaches were investigated.

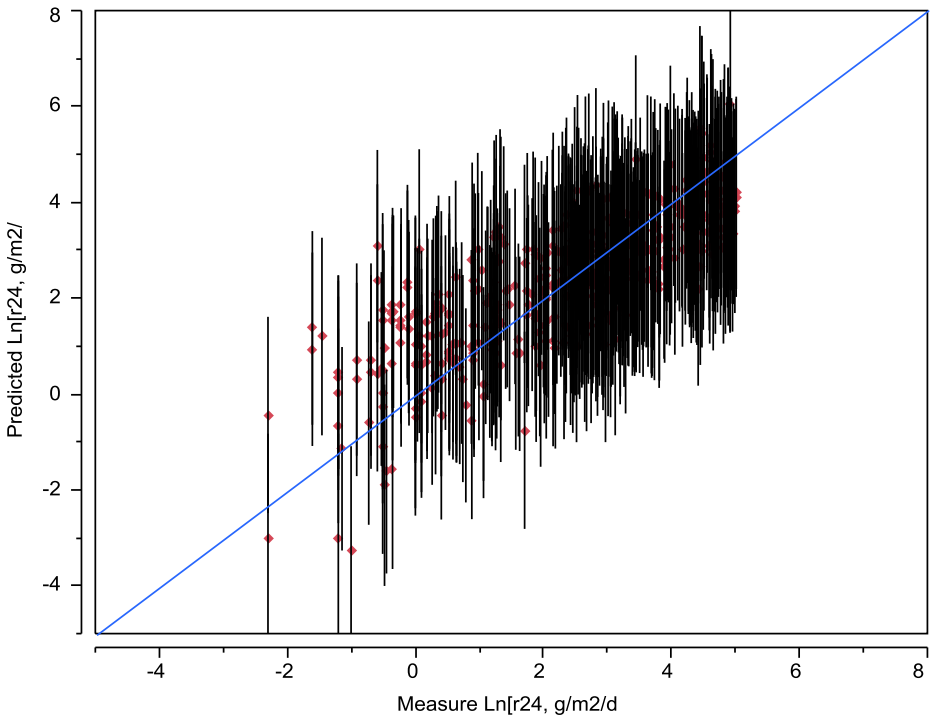

Figure 3.14. Prediction vs. Measured Ln(r24) Partial Quadratic Model with 95% Confidence Interval for Individual Prediction

An NN model is ideal for predicting complex non-linear interactions between the components; this model was used to model VHT response. The final NN model consisted of two first-level nodes and six second level nodes, all using the hyperbolic tangent activation function. These nodes are classified as the hidden layers of the model. Of the possible components, Al_2O_3, B_2O_3, CaO, Fe_2O_3, K_2O, Li_2O, MgO, Na_2O, SiO_2, and ZrO_2 were used for prediction. Analysis was performed using additional components, including F, SO_3, SnO_2, and TiO_2, and ZnO, but these components either altered the predicted effects of other components in non-intuitive ways or did not increase the validity of the model. Additional sensitivity trials were performed using different numbers of NN nodes. The final node selection was made because it optimally fit the data based on complexity and did not result in binning of data.

A graphical representation of the NN used for this model is presented in Figure 3.15. Each of the inputs to the model is listed on the left. The values from these inputs are fed into the six nodes immediately after the input. These are considered the second level of nodes because they are the second level from the output. Each of these nodes contains an intercept and a TanH function that is dependent on each of the inputs. The output of this second level of nodes is fed into the two nodes present in the first layer. The outputs from these nodes are used in Figure 3.15 to create the final predicted values.

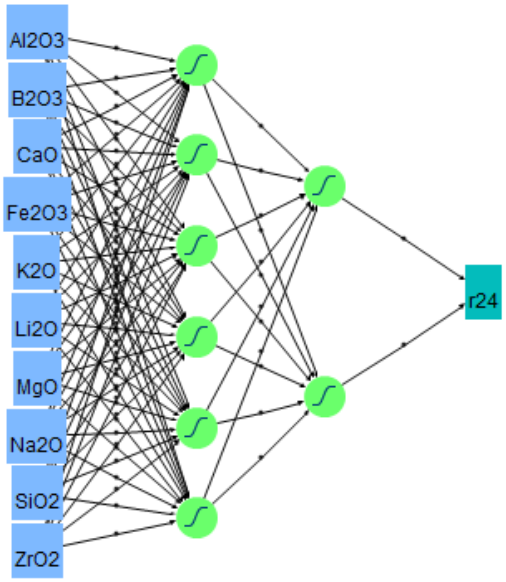

Figure 3.15. Block Diagram of Neural Network

An example node depicted in Figure 3.15 is detailed by the diagram in Figure 3.16. The output from the example node is fed into the first layer nodes, and then used to produce the final answer. The summation of the values input into the node are passed to the next node and then finally to the output.

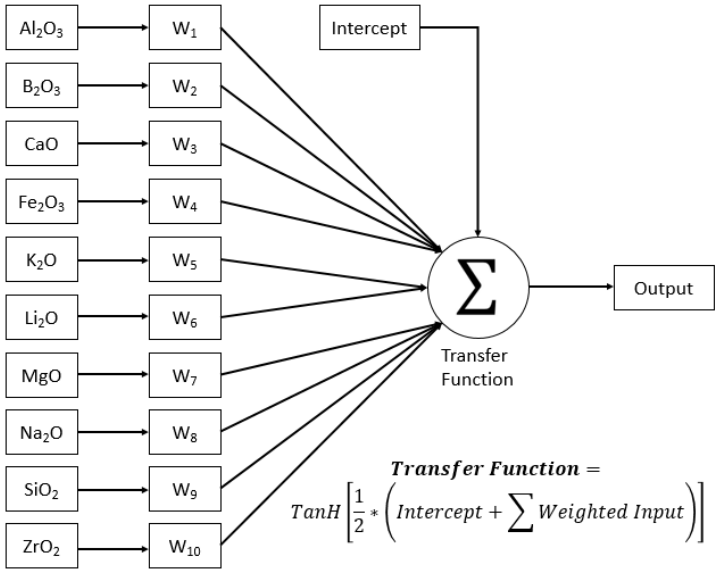

Figure 3.16. Detailed Node Diagram from a Neural Network

A data set of 504 glasses was used to train and validate this NN model. When using the NN with this number of nodes, this is a limited portion of data. To create a predictive model, K-fold cross validation was used to increase the number of data points available for the model while decreasing the likelihood of

overfitting. K-fold cross validation splits the data set into *k* subsets. Each of these subsets uses 1/*k* of the data for validation and 1/(1-*k*) of the data for modeling. In each subset, a unique 1/*k* portion of the data is used for validation. All of the subsets are modeled, and the best model based on the fit of the validation data is presented. This allows maximum use of the data. In all models presented, *k* was set to 12. The resulting model is highly flexible, and care must be taken to avoid overfitting. In all models, a portion of the data is used as a validation set to evaluate the predictive ability of the model. Before creating the final model, the sample set was divided into five equal sets, each containing an equal amount of evenly distributed data based on the r24 value. These sets were modeled using the same procedure as the final model to determine the predictive ability of the method. The overall fit of the models with all of the data included is shown in Table 3.13. The specific performance of the model on only the validation data is shown in Table 3.14. It was noted that subset 5 had a significantly smaller predictive ability compared to the other models. This was quantitatively investigated by evaluating the relative influence from each glass on the final model. The glasses were ranked based on this influence, and it was found that subset 5 contained fewer of the "important" glasses and more of the "unimportant" glasses. The same analysis was applied to the remaining 4 subsets, and a strong correlation was found between the inclusion of the 11 most important glasses and the predictive ability of the model (listed in Table 3.15). There was no correlation between the importance level of the glass and the measured r24 value.

Table 3.13. Subset Models Applied to All Data

All Data	Subset 1	Subset 2	Subset 3	Subset 4	Subset 5
Number of Data Points	504	504	504	504	504
RMSE	16.93	17.00	18.33	16.45	20.58
R^2	0.814	0.811	0.787	0.824	0.735

Table 3.14. Subset Models Applied to Validation Data Only

Validation Set	Subset 1	Subset 2	Subset 3	Subset 4	Subset 5
Number of Data Points	100	101	101	101	101
RMSE	23.76	25.37	29.68	21.68	34.91
R^2	0.773	0.733	0.684	0.805	0.587

Table 3.15. Most Influential Glasses for Neural Network Development

Influence Rank	#	Set	Glass ID
1	525	ICV	AMP2-05
2	311	WTP	LAWM3
3	449	HLP	HLP-37
4	215	WTP	LAWM20
5	95	ORP	ORPLA34
6	216	WTP	LAWM22
7	448	HLP	HLP-36
8	71	ORP	ORPLA14S4
9	21	ORP	LAWA188
10	176	ORP	ORPLG20
11	450	HLP	HLP-38
12	534	ICV	S22-11
13	542	ICV	S22-28
14	472	ICV	AMP2-10
15	416	HLP	HLP-39

The final model had 8% of the data retained to help validate the predictive ability of the model. These glasses were selected randomly based on r24 value, and were not considered to be critical for model development. The final model used the same NN structure, and was developed with K-fold cross validation, k=12. The final predictions of the model performed well. Statistical results are presented in Table 3.16 and a plot is presented in Figure 3.17.

Table 3.16. Final Model Results

Final Model	All Data	K-Fold In Model Validation
Number of Data Points	504	38
RMSE	13.59	12.00
R^2	0.874	0.912

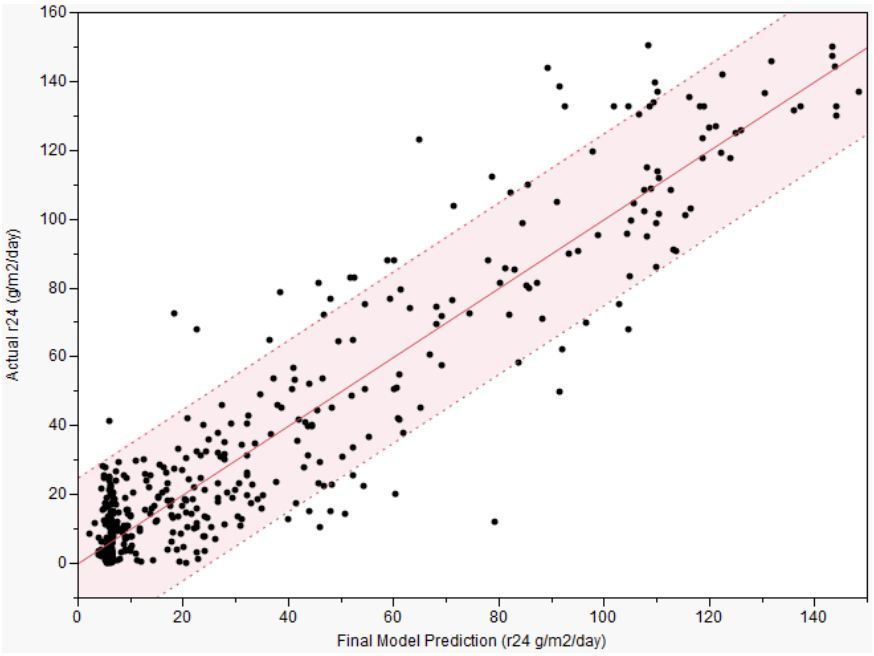

Figure 3.17. Final Model Results − Actual vs. Predicted r24. The shaded band represents the region of "confidence of prediction."

To better understand compositional effects, Figure 3.18 illustrates the composition effect on r24 at five different glass compositions, with VHT responses near the 50 $g/m^2/d$ limit. It is clear that these composition effects are complex, which explains why simple polynomial models were unsuccessful in describing them. More validation of this model and this modeling approach are planned in the future.

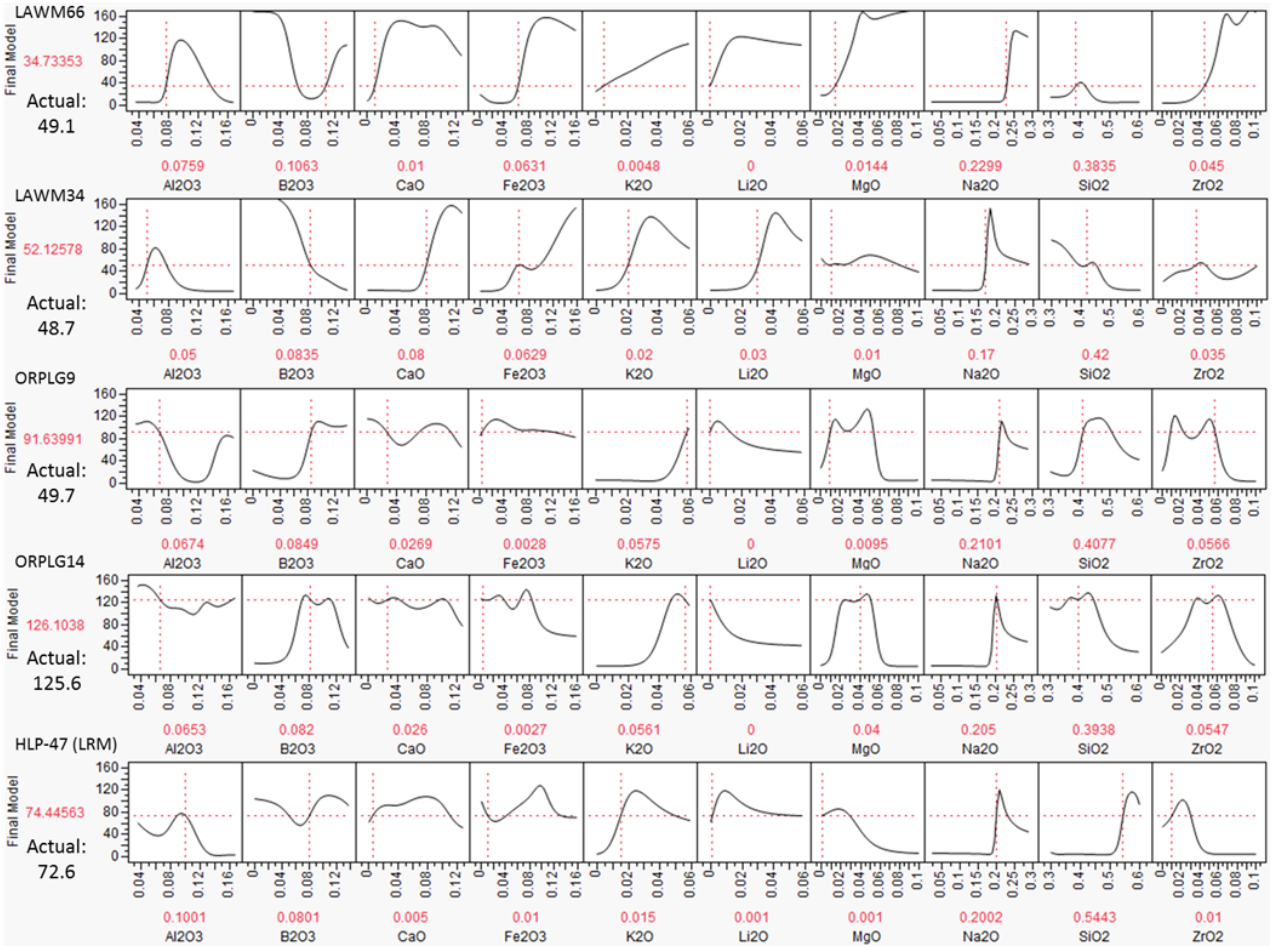

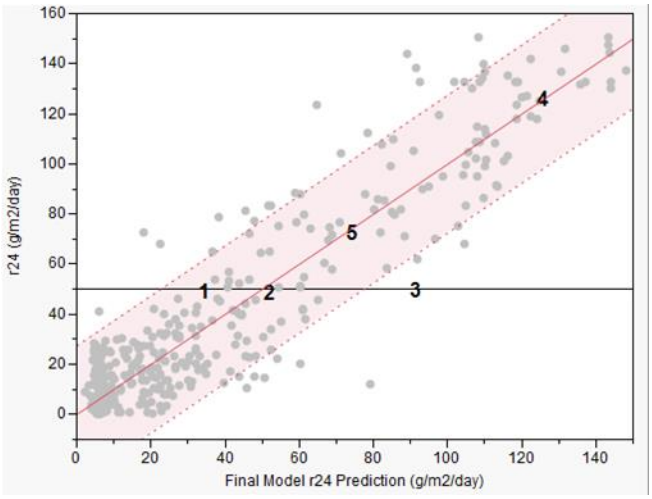

Figure 3.18. Prediction Profiles for Specific Glasses

The model form used is:

r24=22.2368486728788+162.297620340354*TanH(0.5*Fn1)+146.571639705835*TanH(0.5*Fn2) (3.23)

where Fn1 and Fn2 are defined as:

Fn1= -2.0234500345046 +

3.42064364061235 * TanH [0.5 * [19.6032022867479
+ -41.763025292002 * Al2O3
+ -7.2247531165788 * B2O3
+ -71.440190399197 * CaO
+ 21.4866660009179 * Fe2O3
+ -5.8285856407714 * K2O
+ 14.1674908254771 * Li2O
+ -17.712793652953 * MgO
+ 4.90653877435819 * Na2O
+ -23.999070392784 * SiO2
+ -89.261809766372 * ZrO2]] +

-1.5945608677549 * TanH [0.5 * [9.71096479446714
+ -1.7854759769145 * Al2O3
+ 35.9943209948772 * B2O3
+ -49.874405307677 * CaO
+ 23.2401360961441 * Fe2O3
+ -86.620913893724 * K2O
+ 9.56939724758103 * Li2O
+ -238.90360119104 * MgO
+ -3.2019704029069 * Na2O
+ -25.2772019421 * SiO2
+ 140.437932824307 * ZrO2]] +

2.31555079823014 * TanH [0.5 * [3.26429869709493
+ 104.477522837661 * Al2O3
+ 4.58157835900144 * B2O3
+ 0.85255450354859 * CaO
+ 1.1244826601591 * Fe2O3
+ 60.7067527477005 * K2O
+ 62.0556736612157 * Li2O
+ -62.402468467866 * MgO
+ 11.4599614081572 * Na2O
+ -27.425799171143 * SiO2
+ -49.853555611999 * ZrO2]] +

-4.0985855697882 * TanH [0.5 * [54.4850934035448
+ 14.0759354190093 * Al2O3
+ -77.812329749985 * B2O3
+ -24.479879404922 * CaO
+ -15.422081646139 * Fe2O3
+ -64.301191862086 * K2O
+ -106.16853767331 * Li2O
+ -75.957683994829 * MgO
+ -103.98990411707 * Na2O
+ -50.469486676587 * SiO2
+ -29.590974146236 * ZrO2]] +

2.42774575785518 * TanH [0.5 * [10.7282870519699
+ 135.592922593436 * Al2O3
+ -43.364161952728 * B2O3
+ 94.4108021418093 * CaO
+ 106.198181220628 * Fe2O3
+ -95.8928850646 * K2O
+ -62.087358826133 * Li2O
+ 8.17353548499568 * MgO
+ -36.294958232164 * Na2O
+ -44.774632983115 * SiO2
+ 52.2713874914766 * ZrO2]] +

-3.002427812819 * TanH [0.5 * [1.36554171806406
+ 8.39190437614229 * Al2O3
+ 85.1968179640575 * B2O3
+ -54.481478008755 * CaO
+ 87.6692685766409 * Fe2O3
+ -21.332583067516 * K2O
+ -0.0388979586356 * Li2O
+ 155.446663232058 * MgO
+ -25.780955827028 * Na2O
+ -2.3634111816427 * SiO2
+ -165.81210510989 * ZrO2]]

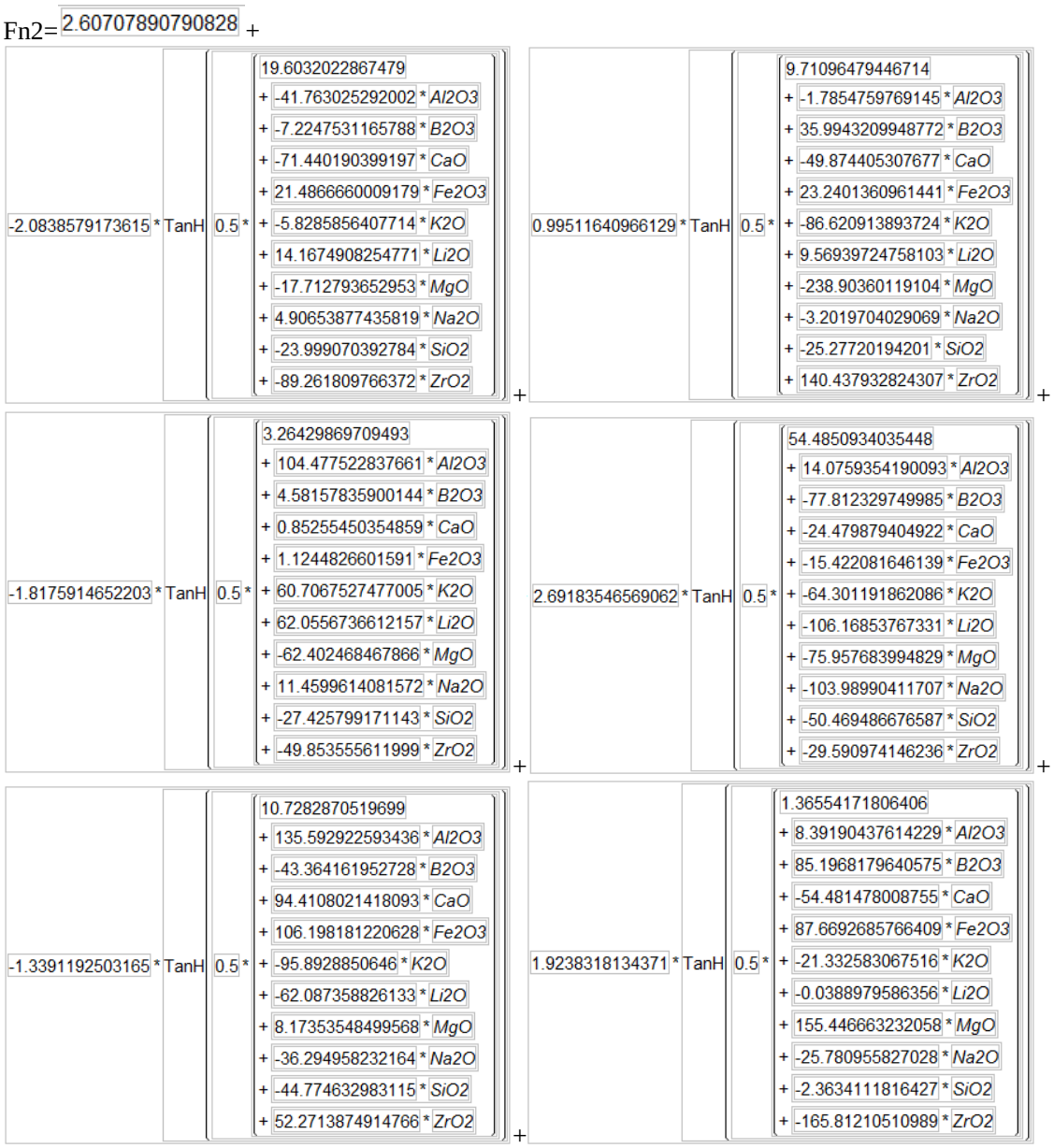

3.5 Viscosity

Viscosity of waste glass melts should be maintained between roughly 20 and 80 P at the melting temperature (nominally 1150°C) [*]. It is not appropriate to fit new viscosity models for advanced LAW glass formulations at this time, because:

- the current WTP models can be extrapolated to the new composition region quite reliably (as shown in Figure 3.19), and

[*] The units used for LAW viscosity are Poise (P), while the units used for HLW viscosity are Pascal Seconds (Pa·s), due only to the history of the models developed for different purposes. These units are easily converted using 1 Pa·s = 10 P.

- the viscosity of glass must be maintained in the correct range to estimate glass composition, but has little influence on the ultimate waste loading of the LAW glasses.

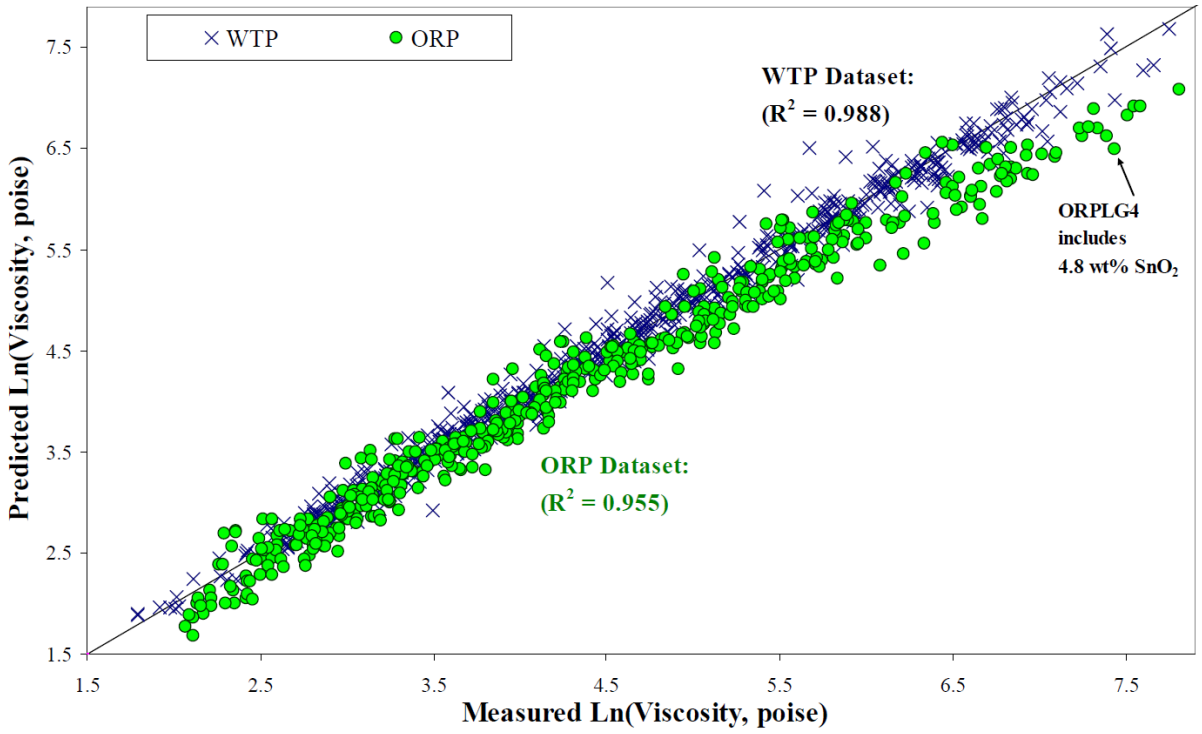

Figure 3.19. Comparison of Predicted and Measured Ln(viscosity) Data for Both WTP Baseline and ORP Advanced LAW Glasses Using the WTP Baseline Viscosity Model (Muller et al. 2012)

It is therefore recommended that the WTP baseline viscosity model be applied to estimate reasonable glass compositions. The form of this model is given by:

$$Ln[\eta_T, P] = \sum_{i=1}^{p}\left(v_i + y_i/\left[T \cdot 1000\right]^2\right) g_i + selected\left\{\sum_{i=1}^{p-1}\sum_{j=i}^{p} v_{ij} g_i g_j\right\} \quad (3.24)$$

where v_i , y_i, and g_i are the i^{th} component temperature-independent coefficient, temperature-dependent coefficient, and mass fraction in glass, respectively; T is the absolute temperature (in K). The model coefficients and parameters are summarized in Table 3.17. Like the other models, composition is in mass fraction and absolute temperature (T) is in Kelvin. Once sufficient data become available to expand the viscosity model, less unusual functional forms will be considered.

Table 3.17. Viscosity-Composition Model Coefficients and Selected Statistical Parameters

Model Term	Coefficient, Ln(η_T, P)	Statistic	Value
Al_2O_3	5.5124	R^2	0.988
B_2O_3	−42.3772	R^2_{Val}	0.983
CaO	−10.6445	RMSE, Ln(P)	0.147
Fe_2O_3	−4.6220	# of glasses	171
K_2O	−0.8689	-	-
Li_2O	10.9390	-	-
MgO	−5.6188	-	-
Na_2O	0.9073	-	-
P_2O_5	−0.8081	-	-
SiO_2	1.5575	-	-
ZrO_2	−12.0741	-	-
Others	−9.3903	-	-
$(B_2O_3)^2$	198.7360	-	-
$(Li_2O)^2$	133.6906	-	-
$Al_2O_3 \times Li_2O$	−136.5095	-	-
$(MgO)^2$	–179.8249	-	-
$Al_2O_3/(T/1000)^2$	24.6423	-	-
$CaO/(T/1000)^2$	13.7793	-	-
$Fe_2O_3/(T/1000^2$	15.2036	-	-
$Li_2O/(T/1000)^2$	−82.4815	-	-
$MgO/(T/1000)^2$	22.7608	-	-
$Na_2O/(T/1000)^2$	−14.5621	-	-
$P_2O_5/(T/1000)^2$	24.0339	-	-
$SiO_2/(T/1000)^2$	24.4077	-	-
$ZrO_2/(T/1000)^2$	48.2286	-	-
Others/$(T/1000)^2$	17.3800	-	-

3.6 Other Property Models and Component Concentration Limits

As described in Section 3.1, the method for estimating the loading of LAW in advanced glasses is to apply both the empirical loading rules in Section 3.1.2 and key waste glass property constraints of sulfur tolerance, PCT response, VHT response, and viscosity through property-composition models. To evaluate whether additional constraints are needed, we first consider the uncertainty in VHT prediction and lack of experience in the waste glass formulation field with the use of NN models. A simple tree model can be used to add additional constraints to help avoid glasses with excessive VHT responses. Figure 3.20 shows a tree model of all VHT data grouped into the glasses that pass (<50 g/m^2/d) and fail (≥50 g/m^2/d) the contract specification. The glasses with *NAlk* <17 wt% all passed, but that is not overly useful for glasses with high waste loading. Of more interest is that for those glasses with *NAlk* < 22.67 wt%, all glasses with Al_2O_3 < 9% passed. Also, for the glasses with *NAlk* ≥ 22.67 wt%, all those with ZrO_2 < 2.54 failed. Based on these results, it is recommended that a maximum concentration of 9 wt% Al_2O_3 and a minimum concentration of 2.6 wt% ZrO_2 be added as constraints.

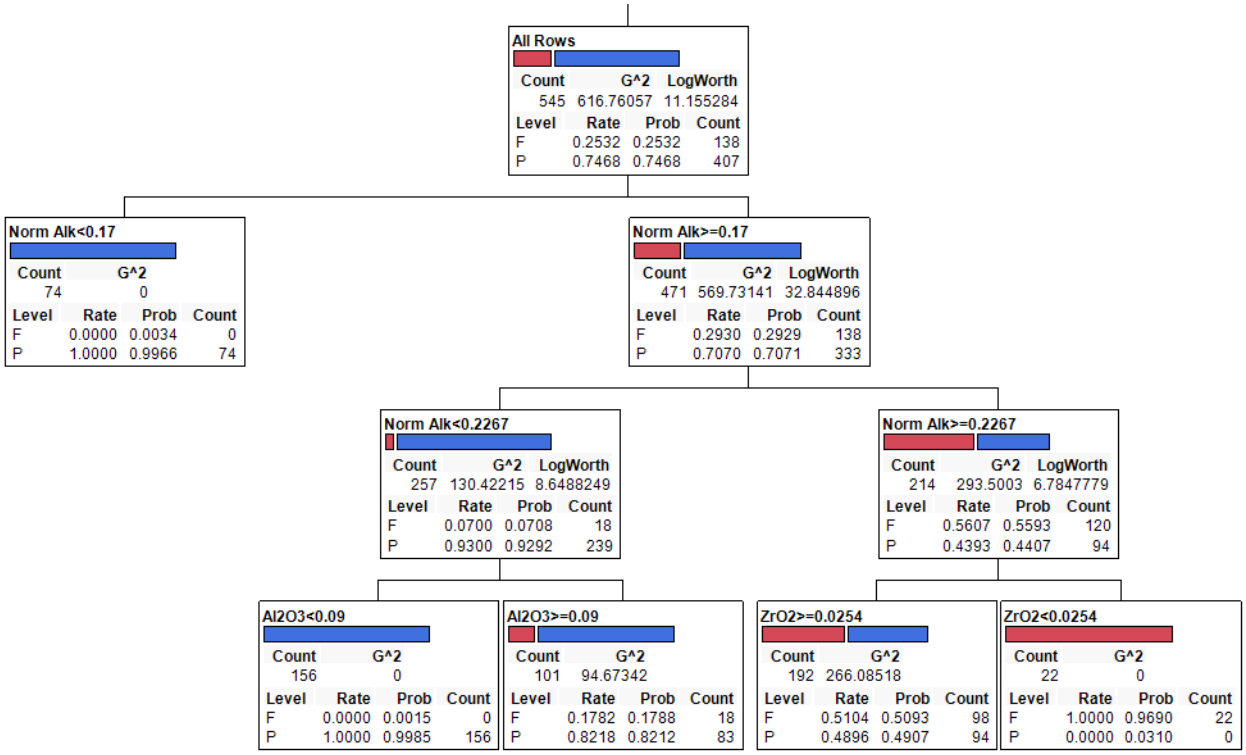

Figure 3.20. Tree Model of VHT Pass and Fail for Different Composition Domains

Lastly, model-validity constraints should be considered when applying the property-composition models. Table 3.18 summarizes these additional constraints.

Table 3.18. Component Concentration Constraints in wt%

Component	Lower Limit	Upper Limit	Component	Lower Limit	Upper Limit
Al_2O_3	5.0	9.0	P_2O_5	0	4.5
B_2O_3	5.0	16.0	SiO_2	30.0	51.0
CaO	0	13.0	SO_3	0	1.6
Fe_2O_3	0	13.0	SnO_2	0	5.0
K_2O	0	8.0	TiO_2	0	4.0
Li_2O	0	6.0	V_2O_5	0	4.5
MgO	0	10.0	ZnO	0	6.0
Na_2O	5.0	26.0	ZrO_2	2.6	7.0

An additional constraint related to the corrosion of metal melter components (e.g., electrodes, bubblers, and thermowells) may be required for advanced LAW glass formulations. However, the data have not yet been fully evaluated to determine if such a constraint is necessary, and how it would be formulated.

3.7 Calculation Examples

Examples are given for use in determining if the application and coding of the LAW models are correct. To create these examples, two hypothetical wastes, based loosely on real projected Hanford HLW feeds, were used in glass optimization calculations. A set of waste compositions was selected to demonstrate the calculations. The waste estimates are from the LAW and secondary LAW vitrification feed, as estimated in case one of System Plan revision 6 (Certa et al. 2011). The waste feeds were converted to mass fractions of reference oxides and halogens, and sorted by the ratios of $Na_2O:SO_3$, $Na_2O:K_2O$, and $Na_2O:(Cl+0.3F)$. The waste with the minimum for each of the ratios was selected for calculation along with a number of data points that systematically varyed the $Na_2O:SO_3$ ratio. The selected waste compositions are listed in Table 3.19.

Table 3.19. Selected Waste Compositions, wt%

Batch Date	6/14/41	4/10/26	6/8/18	7/9/27	4/8/33	6/18/38	8/24/35	7/1/33
Batch #	SLCP-937	LCP-391	LCP-1	SLCP-249	SLCP-539	LCP-1027	LCP-880	SLCP-551
Na_2O	51.86	76.72	73.95	69.52	74.73	80.86	76.68	78.82
SO_3	35.11	0.56	1.35	2.43	7.43	4.04	5.11	2.62
K_2O	0.25	6.55	15.51	2.23	0.37	0.28	0.27	0.30
Cl	2.48	1.48	0.62	5.32	1.36	0.59	0.55	0.50
F	7.66	0.60	0.73	12.63	4.35	0.87	1.60	1.12
P_2O_5	0.66	0.44	0.60	0.82	2.01	3.35	5.89	4.50
Cr_2O_3	0.67	0.12	0.11	0.61	1.03	0.44	0.53	0.71
Al_2O_3	1.15	13.17	6.89	5.95	7.77	8.68	8.25	10.34
SiO_2	0.05	0.16	0.12	0.18	0.64	0.72	0.85	0.79
SUM	99.89	99.81	99.86	99.68	99.70	99.83	99.73	99.69
Na_2O/SO_3	1	136	55	29	10	20	15	30
Na_2O/K_2O	204	12	5	31	202	293	281	265
$Na_2O/(Cl+0.3F)$	11	46	89	8	28	95	74	94

The various constraint sets were used to maximize the loading of each one of the batch compositions; the results are summarized in Table 3.20.

Table 3.20. Glass Composition and Predicted Properties for Example Wastes, wt%

Batch	SLCP-937	LCP-391	LCP-1	LCP-1	SLCP-249	SLCP-249	SLCP-539	SLCP-539	LCP-1027	LCP-880	SLCP-551
Al_2O_3	5.00	5.00	5.00	5.00	5.44	5.00	6.75	5.00	5.43	5.25	5.18
B_2O_3	5.39	5.00	5.00	5.00	5.00	5.00	5.00	5.00	5.00	5.00	5.00
CaO	13.00	8.81	13.00	8.72	12.75	3.68	10.55	8.38	7.03	7.18	4.15
Cl	0.11	0.44	0.10	0.18	0.74	1.70	0.20	0.28	0.16	0.14	0.15
Cr_2O_3	0.03	0.03	0.02	0.03	0.08	0.19	0.16	0.21	0.12	0.13	0.21
F	0.33	0.18	0.12	0.21	1.76	4.03	0.65	0.88	0.23	0.40	0.34
Fe_2O_3	0.35	0.18	0.19	0.16	0.20	0.00	0.00	0.00	0.00	0.00	0.00
K_2O	0.01	1.94	2.53	4.42	0.31	0.71	0.06	0.07	0.07	0.07	0.09
Li_2O	6.00	4.25	6.00	4.21	5.42	5.20	6.00	6.00	6.00	6.00	6.00
MgO	0.27	0.16	0.17	0.15	0.18	0.00	0.00	0.00	0.00	0.00	0.00
Na_2O	5.00	22.72	12.07	21.08	9.67	22.19	11.21	15.09	21.39	19.06	23.94
P_2O_5	0.03	0.13	0.10	0.17	0.11	0.26	0.30	0.41	0.89	1.46	1.37
SiO_2	51.00	43.99	48.48	43.28	51.00	44.25	51.00	49.47	45.56	46.83	45.12
SO_3	1.50	0.17	0.22	0.38	0.34	0.77	1.11	1.50	1.07	1.27	0.80
SnO_2	2.05	0.00	0.00	0.00	0.00	0.00	0.00	0.00	0.00	0.00	0.00
TiO_2	1.05	0.00	0.00	0.00	0.00	0.00	0.00	0.80	0.73	0.74	0.65
V_2O_5	1.04	0.00	0.00	0.00	0.00	0.00	0.00	0.01	0.01	0.01	0.01
ZnO	0.86	0.00	0.00	0.00	0.00	0.00	0.00	0.00	0.00	0.00	0.00
ZrO_2	7.00	7.00	7.00	7.00	7.00	7.00	7.00	6.91	6.32	6.46	7.00
Loading	4.27	29.56	16.29	28.47	13.86	31.82	14.96	20.13	26.41	24.79	30.28
Limiting Factor(s)											
	SO_3 =1.5%	d=24%	ConsH =2.7%	d=24%	ConsH =2.2%	Many	SO_3 =1.5	ConsH =0.74%	S-d limit	S-d limit	d=24%
Predicted Properties											
VHT	6.30	8.44	5.83	45.49	6.30	50.00	6.31	6.24	11.97	4.83	50.00
wSO_3	1.65	1.26	1.66	1.29	1.23	0.77	1.45	1.50	1.68	1.65	1.58
PCT	0.1	1.1	0.2	1.0	0.1	1.3	0.1	0.3	1.0	0.6	1.8
Visc1150	80.0	20.0	40.8	20.0	80.0	20.0	80.0	46.4	20.0	29.0	20.0

To demonstrate the application of these models to the Hanford mission as well as document the current expectations for increased waste loadings across the estimated LAW types, a study was performed and is documented elsewhere (Kim 2013).

4.0 References

DOE. 2011. *Quality Assurance*, DOE O 414.1D. U.S. Department of Energy, Washington, D.C.

DOE. 2013. *Nuclear Safety Management*, 10CFR830. U.S. Department of Energy, Washington, D.C.

Annamalai S, H Gan, M Chaudhuri, WK Kot, and IL Pegg. 2004. "Spinel Crystallization in HLW Glass Melts: Cation Exchange Systematics and the Role of Rh_2O_3 in Spinel Formation." *Ceramic Transactions* 279−288, American Ceramic Society, Westerville, Ohio.

ASME. 2000. "Quality Assurance Requirements for Nuclear Facility Applications." ASME NQA-1-2000, American Society of Mechanical Engineers, New York.

Barnes SM and DE Larson. 1981. *Materials and Design Experience in a Slurry-Fed Electric Glass Melter*. PNL-3959, Pacific Northwest Laboratory, Richland, Washington.

Baron MR and ME Smith. 1988. *Summary of the Drain and Restart of the DWPF Scale Glass Melter*. DPST-88-481, Savannah River Laboratory, Aiken, South Carolina.

Belsher JD and FL Meinert. 2009. *High-Level Waste Glass Formulation Model Sensitivity Study 2009 Glass Formulation Model Versus 1996 Glass Formulation Model*. RPP-RPT-42649, Rev. 0, Washington River Protection Solutions, Richland, Washington.

Bergmann LM. 2010. *Hanford Tank Waste Operations Simulator (HTWOS) Version 6.0 Model Design Document*. RPP-17152, Rev. 4, Washington River Protection Solutions, Richland, Washington.

Bjorklund WJ. 1980. *Defense Waste-Vitrification Studies During FY 1980*. PNL-3818, Pacific Northwest Laboratory, Richland, Washington.

Certa PJ, RD Adams, GK Allen, JD Belsher, PA Empey, JH Foster, TM Hohl, RT Jasper, RA Kirkbride, RL Lytle, FL Meinert, JS Ritari, RM Russell, KR Seniow, EB West, MN Wells, and LM Bergmann. 2011. *River Protection Project System Plan*. ORP-11242, Rev. 6, U.S. Department of Energy, Office of River Protection, Richland, Washington.

Cooper MF, ML Elliott, LL Eyler, CJ Freeman, JJ Higginson, LA Mahoney, and MR Powell. 1994. *Research-Scale Melter Test Report*. PNL-9428, Pacific Northwest Laboratory, Richland, Washington.

Crum JV, JD Vienna, DK Peeler, IA Reamer, and DJ Pittman. 2002. "The Effect of Glass Composition on Crystallinity and Durability for INEEL Run 78 Calcine Waste Simulant." *Environmental Issues and Waste Management Technologies in the Ceramic and Nuclear Industries VII*, 132:267−275, American Ceramic Society, Westerville, Ohio.

Deng YN. 2011. *Dynamic (G2) Model Design Document: 24590-WTP-MDD-PR-01-002, Rev. 12*, ORP-56503, River Protection Project, Waste Treatment Plant, Richland, Washington.

Dierks RD. 1980. *The Design and Performance of A 100-Kg/H, Direct Calcine-Fed Electric-Melter System for Nuclear-Waste Vitrification*. PNL-3387, Pacific Northwest Laboratory, Richland, Washington.

DOE. 2000. *Design, Construction, and Commissioning of the Hanford Tank Waste Treatment and Immobilization Plant*. U.S. Department of Energy, Office of River Protection, Richland, Washington.

DOE. 2008. *Quality Assurance Requirements and Description*. DOE/RW-0333P, Rev. 21, U.S. Department of Energy, Office of Civilian Radioactive Waste Management, Washington, D.C.

DOE. 1996. *Waste Acceptance Product Specifications for Vitrified High-Level Waste Forms (Waps)*. DOE/EM-0093, U.S. Department of Energy, Office of Environmental Management, Washington, D.C.

Feng XD, PR Hrma, JH Westsik, Jr., NR Brown, MJ Schweiger, H Li, JD Vienna, G Chen, GF Piepel, DE Smith, BP Mcgrail, SE Palmer, DS Kim, Y Peng, WK Hahn, AJ Bakel, WL Ebert, DK Peeler, and CY Chang. 1996. *Glass Optimization for Vitrification of Hanford Site Low-Level Tank Waste*. PNNL-10918, Pacific Northwest Laboratory, Richland, Washington.

Fox KM and TB Edwards. 2009. *Experimental Results of the Nepheline Phase III Study*. SRNL-STI-2009-00608, Savannah River National Laboratory, Aiken, South Carolina.

Fox KM and TB Edwards. 2008. *Refinement of the Nepheline Discriminator: Results of a Phase II Study*. SRNS-STI-2008-00099, Savannah River National Laboratory, Aiken, South Carolina.

Fox KM, TB Edwards, DK Peeler, DR Best, IA Reamer, and RJ Workman. 2006. *Nepheline Formation Study for Sludge Batch 4 (SB4): Phase 3 Experimental Results*. WSRC-TR-2006-00093, Savannah River National Laboratory, Aiken, South Carolina.

Fox KM, JD Newell, TB Edwards, DR Best, IA Reamer, and RJ Workman. 2007. *Refinement of the Nepheline Discriminator: Results of a Phase I Study*. WSRC-STI-2007-00659, Westinghouse Savannah River Company, Aiken, South Carolina.

Fox KM, DK Peeler, TB Edwards, DR Best, IA Reamer, RJ Workman, JC Marra, BJ Riley, JD Vienna, JV Crum, J Matyas, AB Edmondson, JB Lang, NM Ibarra, A Fluegel, A Aloy, AV Trofimenko, and R Soshnikov. 2008. *International Study of Aluminum Impacts on Crystallization in U.S. High Level Waste Glass*. SRNL-STI-2008-00057, Savannah River National Laboratory, Aiken, South Carolina.

Gimpel RF. 2010. *Halide, Chromate, and Phosphate Impacts on LAW Glass for Dynamic Flowsheet: 24590-WTP-MCR-PET-09-0037, Rev. 1,* ORP-56504, River Protection Project, Waste Treatment Plant, Richland, Washington.

Gimpel RF. 2009. Memo, "Incorporation of HLW Glass Shell V2.0 into the Flowsheets," to ED Lee, CCN: 184905, October 20, 2009, ORP-56505, River Protection Project, Waste Treatment Plant, Richland, Washington.

Gimpel RF. 2002. *WTP Calculation Sheet: Determining the LAW Glass Former Constituents and Amounts for G2 and Acm Models: 24590-LAW-M4C-LFP-00002, Rev. B,* ORP-56511, River Protection Project, Waste Treatment Plant, Richland, Washington.

Goles RW, WC Buchmiller, CR Hymas, and BD Macisaac. 2002. *Test Summary Report Vitrification Demonstration of an Optimized Hanford C-106/Ay-102 Waste-Glass Formulation*. PNNL-14063, Pacific Northwest National Laboratory, Richland, Washington.

Hrma P. 2002. "Crystallization in High-Level Waste Glasses." *Environmental Issues and Waste Management Technologies in the Ceramic and Nuclear Industries VII* 132:243−256, American Ceramic Society, Westerville, Ohio.

Hrma P. 2010. "Crystallization During Processing of Nuclear Waste Glass," *Journal of Non-Crystalline Solids*, **356**(52-54):3019-3025. DOI 10.1016/j.jnoncryso1.2010.03.039.

Hrma P, J Matyas, and DS Kim. 2003. "Evaluation of Crystallinity Constraint for HLW Glass Processing." *Environmental Issues and Waste Management Technologies in the Ceramic and Nuclear Industries VIII* 143:133−140, American Ceramic Society, Westerville, Ohio.

Hrma P, GF Piepel, MJ Schweiger, DE Smith, DS Kim, PE Redgate, JD Vienna, CA Lopresti, DB Simpson, DK Peeler, and MH Langowski. 1994. *Property/Composition Relationships for Hanford High-Level Waste Glasses Melting at 1150°C*. PNL-10359, Pacific Northwest Laboratory, Richland, Washington.

Hrma, P., JD Vienna, BK Wilson, TJ Plaisted, and SM Heald. 2006. "Chromium Phase Behavior in a Multi-Component Borosilicate Glass Melt," *Journal of Non-Crystalline Solids*, **352**:2114-2122. DOI: 10.1016/j.jnoncrysol.2006.02.051.

Hrma P., BM Arrigoni, and MJ Schweiger. 2009. "Viscosity of Many-Component Glasses," *Journal of Non-Crystalline Solids*, **355**(14-15):891-902. 10.1016/j.jnoncrysol.2009.03.005.

Hrma P, MJ Schweiger, CJ Humrickhouse, JA Moody, RM Tate, TT Rainsdon, NE Tegrotenhuis, BM Arrigoni, J Marcial, CP Rodriguez, and BH Tincher. 2010. "Effect of Glass-Batch Makeup on the Melting Process." *Ceramics-Silikaty*, **54**(3):193−211.

Hrma P., BJ Riley, JV Crum, and J Matyas. 2014. "The Effect of High-Level Waste Glass Composition on Spinel Liquidus Temperature," *Journal of Non-Crystalline Solids*, **384**:32-40. DOI 10.1016/j.jnonaysol.2013.02.014.

Hrma P and JD Vienna. 2003. "Relationship between Liquidus Temperature and Solubility." *Environmental Issues and Waste Management Technologies in the Ceramic and Nuclear Industries VIII* 143:159−167, American Ceramic Society, Westerville, Ohio.

Hutson ND. 1993. *Integrated DWPF Melter System (Idms) Campaign Report, Hanford Waste Vitrification Plant (HWVP) Process Demonstration (U)*. WSRC-TR-92-0403, Rev. 1, Westinghouse Savannah River Company, Aiken, South Carolina.

Jain V and SM Barnes. 1991. "Effect of Glass Pour Cycle on the Crystallization Behavior in the Canistered Product at the West Valley Demonstration Project." *Nuclear Waste Management* IV 23.

Jain V, RA Palmer, and SM Barnes. 1992. "Glass Composition Development and Nuclear Waste Vitrification System Testing − the West Valley Experience." In *Physics of Non-Crystalline Solids*, edited by LD Pye and HJ Stevens, Taylor & Francis, New York.

Jantzen CM. 1986. *Devitrification of Scale Melter Glass in Riser Heater*. DPST-86-461, Savannah River Laboratory, Aiken, South Carolina.

Jantzen CM. 1991a. "Relationship of Glass Composition to Glass Viscosity, Resistivity, Liquidus Temperature, and Durability: First-Principle Process Product Models for Vitrification of Nuclear Waste." *Ceramics Transactions* 23:37−51, American Ceramic Society, Westerville, Ohio.

Jantzen CM. 1991b. *Characterization of Off-Gas System Pluggages, Significance for DWPF and Suggested Remediation*, WSRC-TR-90-205, Westinghouse Savannah River Company, Aiken, South Carolina.

Jantzen CM, NE Bibler, DC Beam, CL Crawford, and MA Pickett. 1993. *Characterization of the Defense Waste Processing Facility (DWPF) Environmental Assessment (EA) Glass Standard Reference Material (U)*. WSRC-TR-92-346, Rev. 1, Westinghouse Savannah River Company, Aiken, South Carolina.

Jantzen CM and D Lambert. 1999. *Inspection and Analysis of the Integrated DWPF Melter System (Idms) after Seven Years of Continuous Operation*. WSRC-MS-99-00336, Westinghouse Savannah River Company, Aiken, South Carolina.

Jantzen CM, AD Cozzi, and NE Bibler. 2004. "High Level Waste Processing Experience with Increased Waste Loadings." *Ceramic Transactions* 168:31−49, American Ceramic Society, Westerville, Ohio.

Jantzen CM and KG Brown. 2007a. "Predicting the Spinel-Nepheline Liquidus for Application to Nuclear Waste Glass Processing: Part I. Primary Phase Analysis, Liquidus Measurement, and Quasicrystalline Approach." *Journal of the American Ceramic Society*, **90**(6):1866-1879.

Jantzen CM and KG Brown. 2007b. "Predicting the Spinel-Nepheline Liquidus for Application to Nuclear Waste Glass Processing. Part II: Quasicrystalline Freezing Point Depression Model." *Journal of the American Ceramic Society*, **90**(6):1880-1891.

Johnson FC and TB Edwards. 2009. *Results of the FY09 Enhanced DOE High-Level Waste Melter Throughput Studies at SRNL*. SRNL-STI-2009-00778, Savannah River National Laboratory, Aiken, South Carolina.

Kim DS, DK Peeler, and P Hrma. 1995. "Effect of Crystallization on the Chemical Durability of Simulated Nuclear Waste Glasses." *Ceramic Transactions* 61:177−185, American Ceramic Society, Westerville, Ohio.

Kim D, JD Vienna, P Hrma, MJ Schweiger, J Matyas, JV Crum, DE Smith, WC Buchmiller, JS Tixier, Jr., JD Yeager, and KB Belew. 2003. *Development and Testing of ICV Glasses for Hanford LAW*. PNNL-14351, Pacific Northwest National Laboratory, Richland, Washington.

Kim D, JD Vienna, DK Peeler, KM Fox, A Aloy, AV Trofimenko, and KD Gerdes. 2008. "Improved Alumina Loading in High Level Waste Glasses." *Waste Management 2008*, p. 10382.

Kim DS, MJ Schweiger, CP Rodriguez, WC Lepry, JB Lang, JV Crum, JD Vienna, FC Johnson, JC Marra, and DK Peeler. 2011. *Formulation and Characterization of Waste Glasses with Varying Processing Temperature*. PNNL-20774, Pacific Northwest National Laboratory, Richland, Washington.

Kim DS and JD Vienna. 2012. *Preliminary ILAW Formulation Algorithm Description*: *24590-LAW-RPT-RT-04-0003, Rev. 1,* ORP-56321, River Protection Project, Hanford Tank Waste Treatment and Immobilization Plant, Richland, Washington.

Kim DS. 2013. Letter, "Estimation of Low-Activity Waste Glass Mass," to AA Kruger, PNNL-SA-92798, January 8, 2013, Pacific Northwest National Laboratory, Richland, Washington.

Li H, JD Vienna, P Hrma, DE Smith, and MJ Schweiger. 1997. "Nepheline Precipitation in High-Level Waste Glasses: Compositional Effects and Impact on the Waste Form Acceptability." *Scientific Basis for Nuclear Waste Management XX* 465*:*261−268, Materials Research Society, Pittsburgh, Pennsylvania.

Matlack KS, M Chaudhuri, H Gan, IS Muller, WK Kot, W Gong, and IL Pegg. 2005. *Glass Formulation Testing to Increase Sulfate Incorporation*: *VSL-04R4960-1,* ORP-51808, Vitreous State Laboratory, The Catholic University of America, Washington, D.C.

Matlack KS, H Gan, M Chaudhuri, WK Kot, W Gong, T Bardakci, IL Pegg, and I Joseph. 2010a. *DM100 and Dm1200 Melter Testing with High Waste Loading Glass Formulations for Hanford High-Aluminum HLW Streams: VSL-10R1690-1,* ORP-44198, Vitreous State Laboratory, The Catholic University of America, Washington, D.C.

Matlack KS, H Gan, M Chaudhuri, WK Kot, W Gong, T Bardakci, IL Pegg, and I Joseph. 2008. *Melt Rate Enhancement for High Aluminum HLW Glass Formulations: VSL-08R1360-1,* ORP-44236, Vitreous State Laboratory, The Catholic University of America, Washington, D.C.

Matlack KS, H Gan, W Gong, IL Pegg, CC Chapman, and I Joseph. 2007a. *High Level Waste Vitrification System Improvements: VSL-07R1010-1,* ORP-56297, Vitreous State Laboratory, The Catholic University of America, Washington, D.C.

Matlack KS, W Gong, IS Muller, I Joseph, and IL Pegg. 2006a. *LAW Envelope A and B Glass Formulations Testing to Increase Waste Loading: VSL-06R6900-1,* ORP-56322, Vitreous State Laboratory, The Catholic University of America, Washington, D.C.

Matlack KS, W Gong, IS Muller, I Joseph, and IL Pegg. 2006b. *LAW Envelope C Glass Formulation Testing to Increase Waste Loading: VSL-05R5900-1*, ORP-56323, Vitreous State Laboratory, The Catholic University of America, Washington, D.C.

Matlack KS, I Joseph, W Gong, IS Muller, and IL Pegg. 2007b. *Enhanced LAW Glass Formulation Testing: VSL-07R1130-1,* ORP-56293, Vitreous State Laboratory, The Catholic University of America, Washington, D.C.

Matlack KS, I Joseph, W Gong, IS Muller, and IL Pegg . 2009a. *Glass Formulation Development and Dm10 Melter Testing with ORP LAW Glasses: VSL-09R1510-2,* ORP-56296, Vitreous State Laboratory, The Catholic University of America, Washington, D.C.

Matlack KS, WK Kot, H Gan, and IL Pegg. 2010b. *Glass Formulation Development and Testing for DWPF High-Al_2O_3 HLW Sludges: VSL-10R1670-1,* ORP-56290, Vitreous State Laboratory, The Catholic University of America, Washington, D.C.

Matlack KS, WK Kot, W Gong, W Lutze, IL Pegg, and I Joseph. 2009b. *Effects of High Spinel and Chromium Oxide Crystal Contents on Simulated HLW Vitrification in DM100 Melter Tests: VSL-09R1520-1,* ORP-56327, Vitreous State Laboratory, The Catholic University of America, Washington, D.C.

Matyas J, AR Huckleberry, CP Rodriguez, JB Lang, AT Owen, and AA Kruger. 2013. "Crystal-Tolerant Glass Approach for Mitigation of Crystal Accumulation in Continuous Melters Processing Radioactive Waste." *Journal of the American Ceramic Society* (Submitted).

Matyas J, M Schaible, and JD Vienna. 2011. "Determination of Stokes Shape Factor for Single Particles and Agglomerates." *Advances in Materials Science for Environmental and Nuclear Technology II* 227:195−202.

Matyas J, JD Vienna, A Kimura, M Schaible, and RM Tate. 2010a. "Development of Crystal-Tolerant Waste Glasses." *Advances in Materials Science for Environmental and Nuclear Technology* 222:41−50.

Matyas J, JD Vienna, M Schaible, C Rodriguez, JV Crum, A Kimura, and RM Tate. 2010b. *Development of Crystal-Tolerant High-Level Waste Glasses.* PNNL-20072, Pacific Northwest National Laboratory, Richland, Washington.

McCloy JS, C Rodriguez, C Windisch, C Leslie, MJ Schweiger, BJ Riley, and JD Vienna. 2010. "Alkali/Alkaline-Earth Content Effects of Properties of High-Alumina Nuclear Waste Glasses." *Ceramic Transactions* 222:63−76, American Ceramic Society, Westerville, Ohio.

McCloy JS, MJ Schweiger, CP Rodriguez, and JD Vienna. 2011. "Nepheline Crystallization in Nuclear Waste Glasses: Progress toward Acceptance of High-Alumina Formulations." *International Journal of Applied Glass Science* 2(3):201−214. DOI 10.1111/j.2041-1294.2011.00055.x.

McCloy JS and JD Vienna. 2010. *Glass Composition Constraint Recommendations for Use in Life-Cycle Mission Modeling*. PNNL-19372, Pacific Northwest National Laboratory, Richland, Washington.

McElroy JL. 1976. *Quarterly Progress Report Research and Development Activities Waste Fixation Program, January through March 1976.* BNWL-2070, Pacific Northwest Laboratory, Richland, Washington.

McElroy JL, JE Mendel, WF Bonner, and MH Henry. 1979a. *Quarterly Progress Report − Research and Development Activities − High-Level Waste Immobilization Program: January through March 1979.* PNL-3050-1, Pacific Northwest Laboratory, Richland, Washington.

McElroy JL, JE Mendel, WF Bonner, and MH Henry. 1979b. *Quarterly Progress Reports Research and Development Activities − High-Level Waste Immobilization Program: January through December 1978.* PNL-2999, Pacific Northwest Laboratory, Richland, Washington.

Mendel JE, WA Ross, FP Roberts, YB Katayama, J Westsik, JH, RP Turcotte, JW Wald, and DJ Bradley. 1977. *Annual Report on the Characteristics of High-Level Waste Glasses*. BNWL-2252, Pacific Northwest Laboratory, Richland, Washington.

Muller IS, AC Buechele, and IL Pegg. 2001. *Glass Formulation and Testing with Rpp-WTP LAW Simulants: VSL-01R3560-2,* ORP-56327, Vitreous State Laboratory, The Catholic University of America, Washington, D.C.

Muller IS, G Diener, I Joseph, and IL Pegg. 2004. *Proposed Approach for Development of LAW Glass Formulation Correlation: VSL-04L4460-1, Rev. 2,* ORP-56326, Vitreous State Laboratory, The Catholic University of America, Washington, D.C.

Muller IS, WK Kot, HK Pasieka, K Gilbo, FC Perez-Cardenas, I Joseph, and IL Pegg. 2012. *Compilation and Management of ORP Glass Formulation Database: VSL-12R2470-1,* ORP-53934, Vitreous State Laboratory, The Catholic University of America, Washington, D.C.

Muller IS, KS Matlack, H Gan, I Joseph, and IL Pegg. 2010. *Waste Loading Enhancements for Hanford LAW Glasses: VSL-10R1790-1,* ORP-48578, Vitreous State Laboratory, The Catholic University of America, Washington, D.C.

Muller IS and IL Pegg. 2003. *Baseline LAW Glass Formulation Testing: VSL-03R3460-1,* ORP-55237, Vitreous State Laboratory, The Catholic University of America, Washington, D.C.

Muller IS, IL Pegg, AC Buechele, H Gan, C Kim, ST Lai, G Del Rosario, and Q Yan. 1998. *Glass Formulation and Testing with TWRS LAW Simulants*. ORP-56328, The Catholic University of America, Washington, D.C.

OCRWM. 2008. *Civilian Radioactive Waste Management System Waste Acceptance System Requirements Document (WASRD*. DOEIRW-0351, Rev. 5, ICN 01, U.S. Department of Energy, Office of Civilian Radioactive Waste Management, Washington, D.C.

Peeler DK, TB Edwards, DR Best, IA Reamer, and RJ Workman. 2006. *Nepheline Formation Study for Sludge Batch 4 (SB4): Phase 2 Experimental Results*. WSRC-TR-2006-00006, Savannah River National Laboratory, Aiken, South Carolina.

Peeler DK, TB Edwards, IA Reamer, and RJ Workman. 2005. *Nepheline Formation Study for Sludge Batch 4 (SB4): Phase 1 Experimental Results*. WSRC-TR-2005-00371, Savannah River National Laboratory, Aiken, South Carolina.

Piepel GF, SK Cooley, A Heredia-Langner, SM Landmesser, WK Kot, H Gan, and IL Pegg. 2008. *IHLW PCT, Spinel $T_{1\%}$, Electrical Conductivity, and Viscosity Model Development: VSL-07R1240-4, Rev. 0,* ORP-56320, Vitreous State Laboratory, The Catholic University of America, Washington, D.C.

Piepel GF, SK Cooley, IS Muller, H Gan, I Joseph, and IL Pegg. 2007. *ILAW PCT, VHT, Viscosity, and Electrical Conductivity Model Development: VSL-07R1240-4, Rev. 0*, ORP-56502, Vitreous State Laboratory, The Catholic University of America, Washington, D.C.

Rankin WN, PE O'rourke, PD Soper, MB Cosper, and BC Osgood. 1982. *Evaluation of Corrosion and Deposition in the 1941 Melter*. DPST-82-231, Savannah River Laboratory, Aiken, South Carolina.

Riley BJ, JA Rosaria, and P Hrma. 2001. *Impact of HLW Glass Crystallinity on PCT Response*. PNNL-13491, Pacific Northwest National Laboratory, Richland, Washington.

Rodriguez CP, J McCloy, MJ Schweiger, JV Crum, and A Winschell. 2011. *Optical Basicity and Nepheline Crystallization in High Alumina Glasses*. PNNL-20184, Pacific Northwest National Laboratory, Richland, Washington.

Ross WA and JE Mendel. 1979. *Annual Report on the Development and Characterization of Solidified Forms for High-Level Wastes: 1978*. PNL-3060, Pacific Northwest Laboratory, Richland, Washington.

Vienna JD, A Fluegel, DS Kim, and P Hrma. 2009. *Glass Property Data and Models for Estimating High-Level Waste Glass Volume*. PNNL-18501, Pacific Northwest National Laboratory, Richland, Washington.

Vienna JD, P Hrma, A Jiricka, DE Smith, TH Lorier, IA Reamer, and RL Schulz. 2001a. *Hanford Immobilized LAW Product Acceptance Testing: Tanks Focus Area Results*. PNNL-13744, Pacific Northwest National Laboratory, Richland, Washington.

Vienna JD, P Hrma, MJ Schweiger, and MH Langowski. 1996a. "Compositional Dependence of Elemental Release from HLW Glasses by the Product Consistency Test: A One Component-at-a-Time Study." *Ceramic Transactions* 72:307−316, American Ceramic Society, Westerville, Ohio.

Vienna JD, P Hrma, MJ Schweiger, MH Langowski, PE Redgate, DS Kim, GF Peipel, DE Smith, CY Chang, DE Rinehart, SE Palmer, and H Li. 1996b. *Effect of Composition and Temperature on the Properties of High-Level Waste (HLW) Glass Melting above 1200°C*. PNNL-10987, Pacific Northwest National Laboratory, Richland, Washington.

Vienna JD, A Jiřička, PR Hrma, DE Smith, TH Lorier, RL Schulz, and IA Reamer. 2001b. *Hanford Immobilized LAW Product Acceptance Testing: Tanks Focus Area Results*. PNNL-13744, Pacific Northwest National Laboratory, Richland, Washington.

Vienna JD and DS Kim. 2008. *Preliminary IHLW Formulation Algorithm Description*. 24590-HLW-RPT-RT-05-001, Rev 0, River Protection Project, Hanford Tank Waste Treatment and Immobilization Plant, Richland, Washington.

Vienna JD, DS Kim, MJ Schweiger, JS McCloy, J Matyas, GF Piepel, and SK Cooley. 2013. *Test Plan: Enhanced Hanford Waste Glass Models*. TP-EWG-00001, Rev. 0, Pacific Northwest National Laboratory, Richland, Washington.

Appendix A

High-Level Waste Glass Volume Estimates

Appendix A

High-Level Waste Glass Volume Estimates

Abstract

The glass property-composition models, property constraints, and component concentration constraints described in Section 2.0 of this report were applied to estimates of the HLW to be treated in the WTP HLW vitrification facility during the life of the mission. The resulting maximum waste loadings and glass masses were determined. The calculation was also performed using the constraints currently applied in the HTWOS model runs in support of system planning as verification of the method as well as a point of comparison. It was found that the HLW glass mass for the whole mission was roughly 23,000 MT, which translates to roughly 7,600 canisters of glass. These results show a significant glass mass reduction compared to either the System Plan Rev. 6 base case (31,500 MT) or the current fully qualified WTP formulation algorithm (55,000 MT).

Waste Composition Estimates

It has long been recognized that the waste composition estimates change to some extent with assumptions on retrieval sequence, retrieval efficiency, leaching efficiency, system recycles, inclusion of transuranic tank wastes, and other system variables. Therefore, two waste composition estimates or feed vectors were used to evaluate the impacts of advanced glass formulation constraints on glass volumes. The first feed vector was generated in May of 2008 using RPP system plan revision 3 baseline assumptions (Certa et al. 2008). This "2008" feed vector was used to generate the 2010 WTP tank utilization assessment (TUA-2010) (Jenkins et al. 2010). The HLW feed compositions generated by the WTP Dynamic Flowsheet Model (G2) run (MRQ 10-0063 Scenario 6.0.1a) in support of the TUA-2010 base case were used as the "2008" waste in this study. Specifically, the compositions of HLW at a node between the high-level waste blend vessel (HLP, HLP-VSL-0028) and the melter feed preparation vessel (MFPV, HFP-VSL-00001 and 5) were used (G2 node HLP-4).

The second waste composition estimate (feed vector) was based on the RPP system plan revision 6 baseline assumptions (Certa et al. 2011). This "2011" feed vector was used to generate the 2012 WTP tank utilization assessment (TUA-2012) (Jenkins et al. 2012). The HLW feed compositions generated by the G2 run (MRQ 11-0056) in support of the TUA-2012 Case 3 were used as the "2011" waste in this study. Similar to the "2008" waste, the compositions of HLW at a node between HBV and MFPV were used (HLP-4).

Cluster analyses were performed to reduce the roughly 380 ("2008" waste) and 580 ("2011" waste) waste batches to a manageable number for calculation. These analyses were performed using the *K*-Means Cluster method in JMP® Version 10.0 (SAS Institute, Inc., Cary, NC) based on the 15 components, Al_2O_3, Bi_2O_3, CaO, CdO, Cr_2O_3, F, Fe_2O_3, MnO, Na_2O, NiO, P_2O_5, SO_3, ThO_2, UO_3, and ZrO_2, which represent the components that are present in large concentrations or have a strong effect on waste loading in glass. In cluster analysis, as the number of clusters increases, the average distance (a measure of closeness of data points or waste compositions to the centroid of each cluster used by JMP® software) over all clusters analyzed decreases, (i.e., the higher the number of clusters, the more accurate

the partitioning of composition becomes). However, it is desirable to keep the number of clusters small so that the glass formulation is manageable. The 20 clusters were found reasonable in a previous study (Kim et al. 2011) and were used in this study without additional evaluation.

The resulting clusters of like compositions are given in Table A.1 for the 2008 waste and Table A.2 for the 2011 waste.

Table A.1. 2008 Waste Cluster Mean Compositions in Mass Fractions and Total Oxide Mass (*M*) in MT

Cluster #	08-C01	08-C02	08-C03	08-C04	08-C05	08-C06	08-C07	08-C08	08-C09	08-C10	08-C11	08-C12	08-C13	08-C14	08-C15	08-C16	08-C17	08-C18	08-C19	08-C20
Ag2O	0.0001	0.0002	0.0001	0.0001	0.0003	0.0002	0.0011	0.0002	0.0011	0.0002	0.0010	0.0002	0.0004	0.0014	0.0006	0.0002	0.0001	0.0001	0.0003	0.0003
Al2O3	0.1948	0.1698	0.2274	0.4105	0.2274	0.2659	0.1646	0.2844	0.1839	0.4166	0.1494	0.1505	0.0869	0.1252	0.2057	0.3090	0.5627	0.1572	0.1197	0.3817
As2O5	0.0005	0.0006	0.0002	0.0005	0.0005	0.0003	0.0002	0.0006	0.0003	0.0003	0.0006	0.0002	0.0009	0.0005	0.0007	0.0002	0.0003	0.0005	0.0002	0.0011
B2O3	0.0020	0.0038	0.0011	0.0029	0.0032	0.0019	0.0026	0.0028	0.0025	0.0021	0.0029	0.0020	0.0050	0.0076	0.0041	0.0010	0.0019	0.0012	0.0018	0.0047
BaO	0.0004	0.0004	0.0005	0.0007	0.0009	0.0006	0.0027	0.0003	0.0013	0.0002	0.0029	0.0004	0.0006	0.0006	0.0014	0.0007	0.0002	0.0005	0.0005	0.0009
BeO	0.0004	0.0002	0.0002	0.0001	0.0001	0.0010	0.0001	0.0008	0.0001	0.0002	0.0001	0.0001	0.0001	0.0002	0.0008	0.0001	0.0001	0.0001	0.0000	0.0001
Bi2O3	0.0691	0.0246	0.0160	0.0378	0.0488	0.0514	0.0117	0.0156	0.0031	0.0183	0.0178	0.0313	0.0122	0.0226	0.0328	0.0081	0.0142	0.0105	0.0529	0.0140
CaO	0.0535	0.0332	0.0195	0.0217	0.0367	0.0225	0.0228	0.0191	0.0203	0.0144	0.0245	0.0277	0.0240	0.0354	0.0169	0.0309	0.0076	0.0762	0.0491	0.0154
CdO	0.0005	0.0004	0.0005	0.0001	0.0003	0.0003	0.0008	0.0007	0.0295	0.0002	0.0006	0.0002	0.0004	0.0043	0.0006	0.0036	0.0000	0.0031	0.0002	0.0001
Ce2O3	0.0008	0.0003	0.0003	0.0004	0.0005	0.0004	0.0019	0.0007	0.0021	0.0002	0.0015	0.0002	0.0007	0.0006	0.0010	0.0008	0.0003	0.0013	0.0009	0.0009
Cl	0.0016	0.0018	0.0026	0.0014	0.0013	0.0021	0.0019	0.0021	0.0021	0.0018	0.0024	0.0018	0.0016	0.0018	0.0015	0.0020	0.0014	0.0021	0.0022	0.0009
CoO	0.0001	0.0002	0.0001	0.0001	0.0002	0.0003	0.0001	0.0001	0.0001	0.0001	0.0001	0.0001	0.0002	0.0001	0.0002	0.0001	0.0001	0.0001	0.0000	0.0002
Cr2O3	0.0132	0.0201	0.0319	0.0164	0.0172	0.0201	0.0060	0.0653	0.0056	0.0201	0.0128	0.0708	0.0255	0.0113	0.0276	0.0120	0.0203	0.0125	0.0035	0.0218
Cs2O	0.0001	0.0001	0.0003	0.0001	0.0001	0.0001	0.0003	0.0003	0.0003	0.0003	0.0004	0.0001	0.0002	0.0002	0.0002	0.0003	0.0001	0.0003	0.0003	0.0001
CuO	0.0002	0.0003	0.0001	0.0001	0.0003	0.0001	0.0007	0.0001	0.0004	0.0002	0.0007	0.0001	0.0002	0.0003	0.0003	0.0002	0.0002	0.0003	0.0004	0.0002
Eu2O3	0.0000	0.0000	0.0000	0.0000	0.0000	0.0000	0.0000	0.0000	0.0000	0.0000	0.0000	0.0000	0.0000	0.0000	0.0000	0.0000	0.0000	0.0000	0.0000	0.0000
F	0.0269	0.0305	0.0157	0.0059	0.0187	0.0541	0.0020	0.0039	0.0011	0.0122	0.0124	0.0460	0.0065	0.0015	0.0041	0.0012	0.0028	0.0022	0.0113	0.0062
Fe2O3	0.1086	0.1176	0.0936	0.0991	0.1340	0.0865	0.2936	0.0749	0.3188	0.0528	0.2309	0.1124	0.0622	0.1719	0.1472	0.1355	0.0432	0.1184	0.2167	0.0819
I	0.0000	0.0000	0.0000	0.0000	0.0000	0.0000	0.0000	0.0000	0.0000	0.0000	0.0000	0.0000	0.0000	0.0000	0.0000	0.0000	0.0000	0.0000	0.0000	0.0000
K2O	0.0047	0.0041	0.0042	0.0039	0.0038	0.0050	0.0059	0.0064	0.0088	0.0049	0.0107	0.0096	0.0236	0.0095	0.0077	0.0047	0.0015	0.0085	0.0196	0.0042
La2O3	0.0004	0.0006	0.0024	0.0008	0.0030	0.0003	0.0019	0.0007	0.0077	0.0026	0.0039	0.0044	0.0002	0.0061	0.0083	0.0021	0.0010	0.0019	0.0003	0.0003
Li2O	0.0004	0.0004	0.0002	0.0002	0.0003	0.0008	0.0003	0.0008	0.0004	0.0003	0.0004	0.0003	0.0006	0.0002	0.0008	0.0003	0.0002	0.0005	0.0002	0.0004
MgO	0.0016	0.0036	0.0014	0.0016	0.0051	0.0013	0.0056	0.0010	0.0024	0.0019	0.0082	0.0019	0.0036	0.0037	0.0055	0.0014	0.0018	0.0010	0.0018	0.0033
MnO	0.0094	0.0080	0.0179	0.0301	0.0244	0.0050	0.0288	0.0401	0.0113	0.0291	0.0239	0.0118	0.0203	0.0315	0.0881	0.0125	0.0189	0.0370	0.0222	0.1407
MoO3	0.0004	0.0007	0.0002	0.0004	0.0006	0.0005	0.0002	0.0005	0.0002	0.0002	0.0005	0.0004	0.0012	0.0003	0.0005	0.0002	0.0003	0.0005	0.0002	0.0007
Na2O	0.2791	0.2416	0.3051	0.1758	0.1820	0.1981	0.2174	0.2658	0.1727	0.2175	0.2241	0.2112	0.5558	0.1968	0.2320	0.2310	0.2116	0.4378	0.1993	0.1364
Nd2O3	0.0007	0.0003	0.0004	0.0005	0.0006	0.0003	0.0023	0.0009	0.0059	0.0003	0.0018	0.0002	0.0007	0.0010	0.0012	0.0018	0.0007	0.0028	0.0003	0.0011
NiO	0.0074	0.0126	0.0174	0.0062	0.0133	0.0069	0.0176	0.0034	0.0250	0.0133	0.0193	0.0288	0.0045	0.0382	0.0260	0.0202	0.0035	0.0049	0.0282	0.0039
P2O5	0.0643	0.0739	0.0987	0.0275	0.0295	0.0402	0.0158	0.0984	0.0089	0.0399	0.0141	0.1031	0.0232	0.0391	0.0406	0.0113	0.0117	0.0275	0.0518	0.0179
PbO	0.0060	0.0057	0.0036	0.0050	0.0079	0.0026	0.0137	0.0037	0.0062	0.0022	0.0124	0.0036	0.0054	0.0058	0.0075	0.0053	0.0017	0.0027	0.0113	0.0060
PdO	0.0000	0.0000	0.0000	0.0000	0.0000	0.0000	0.0000	0.0000	0.0000	0.0000	0.0000	0.0000	0.0000	0.0000	0.0000	0.0002	0.0000	0.0002	0.0000	0.0000
Rb2O	0.0000	0.0000	0.0000	0.0000	0.0000	0.0000	0.0001	0.0000	0.0001	0.0000	0.0001	0.0000	0.0000	0.0003	0.0001	0.0001	0.0000	0.0001	0.0000	0.0000
Re2O7	0.0000	0.0000	0.0001	0.0000	0.0000	0.0000	0.0000	0.0000	0.0000	0.0000	0.0000	0.0000	0.0001	0.0000	0.0001	0.0000	0.0000	0.0000	0.0000	0.0000
Rh2O3	0.0000	0.0000	0.0000	0.0000	0.0000	0.0000	0.0001	0.0000	0.0000	0.0000	0.0001	0.0000	0.0000	0.0002	0.0001	0.0001	0.0000	0.0002	0.0000	0.0000
RuO2	0.0001	0.0000	0.0003	0.0000	0.0000	0.0000	0.0014	0.0001	0.0001	0.0000	0.0013	0.0000	0.0000	0.0001	0.0005	0.0007	0.0000	0.0004	0.0003	0.0000

Cluster #	08-C01	08-C02	08-C03	08-C04	08-C05	08-C06	08-C07	08-C08	08-C09	08-C10	08-C11	08-C12	08-C13	08-C14	08-C15	08-C16	08-C17	08-C18	08-C19	08-C20
Sb2O3	0.0003	0.0001	0.0002	0.0002	0.0002	0.0003	0.0001	0.0002	0.0001	0.0001	0.0002	0.0003	0.0004	0.0002	0.0003	0.0001	0.0002	0.0002	0.0002	0.0004
SeO2	0.0000	0.0000	0.0000	0.0000	0.0000	0.0000	0.0000	0.0000	0.0000	0.0000	0.0001	0.0000	0.0002	0.0000	0.0000	0.0000	0.0000	0.0000	0.0000	0.0001
SiO2	0.0891	0.0969	0.0534	0.0801	0.1327	0.1659	0.0620	0.0381	0.0289	0.0301	0.0578	0.0538	0.0792	0.0376	0.0490	0.0865	0.0412	0.0206	0.1290	0.1005
Sm2O3	0.0000	0.0000	0.0000	0.0000	0.0000	0.0000	0.0000	0.0000	0.0000	0.0000	0.0000	0.0000	0.0000	0.0000	0.0000	0.0000	0.0000	0.0000	0.0000	0.0000
SnO2	0.0000	0.0000	0.0000	0.0000	0.0000	0.0000	0.0000	0.0000	0.0000	0.0000	0.0000	0.0000	0.0000	0.0000	0.0000	0.0000	0.0000	0.0000	0.0000	0.0000
SO3	0.0086	0.0112	0.0089	0.0078	0.0089	0.0193	0.0033	0.0175	0.0017	0.0108	0.0097	0.0201	0.0033	0.0061	0.0130	0.0024	0.0041	0.0038	0.0014	0.0067
SrO	0.0093	0.0128	0.0167	0.0022	0.0081	0.0048	0.0016	0.0046	0.0006	0.0066	0.0008	0.0224	0.0038	0.0012	0.0023	0.0105	0.0017	0.0255	0.0014	0.0019
TeO2	0.0000	0.0000	0.0000	0.0000	0.0000	0.0000	0.0003	0.0000	0.0000	0.0000	0.0002	0.0000	0.0000	0.0000	0.0001	0.0001	0.0000	0.0001	0.0000	0.0000
ThO2	0.0036	0.0023	0.0055	0.0008	0.0028	0.0020	0.0176	0.0003	0.0156	0.0005	0.0150	0.0035	0.0059	0.0461	0.0088	0.0253	0.0005	0.0012	0.0027	0.0014
TiO2	0.0001	0.0003	0.0001	0.0001	0.0002	0.0002	0.0005	0.0001	0.0003	0.0002	0.0005	0.0002	0.0001	0.0003	0.0002	0.0001	0.0001	0.0001	0.0001	0.0003
Tl2O	0.0003	0.0006	0.0003	0.0003	0.0008	0.0004	0.0003	0.0007	0.0000	0.0003	0.0001	0.0001	0.0012	0.0002	0.0005	0.0002	0.0019	0.0006	0.0004	0.0001
UO3	0.0374	0.1171	0.0446	0.0558	0.0817	0.0317	0.0523	0.0316	0.0684	0.0499	0.0880	0.0670	0.0327	0.0865	0.0417	0.0479	0.0395	0.0220	0.0461	0.0408
V2O5	0.0003	0.0004	0.0002	0.0003	0.0003	0.0005	0.0001	0.0004	0.0001	0.0002	0.0004	0.0003	0.0006	0.0002	0.0004	0.0001	0.0002	0.0002	0.0001	0.0007
WO3	0.0000	0.0000	0.0001	0.0000	0.0000	0.0000	0.0005	0.0002	0.0000	0.0000	0.0007	0.0000	0.0000	0.0000	0.0004	0.0002	0.0000	0.0003	0.0001	0.0000
Y2O3	0.0000	0.0000	0.0000	0.0000	0.0000	0.0000	0.0003	0.0000	0.0002	0.0000	0.0002	0.0000	0.0000	0.0001	0.0001	0.0001	0.0000	0.0002	0.0000	0.0000
ZnO	0.0003	0.0008	0.0003	0.0003	0.0006	0.0005	0.0008	0.0005	0.0012	0.0009	0.0009	0.0006	0.0010	0.0013	0.0006	0.0003	0.0004	0.0006	0.0008	0.0006
ZrO2	0.0032	0.0019	0.0075	0.0018	0.0026	0.0056	0.0362	0.0120	0.0603	0.0474	0.0436	0.0119	0.0049	0.1017	0.0181	0.0284	0.0018	0.0119	0.0220	0.0013
M, MT	355.67	274.54	138.15	3045.4	1416.5	618.44	1148.2	196.37	135.43	891.44	139.37	299.63	154.28	291.41	331.00	449.01	1300.5	192.30	356.33	312.49

Table A.2. 2011 Waste Cluster Mean Compositions in Mass Fractions and Total Oxide Mass (*M*) in MT

#	11-C1	11-C2	11-C3	11-C4	11-C5	11-C6	11-C7	11-C8	11-C9	11-C10	11-C11	11-C12	11-C13	11-C14	11-C15	11-C16	11-C17	11-C18	11-C19	11-C20
Ag2O	0.0002	0.0001	0.0001	0.0001	0.0010	0.0003	0.0005	0.0002	0.0010	0.0009	0.0001	0.0002	0.0004	0.0003	0.0006	0.0002	0.0001	0.0010	0.0005	0.0003
Al2O3	0.3564	0.5086	0.2738	0.0844	0.1494	0.2367	0.2737	0.2559	0.1657	0.1852	0.1823	0.2262	0.1775	0.3532	0.1412	0.3508	0.3129	0.1693	0.2853	0.1746
As2O5	0.0004	0.0004	0.0003	0.0006	0.0003	0.0005	0.0002	0.0007	0.0001	0.0003	0.0007	0.0003	0.0001	0.0008	0.0003	0.0006	0.0003	0.0007	0.0006	0.0008
B2O3	0.0032	0.0028	0.0025	0.0015	0.0045	0.0029	0.0013	0.0035	0.0006	0.0032	0.0028	0.0020	0.0005	0.0051	0.0028	0.0038	0.0024	0.0026	0.0047	0.0045
BaO	0.0005	0.0003	0.0006	0.0002	0.0010	0.0015	0.0008	0.0004	0.0025	0.0021	0.0005	0.0003	0.0017	0.0005	0.0014	0.0004	0.0002	0.0016	0.0005	0.0003
BeO	0.0001	0.0003	0.0001	0.0001	0.0002	0.0001	0.0000	0.0001	0.0000	0.0001	0.0002	0.0001	0.0000	0.0003	0.0001	0.0004	0.0000	0.0001	0.0002	0.0001
Bi2O3	0.0428	0.0119	0.0755	0.0784	0.0069	0.0088	0.0071	0.0534	0.0133	0.0115	0.0169	0.0472	0.0366	0.0221	0.0115	0.0092	0.0472	0.0016	0.0039	0.0580
CaO	0.0170	0.0182	0.0268	0.0181	0.0198	0.0237	0.0217	0.0153	0.0199	0.0233	0.0781	0.1407	0.0351	0.0124	0.0385	0.0172	0.0669	0.0196	0.0151	0.0189
CdO	0.0001	0.0002	0.0001	0.0001	0.0005	0.0003	0.0040	0.0004	0.0009	0.0014	0.0004	0.0001	0.0029	0.0004	0.0008	0.0002	0.0000	0.0238	0.0003	0.0003
Ce2O3	0.0005	0.0004	0.0004	0.0005	0.0003	0.0002	0.0011	0.0006	0.0021	0.0009	0.0006	0.0003	0.0011	0.0007	0.0003	0.0005	0.0002	0.0027	0.0005	0.0006
Cl	0.0007	0.0010	0.0008	0.0011	0.0015	0.0015	0.0017	0.0010	0.0010	0.0015	0.0008	0.0014	0.0016	0.0007	0.0015	0.0011	0.0011	0.0011	0.0011	0.0014
CoO	0.0001	0.0001	0.0001	0.0001	0.0001	0.0001	0.0001	0.0001	0.0001	0.0002	0.0002	0.0001	0.0001	0.0001	0.0001	0.0002	0.0000	0.0002	0.0001	0.0002
Cr2O3	0.0134	0.0239	0.0217	0.0123	0.0152	0.0195	0.0091	0.0245	0.0061	0.0081	0.0192	0.0083	0.0072	0.0210	0.0098	0.0298	0.0146	0.0087	0.0094	0.0193
Cs2O	0.0001	0.0001	0.0000	0.0002	0.0004	0.0002	0.0005	0.0001	0.0002	0.0004	0.0001	0.0001	0.0004	0.0001	0.0003	0.0001	0.0000	0.0006	0.0004	0.0002

#	11-C1	11-C2	11-C3	11-C4	11-C5	11-C6	11-C7	11-C8	11-C9	11-C10	11-C11	11-C12	11-C13	11-C14	11-C15	11-C16	11-C17	11-C18	11-C19	11-C20
CuO	0.0003	0.0001	0.0002	0.0001	0.0002	0.0003	0.0003	0.0003	0.0007	0.0004	0.0001	0.0002	0.0004	0.0003	0.0002	0.0001	0.0002	0.0006	0.0002	0.0002
Eu2O3	0.0000	0.0000	0.0000	0.0000	0.0000	0.0000	0.0000	0.0000	0.0000	0.0000	0.0000	0.0000	0.0000	0.0000	0.0000	0.0000	0.0000	0.0000	0.0000	0.0000
F	0.0084	0.0101	0.0199	0.0689	0.0309	0.0050	0.0037	0.0083	0.0035	0.0191	0.0259	0.0040	0.0059	0.0060	0.0148	0.0148	0.0038	0.0039	0.0185	0.0256
Fe2O3	0.1116	0.0517	0.1387	0.0759	0.0865	0.0936	0.2071	0.0872	0.3627	0.1894	0.0758	0.0681	0.2792	0.0780	0.1356	0.0619	0.0665	0.3484	0.0679	0.0811
I	0.0000	0.0000	0.0000	0.0000	0.0000	0.0000	0.0000	0.0000	0.0000	0.0000	0.0000	0.0000	0.0000	0.0000	0.0000	0.0000	0.0000	0.0000	0.0000	0.0000
K2O	0.0032	0.0028	0.0013	0.0257	0.0076	0.0064	0.0097	0.0132	0.0041	0.0090	0.0040	0.0116	0.0063	0.0096	0.0091	0.0058	0.0053	0.0283	0.0068	0.0392
La2O3	0.0015	0.0009	0.0005	0.0222	0.0014	0.0007	0.0024	0.0109	0.0022	0.0021	0.0003	0.0121	0.0024	0.0024	0.0014	0.0012	0.0054	0.0070	0.0009	0.0147
Li2O	0.0003	0.0004	0.0002	0.0004	0.0002	0.0003	0.0002	0.0004	0.0005	0.0003	0.0004	0.0002	0.0003	0.0004	0.0001	0.0005	0.0002	0.0006	0.0004	0.0005
MgO	0.0028	0.0015	0.0014	0.0082	0.0044	0.0040	0.0019	0.0053	0.0063	0.0065	0.0018	0.0053	0.0036	0.0028	0.0046	0.0019	0.0036	0.0030	0.0025	0.0066
MnO	0.0366	0.0197	0.0112	0.0413	0.0191	0.0279	0.0259	0.1477	0.0423	0.0295	0.0715	0.0321	0.0233	0.1229	0.0193	0.0242	0.0195	0.0478	0.0512	0.0438
MoO3	0.0004	0.0004	0.0003	0.0005	0.0002	0.0004	0.0002	0.0007	0.0002	0.0003	0.0005	0.0003	0.0001	0.0007	0.0003	0.0007	0.0002	0.0006	0.0005	0.0007
Na2O	0.1869	0.2008	0.2046	0.2630	0.1883	0.2589	0.1958	0.1780	0.1559	0.1742	0.2788	0.2298	0.1713	0.1861	0.1539	0.2762	0.2169	0.1066	0.2447	0.2423
Nd2O3	0.0010	0.0004	0.0004	0.0003	0.0005	0.0003	0.0016	0.0011	0.0023	0.0013	0.0006	0.0005	0.0014	0.0013	0.0004	0.0006	0.0008	0.0059	0.0009	0.0006
NiO	0.0067	0.0058	0.0053	0.0530	0.0120	0.0146	0.0186	0.0287	0.0154	0.0160	0.0118	0.0295	0.0262	0.0094	0.0235	0.0090	0.0132	0.0214	0.0095	0.0363
P2O5	0.0347	0.0166	0.0300	0.0913	0.0103	0.0212	0.0085	0.0334	0.0109	0.0141	0.0213	0.0889	0.0315	0.0216	0.0174	0.0370	0.0504	0.0144	0.0111	0.0631
PbO	0.0052	0.0017	0.0062	0.0036	0.0044	0.0060	0.0076	0.0044	0.0180	0.0083	0.0026	0.0025	0.0151	0.0041	0.0066	0.0028	0.0034	0.0087	0.0037	0.0063
PdO	0.0000	0.0000	0.0000	0.0000	0.0000	0.0000	0.0000	0.0005	0.0000	0.0000	0.0000	0.0000	0.0000	0.0004	0.0000	0.0000	0.0000	0.0000	0.0001	0.0000
Rb2O	0.0000	0.0000	0.0000	0.0000	0.0000	0.0000	0.0000	0.0000	0.0000	0.0000	0.0000	0.0000	0.0000	0.0000	0.0001	0.0000	0.0000	0.0000	0.0000	0.0000
Re2O7	0.0000	0.0000	0.0000	0.0001	0.0000	0.0000	0.0000	0.0000	0.0000	0.0001	0.0000	0.0000	0.0000	0.0000	0.0001	0.0000	0.0000	0.0000	0.0000	0.0001
Rh2O3	0.0000	0.0000	0.0000	0.0000	0.0000	0.0000	0.0000	0.0000	0.0001	0.0000	0.0000	0.0000	0.0000	0.0000	0.0000	0.0000	0.0000	0.0000	0.0000	0.0000
RuO2	0.0002	0.0000	0.0001	0.0002	0.0001	0.0000	0.0006	0.0006	0.0021	0.0008	0.0000	0.0002	0.0014	0.0005	0.0001	0.0000	0.0001	0.0002	0.0000	0.0002
Sb2O3	0.0002	0.0002	0.0002	0.0001	0.0001	0.0001	0.0001	0.0004	0.0001	0.0001	0.0004	0.0001	0.0000	0.0004	0.0001	0.0003	0.0001	0.0003	0.0002	0.0003
SeO2	0.0000	0.0001	0.0000	0.0001	0.0000	0.0001	0.0000	0.0001	0.0000	0.0000	0.0001	0.0000	0.0000	0.0001	0.0001	0.0001	0.0000	0.0001	0.0001	0.0001
SiO2	0.0900	0.0600	0.1047	0.0641	0.0522	0.0599	0.0863	0.0634	0.0943	0.0885	0.1078	0.0502	0.0954	0.0521	0.0717	0.0648	0.1025	0.0390	0.0275	0.0795
Sm2O3	0.0000	0.0000	0.0000	0.0000	0.0000	0.0000	0.0000	0.0000	0.0000	0.0000	0.0000	0.0000	0.0000	0.0000	0.0000	0.0000	0.0000	0.0000	0.0000	0.0000
SnO2	0.0000	0.0000	0.0000	0.0000	0.0000	0.0000	0.0000	0.0000	0.0000	0.0000	0.0000	0.0000	0.0000	0.0000	0.0000	0.0000	0.0000	0.0000	0.0000	0.0000
SO3	0.0111	0.0050	0.0101	0.0462	0.0019	0.0024	0.0029	0.0101	0.0026	0.0022	0.0127	0.0085	0.0026	0.0068	0.0044	0.0061	0.0128	0.0070	0.0023	0.0199
SrO	0.0034	0.0058	0.0040	0.0016	0.0009	0.0029	0.0007	0.0041	0.0008	0.0007	0.0142	0.0035	0.0013	0.0082	0.0009	0.0114	0.0017	0.0009	0.0234	0.0044
TeO2	0.0000	0.0000	0.0000	0.0000	0.0000	0.0000	0.0001	0.0004	0.0004	0.0001	0.0000	0.0000	0.0002	0.0003	0.0000	0.0000	0.0000	0.0000	0.0000	0.0001
ThO2	0.0011	0.0016	0.0016	0.0008	0.0217	0.0260	0.0191	0.0008	0.0045	0.0066	0.0018	0.0005	0.0036	0.0013	0.0449	0.0036	0.0006	0.0058	0.0084	0.0007
TiO2	0.0002	0.0002	0.0001	0.0001	0.0001	0.0001	0.0002	0.0001	0.0005	0.0002	0.0002	0.0001	0.0002	0.0002	0.0001	0.0002	0.0001	0.0004	0.0002	0.0002
Tl2O	0.0016	0.0003	0.0004	0.0004	0.0001	0.0002	0.0001	0.0021	0.0003	0.0001	0.0001	0.0008	0.0000	0.0015	0.0000	0.0005	0.0020	0.0001	0.0003	0.0012
UO3	0.0536	0.0365	0.0533	0.0300	0.0866	0.1047	0.0396	0.0369	0.0255	0.0463	0.0620	0.0211	0.0428	0.0403	0.1169	0.0446	0.0430	0.0541	0.0646	0.0484
V2O5	0.0003	0.0003	0.0002	0.0002	0.0002	0.0002	0.0001	0.0003	0.0001	0.0002	0.0005	0.0002	0.0001	0.0004	0.0002	0.0004	0.0002	0.0004	0.0004	0.0003
WO3	0.0000	0.0000	0.0000	0.0001	0.0001	0.0001	0.0000	0.0009	0.0008	0.0002	0.0000	0.0000	0.0006	0.0007	0.0000	0.0000	0.0000	0.0000	0.0002	0.0001
Y2O3	0.0000	0.0000	0.0000	0.0000	0.0001	0.0000	0.0001	0.0001	0.0003	0.0001	0.0000	0.0000	0.0001	0.0001	0.0000	0.0000	0.0000	0.0003	0.0001	0.0000

#	11-C1	11-C2	11-C3	11-C4	11-C5	11-C6	11-C7	11-C8	11-C9	11-C10	11-C11	11-C12	11-C13	11-C14	11-C15	11-C16	11-C17	11-C18	11-C19	11-C20
ZnO	0.0004	0.0004	0.0005	0.0002	0.0005	0.0007	0.0003	0.0007	0.0005	0.0004	0.0004	0.0003	0.0004	0.0008	0.0004	0.0006	0.0004	0.0013	0.0008	0.0006
ZrO2	0.0027	0.0083	0.0018	0.0037	0.2681	0.0666	0.0443	0.0025	0.0286	0.1437	0.0012	0.0019	0.0190	0.0226	0.1633	0.0158	0.0009	0.0592	0.1300	0.0033
M, MT	1539.0	1616.0	3164.0	155.54	829.19	249.72	181.42	193.08	565.20	507.96	131.59	92.925	433.61	175.65	208.10	1420.6	106.79	157.25	689.81	138.10

Waste Loading Calculations and Results

The maximum waste loadings were estimated for each of the forty clusters using the sets of constraints in Table 2.24 and Table 2.25 for the qualified WTP algorithm constraints (Vienna and Kim 2008), the HTWOS 2009 constraints (Vienna et al. 2009), and the HTWOS 2010 constraints (McCloy and Vienna 2010). These calculations were performed using an iterative solution method in Excel 2010 (Microsoft Corp., Redmond, WA).

The results for the WTP qualified algorithm constraint set are summarized in Table A.3. Each cluster was limited by model validity constraints for waste components. Although the fraction of glass limited by each component constraint differs between the two feed vectors, the total estimated glass mass is surprisingly similar at 55,500 ± 600 MT, translating to just over 18,000 canisters of HLW glass (assuming an average of 3.02 MT of glass per canister).

Table A.3. Summary of Waste Loading Estimates for the WTP Baseline Set of Constraints

Cluster	WL, %	Limits(a)	waste, MT	glass, MT	Cluster	WL, %	Limits(a)	waste, MT	Glass, MT
08-C01	16.35	mv(F)	355.67	2175.3	11-C01	36.50	mv(Al)	1539.0	4216.6
08-C02	14.43	mv(F)	274.54	1902.7	11-C02	25.09	mv(Cr)	1616.0	6441.9
08-C03	18.80	mv(Cr)	138.15	734.80	11-C03	22.11	mv(F)	3164.0	14307
08-C04	31.67	mv(Al)	3045.5	9615.8	11-C04	6.39	mv(F)	155.5	2435.6
08-C05	23.58	mv(F)	1416.5	6007.3	11-C05	14.26	mv(F)	829.2	5816.3
08-C06	8.13	mv(F)	618.44	7602.8	11-C06	30.81	mv(Cr)	249.72	810.44
08-C07	43.87	mv(Ca)	1148.2	2617.2	11-C07	31.10	mv(Al)	181.4	583.26
08-C08	9.19	mv(Cr)	196.37	2136.1	11-C11	24.56	mv(Cr)	193.08	786.22
08-C09	40.00	mv(Ni)	135.43	338.59	11-C09	41.44	mv(Fe)	565.20	1363.9
08-C10	29.80	mv(Cr)	891.44	2991.4	11-C10	23.01	mv(F)	507.96	2207.2
08-C11	35.56	mv(F)	139.37	391.88	11-C11	12.81	mv(Ca)	131.59	1027.1
08-C12	8.48	mv(Cr)	299.63	3534.9	11-C12	7.11	mv(Ca)	92.925	1306.3
08-C13	23.55	mv(Cr)	154.28	655.15	11-C13	28.50	mv(Ca)	433.61	1521.5
08-C14	26.21	mv(Ni)	291.41	1111.9	11-C14	28.62	mv(Cr)	175.65	613.74
08-C15	21.78	mv(Cr)	331.00	1519.9	11-C15	26.03	mv(Ca)	208.10	799.45
08-C16	27.76	mv(Al)	449.02	1617.6	11-C16	20.16	mv(Cr)	1420.6	7045.1
08-C17	23.10	mv(Al)	1300.5	5628.7	11-C17	14.96	mv(Ca)	106.8	713.59
08-C18	13.14	mv(Ca)	192.30	1464.0	11-C18	39.88	mv(SoM)	157.25	394.35
08-C19	20.36	mv(Ca)	356.33	1750.0	11-C19	23.74	mv(F)	689.81	2905.8
08-C20	27.53	mv(Cr)	312.49	1134.9	11-C20	17.22	mv(F)	138.10	802.16
Average	21.93	Total	12,047	54,931	Average	22.38	Total	12,555	56,098

(a) mv – is model validity single component constraint with the constraining component listed after, SoM is the sum of minor components

The results for the HTWOS 2009 constraint set are summarized in Table A.4. Unlike the WTP constraint set, a majority of clusters were limited by glass properties (70% for the 2008 feed and 44% for the 2011 feed). Under the optimization process used, when the composition is limited by properties, there must be as many limiting factors as there are additives (i.e., all degrees of freedom are used). Although the fraction of glass limited by each component constraint differs between the two feed vectors, the total estimated glass mass is surprisingly similar at 31,350 ± 100 MT, translating to roughly 10,400 canisters of HLW glass (assuming an average of 3.02 MT of glass per canister).

Table A.4. Summary of Waste Loading Estimates for the HTWOS 2009 Set of Constraints

Cluster	WL, %	Limits	waste, MT	glass, MT	Cluster	WL, %	Limits	waste, MT	glass, MT
08-C01	38.85	mv(P) mv(P)	355.67	915.41	11-C01	45.23	SO3 mv(Fe), mv(Li), UV,	1539.0	3402.7
08-C02	33.84		274.54	811.38	11-C02	35.43	ND	1616.0	4561.4
08-C03	25.32	mv(P)	138.15	545.60	11-C03	42.39	mv(Bi)	3164.0	7463.8
08-C04	42.86	mv(Li), UV, ND	3045.5	7105.4	11-C04	10.82	SO3	155.5	1438.0
08-C05	52.89	LV, T1%, ND	1416.5	2678.4	11-C05	49.37	mv(B), LV, TL, ND	829.2	1679.4
08-C06	25.97	SO3	618.44	2381.7	11-C06	51.75	mv(B), T1%, ND	249.72	482.5
08-C07	45.78	LV, T1%, ND	1148.2	2508.0	11-C07	44.96	mv(B), LV, T1%, ND	181.4	403.5
08-C08	18.38	mv(Cr)	196.37	1068.4	11-C08	40.87	mv(B), mv(Fe), LV, T1%, ND	193.08	472.4
08-C09	41.84	LV, T1%, ND	135.43	323.69	11-C09	41.53	mv(B), LV, T1%, ND	565.20	1361.0
08-C10	39.73	mv(Fe), mv(Li), UV, ND	891.44	2243.9	11-C10	48.05	mv(B), LV, T1%, ND	507.96	1057.2
08-C11	48.06	mv(B), LV, T1%, ND	139.37	289.96	11-C11	39.41	SO3	131.59	333.88
08-C12	16.95	mv(Cr)	299.63	1767.7	11-C12	22.79	CaP	92.925	407.7
08-C13	38.50	mv(Na)	154.28	400.70	11-C13	44.21	mv(B), LV, T1%, ND	433.61	980.83
08-C14	46.58	mv(B), LV, T1%, ND	291.41	625.64	11-C14	42.06	mv(Fe), T1%, LV, ND	175.65	417.60
08-C15	38.46	SO3	331.00	860.57	11-C15	50.95	LV, T1%, TL, ND	208.10	408.41
08-C16	47.16	mv(Li), T1%, ND	449.02	952.01	11-C16	40.30	mv(Cr)	1420.6	3524.8
08-C17	32.16	mv(Fe), mv(Li), UV, ND	1300.5	4043.5	11-C17	38.94	SO3	106.8	274.2
08-C18	48.33	mv(B), UV, ND	192.30	397.88	11-C18	39.41	mv(B), LV, T1%, ND	157.25	398.96
08-C19	48.27	mv(P)	356.33	738.15	11-C19	41.82	mv(B), mv(Fe), mv(Li), TL, ND	689.81	1649.7
08-C20	41.67	mv(B), mv(Fe), LV, T1%, ND	312.49	750.00	11-C20	25.13	SO3	138.10	549.55
Average	38.36	Total	12,047	31,408	Average	40.16	Total	12,555	31,268

(a) mv – is model validity single component constraint with the constraining element listed after, UV and LV - the upper and lower viscosity limits, ND – nepheline discriminator, T1% - spinel $T_{1\%}$, SO3 – sulfate salt limit, CaP – $CaO \times P_2O_5$ limit, TL – zirconia-containing phase T_L

This set of assumptions is the most appropriate to compare with mission estimates. Table A.5 compares the estimates generated here with those reported in literature. The calculations performed in this study are 2.2% lower than those reported by Certa et al. (2011). This compares quite closely to the 2.5% relative differences (RPD) identified by Perez et al. (2001) between glass volumes estimated by formulation of waste clusters to those for every batch using HTWOS for four well controlled cases. This difference is directly attributed to the slight increase in waste loadings for the clusters over the individual batches within the cluster due to the effective blending of those batches to generate a cluster average composition (Perez et al. 2001). Larger differences are seen (6.6 to 8.5% RPD) between these calculations and those from the G2 model estimates of Jenkins et al. (2010 and 2012). In addition to the roughly 2.5% difference caused by blending of waste into cluster averages, there is an unexplained 4-6% relative difference. No attempt was made to determine the cause of this small difference.

Table A.5. Comparison of Glass Canister Estimates Between This Study and Literature Values for the HTWOS 2009 Constraint Set

Source of estimate	glass, cans	RPD	Reference
2008 feed, this study	10,400	-	-
2008 feed, TUA-2010	11,365	-8.5	Jenkins et al. 2010
2011 feed, this study	10,353	-	-
2011 feed, SP-6	10,586	-2.2	Certa et al. 2011
2011 feed, TUA-2012	11,079	-6.6	Jenkins et al. 2012

The results for the HTWOS 2010 constraint set are summarized in Table A.6. Although the fraction of glass limited by each component constraint differs between the two feed vectors, the total estimated glass mass is surprisingly similar at 28,450 ± 200 MT, translating to roughly 9,400 canisters of HLW glass.

Table A.6. Summary of Waste Loading Estimates for the HTWOS 2010 Set of Constraints

Cluster	WL, %	Limits	waste, MT	glass, MT	Cluster	WL, %	Limits	waste, MT	glass, MT
08-C01	43.45	CaP	355.67	818.65	11-C01	51.68	mv(Si), LV, T1%, OB	1539.0	2978.0
08-C02	51.48	CaP	274.54	533.29	11-C02	39.33	mv(Al)	1616.0	4109.3
08-C03	37.59	mv(Cr)	138.15	367.49	11-C03	54.25	mv(Si), LV, T1%, OB	3164.0	5831.7
08-C04	48.72	mv(Al)	3045.5	6251.6	11-C04	12.98	SO3	155.5	1198.3
08-C05	54.67	LV, T1%, OB	1416.5	2590.9	11-C05	49.37	mv(B), LV, TL, ND	829.2	1679.4
08-C06	31.16	SO3	618.44	1984.8	11-C06	54.24	mv(Si), T1%, OB	249.72	460.4
08-C07	45.73	LV, T1%, ND	1148.2	2510.9	11-C07	46.82	LV, T1%, OB	181.4	387.5
08-C08	18.38	mv(Cr)	196.37	1068.4	11-C08	41.17	mv(B), mv(Fe), LV, T1%	193.08	468.9
08-C09	41.89	LV, T1%, OB	135.43	323.32	11-C09	41.53	mv(B), LV, T1%, ND	565.20	1361.0
08-C10	45.03	mv(Fe), mv(Si), LV, T1%, OB	891.44	1979.7	11-C10	48.26	LV, TL, OB	507.96	1052.5
08-C11	47.99	LV, T1%, ND	139.37	290.44	11-C11	47.30	SO3	131.59	278.24
08-C12	16.95	mv(Cr)	299.63	1767.7	11-C12	22.79	CaP	92.925	407.7
08-C13	38.50	mv(Na)	154.28	400.70	11-C13	44.21	mv(B), LV, T1%, ND	433.61	980.83
08-C14	46.58	mv(B), LV, T1%, ND	291.41	625.64	11-C14	45.13	mv(Fe), LV, T1%, OB	175.65	389.17
08-C15	43.39	LV, T1%, OB	331.00	762.90	11-C15	50.95	LV, T1%, TL, ND	208.10	408.41
08-C16	50.42	mv(Si), LV, T1%, OB	449.02	890.59	11-C16	40.30	mv(Cr)	1420.6	3524.8
08-C17	35.54	mv(Al)	1300.5	3659.1	11-C17	43.90	CaP	106.8	243.2
08-C18	48.33	mv(B), UV, ND	192.30	397.88	11-C18	39.41	mv(B), LV, T1%, ND	157.25	398.96
08-C19	50.54	CaP	356.33	704.98	11-C19	41.82	mv(B), mv(Fe), mv(Li), TL, ND	689.81	1649.7
08-C20	44.97	mv(Fe), LV, T1%, OB	312.49	694.95	11-C20	30.16	SO3	138.10	457.96
Average	42.09	Total	12,047	28,624	Average	44.42	Total	12,555	28,266

(a) mv – is model validity single component constraint with the constraining element listed after, UV and LV - the upper and lower viscosity limits, ND – nepheline discriminator, OB – optical basicity, T1% - spinel $T_{1\%}$, SO3 – sulfate salt limit, CaP – $CaO \times P_2O_5$ limit, TL – zirconia-containing phase T_L

The results for the advanced constraint sets are summarized in Table A.7. Although the fraction of glass limited by each component constraint differs between the two feed vectors, the total estimated glass mass is surprisingly similar at 23,000 ± 120 MT, translating to roughly 7,650 canisters of HLW glass.

Table A.7. Summary of Waste Loading Estimates for the Advanced Set of Constraints

Cluster	WL, %	Limits	waste, MT	glass, MT	Cluster	WL, %	Limits	waste, MT	glass, MT
08-C01	43.45	CaP	355.67	818.65	11-C01	56.74	mv(Si), UV, C2, NP	1539.0	2712.4
08-C02	51.48	CaP	274.54	533.29	11-C02	51.50	mv(Si), UV, NP	1616.0	3138.1
08-C03	45.58	mv(P)	138.15	303.11	11-C03	61.84	mv(Si), SO3, C2, NP	3164.0	5116.4
08-C04	54.92	mv(Si), UV, C2, NP	3045.5	5545.0	11-C04	28.51	mv(Li), SO3, mv(Zn), LV, C2	155.5	545.62
08-C05	61.68	mv(Si), C2, NP	1416.5	2296.4	11-C05	50.35	mv(Zr)	829.2	1647.0
08-C06	46.21	mv(F)	618.44	1338.2	11-C06	60.18	mv(U)	249.72	414.99
08-C07	55.02	LV, C2, NP	1148.2	2087.0	11-C07	56.35	mv(Si), UV, C2, NP	181.4	321.93
08-C08	45.74	mv(P)	196.37	429.3	11-C08	46.10	LV, C2, NP	193.08	418.78
08-C09	50.84	mv(Cd)	135.43	266.38	11-C09	49.88	LV, C2, NP	565.20	1133.2
08-C10	52.42	mv(Si), UV, C2, NP	891.44	1700.7	11-C10	57.16	mv(Si), C2, NP	507.96	888.65
08-C11	54.90	SO3	139.37	253.86	11-C11	61.70	SO3, LV, NP	131.59	213.29
08-C12	42.37	Cr2O3	299.63	707.1	11-C12	22.79	CaP	92.925	407.69
08-C13	41.38	mv(Na)	154.28	372.83	11-C13	53.14	LV, C2, NP	433.61	815.95
08-C14	54.39	LV, C2, NP	291.41	535.82	11-C14	51.10	mv(Si), C2, NP	175.65	343.74
08-C15	48.97	LV, C2, NP	331.00	675.92	11-C15	53.88	mv(U)	208.10	386.22
08-C16	59.26	mv(Si), UV, C2, NP	449.02	757.69	11-C16	57.61	mv(Si), UV, NP	1420.6	2465.8
08-C17	48.86	mv(Si), UV, NP	1300.5	2661.6	11-C17	43.90	CaP	106.8	243.25
08-C18	52.53	mv(Na)	192.30	366.06	11-C18	46.88	LV, C2, NP	157.25	335.43
08-C19	50.54	CaP	356.33	704.98	11-C19	50.83	mv(Si), LV, TL, NP	689.81	1357.2
08-C20	49.77	mv(Mn)	312.49	627.90	11-C20	46.30	SO3, mv(Zn), LV, C2	138.10	298.29
Average	52.42	Total	12,047	22,982	Average	54.11	Total	12,555	23,204

(a) mv – is model validity single component constraint with the constraining element listed after, UV and LV - the upper and lower viscosity limits, NP – nepheline constraint, C2 – 2 vol% spinel at 950°C, SO3 – sulfate salt limit, CaP – $CaO \times P_2O_5$ limit, TL – zirconia-containing phase T_L

Summary and Conclusions

Table A.8 summarizes the glass mass (MT) by constraint for each of the constraint sets and feed vectors. The constraint sets evolve in time with the addition of more glass formulation and property data. In 2008 (WTP algorithm) 100% of the glass was limited by model validity constraints. As time progressed, less and less of the glass was limited by model validity, and more and more glass was limited by property constraints. Ultimately, it is the properties that should limit the loading of waste in glass as model validity constraints represent only the bounds of current data or the bounds over which the current models are predictive. Additional data and improved models should eventually remove those constraints until all wastes are limited by property constraints. Although the table suggests that 70 to 90% of all the glasses in the advanced constraint set are limited by properties, it needs to be recognized that among the property constraints there do exist model validity constraints. This is because when optimizing glass formulations for a given waste, the additive mix is continually changed until as many limits are reached as there are additives in the glass (to use up all remaining degrees of freedom). The nominal "property-limited" glasses therefore have between three and five limits which include model validity constraints.

Table A.8. Summary of Glass Mass (MT) by Constraint for Each of the Constraint Sets

Constraint	WTP		HTWOS 2009		HTWOS 2010		Advanced	
Feed	2008	2011	2008	2011	2008	2011	2008	2011
Properties	0	0	21,918	13,873	11,067	18,047	16,260	20,105
mv(F)	18,080	28,474	0	0	0	0	1,338	0
mv(Al)	16,862	4,800	0	0	9,911	4,109	0	0
mv(Cr)	12,707	15,697	2,836	3,525	3,204	3,525	707	0
mv(Bi)	0	0	0	7,464	0	0	0	0
SO3	0	0	3,242	5,998	1,985	1,935	254	0
CaP	5,831	5,368	3,011	408	2,057	651	2,789	651
mv(Zr)	0	0	0	0	0	0	0	1,647
mv(Ni)	1,451	0	0	0	0	0	0	0
mv(Fe)	0	1,364	0	0	0	0	0	0
mv(U)	0	0	0	0	0	0	0	801
mv(Na)	0	0	401	0	401	0	739	0
mv(Mn)	0	0	0	0	0	0	628	0
mv(Cd)	0	0	0	0	0	0	266	0
SoM	0	394	0	0	0	0	0	0
Total	54,931	56,098	31,408	31,268	28,624	28,266	22,982	23,204

The results of these calculations can best be summarized in a single figure showing the amount of glass estimated for each of the constraints (Figure A.1). If we were to process HLW today, we would need to use the WTP baseline constraint set, as that is the only fully qualified set of constraints and models. This would yield roughly 2.5× the amount of glass that is possible by applying the advanced glass formulation results. We conclude and recommend that the efforts necessary to develop the advanced glass formulation and to qualify those compositions for production in the WTP be completed.

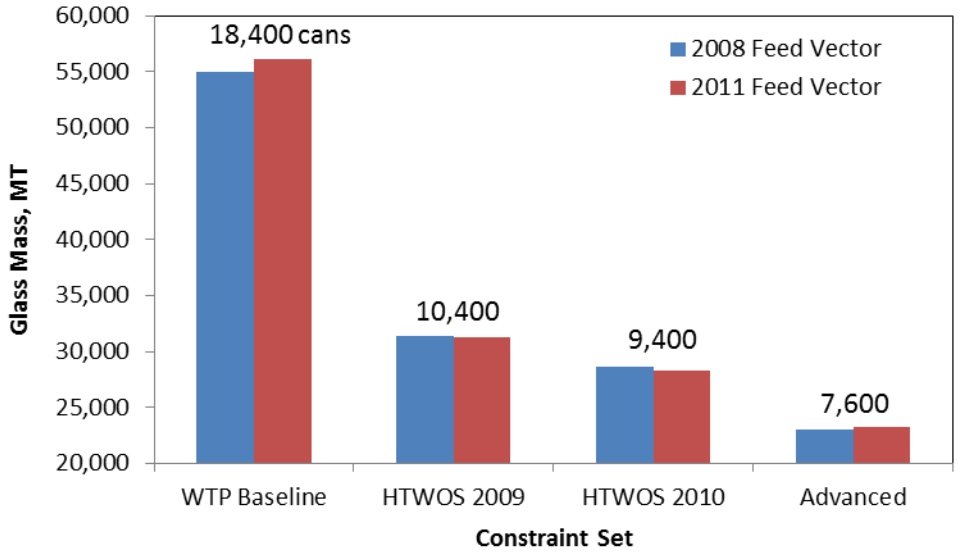

Figure A.1. Comparison of Glass Mass Estimates for Each Constraint Set and Feed Vector

Developing and applying the advanced glass formulations will certainly reduce the cost of Hanford tank waste management, if only by reducing the cost of fabrication, storage, transportation, and disposal

of the HLW glass. More significant benefits may also be realized. These advanced formulations are far more tolerable to key components in the waste, such as Al_2O_3 (with concentrations of up to 28 wt%), Cr_2O_3 (with concentrations up to 3 wt%), SO_3 (with concentrations up to nearly 1 wt%), and Na_2O (with concentrations up to 23 wt%). Tolerating these higher concentrations of key glass limiters may reduce the burden on waste pretreatment, which currently strives to effectively leach Cr and Al and wash S and Na from the HLW fraction. This may also make direct vitrification of the HLW fraction without significant pretreatment more cost effective. Finally, the advanced glass formulation efforts seek not only to increase waste loading in glass, but also glass production rate. All of the advanced glass formulations are processable at or above the current nominal processing rate estimates (1000 $kg/m^2/d$) and well above the current contract (807 $kg/m^2/d$) processing rate limit. Therefore, if waste can be delivered to the HLW vitrification facility fast enough to match the enhanced waste throughput rates (waste throughput = waste loading times glass production rate), then the mission life may be significantly reduced.

References

Certa PJ, GK Allen, TW Crawford, TM Hohl, KN Jordan, RA Kirkbride, and RL Lytle. 2008. *River Protection Project System Plan*, ORP-11242, Rev. 3A, U.S. Department of Energy, Office of River Protection, Richland, Washington.

Certa PJ, RD Adams, GK Allen, JD Belsher, PA Empey, JH Foster, TM Hohl, RT Jasper, RA Kirkbride, RL Lytle, FL Meinert, JS Ritari, RM Russell, KR Seniow, EB West, MN Wells, and LM Bergmann. 2011. *River Protection Project System Plan*, ORP-11242, Rev. 6, U.S. Department of Energy, Office of River Protection, Richland, Washington.

Jenkins KD, RF Gimpel, YN Deng, VS Arakali, SL Orcutt, and IZ Stone. 2010. *2010 WTP Tank Utilization Assessment.* 24590-WTP-RPT-PET-10-020, Rev. 0, River Protection Project, Hanford Tank Waste Treatment and Immobilization Plant, Richland, Washington.

Jenkins KD, YN Deng, and SL Orcutt. 2012. *2012 WTP Tank Utilization Assessment.* 24590-WTP-RPT-PE-12-001, Rev 0, River Protection Project, Hanford Tank Waste Treatment and Immobilization Plant, Richland, Washington.

Kim DS, MJ Schweiger, CP Rodriguez, WC Lepry, JB Lang, JV Crum, JD Vienna, FC Johnson, JC Marra, and DK Peeler. 2011. *Formulation and Characterization of Waste Glasses with Varying Processing Temperature.* PNNL-20774, Pacific Northwest National Laboratory, Richland, Washington.

McCloy JS and JD Vienna. 2010. *Glass Composition Constraint Recommendations for Use in Life-Cycle Mission Modeling.* PNNL-19372, Pacific Northwest National Laboratory, Richland, Washington.

Perez JM, DF Bickford, DE Day, D-S Kim, SL Lambert, SL Marra, DK Peeler, DM Strachan, MB Triplett, JD Vienna, and RS Wittman. 2001. *High-Level Waste Melter Study Report.* PNNL-13582, Pacific Northwest National Laboratory, Richland, Washington.

Vienna JD and DS Kim. 2008. *Preliminary IHLW Formulation Algorithm Description.* 24590-HLW-RPT-RT-05-001, Rev 0, River Protection Project, Hanford Tank Waste Treatment and Immobilization Plant, Richland, Washington.

Vienna JD, A Fluegel, DS Kim, and P Hrma. 2009. *Glass Property Data and Models for Estimating High-Level Waste Glass Volume*. PNNL-18501, Pacific Northwest National Laboratory, Richland, Washington.

Pacific Northwest
NATIONAL LABORATORY

U.S. DEPARTMENT OF
ENERGY

Proudly Operated by **Battelle** *Since 1965*

902 Battelle Boulevard
P.O. Box 999
Richland, WA 99352
1-888-375-PNNL (7665)

www.pnnl.gov